Analysis of cone-like singularities in twisted elastic ribbons

Basile Audoly, G.H.M. van der Heijden

Analysis of cone-like singularities in twisted elastic ribbons

Basile Audoly[†] and G.H.M. van der Heijden[⋆]

[†]Laboratoire de mécanique des solides, CNRS, Institut Polytechnique de Paris, Palaiseau, France
[⋆]Department of Civil, Environmental and Geomatic Engineering, University College London, London WC1E 6BT, UK

August 27, 2022

Abstract

Twisting a thin elastic ribbon is known to produce a localised deformation pattern resembling a cone whose tip is located on the edge of the ribbon. Using the theory of inextensional ribbons, we present a matched asymptotic analysis of these singularities for ribbons whose width-to-length ratio $w/\ell \ll 1$ is small. An inner layer solution is derived from the finite-w Wunderlich model and captures the fast, local variations of the bending and twisting strains in the neighbourhood of the cone-like region; it is universal up to a load intensity factor. The outer solution is given by the zero-w Sadowsky model. Based on this analysis, we propose a new standalone ribbon model that combines the Sadowsky equations with jump conditions providing a coarse-grained description of cone-like singularities, and give a self-contained variational derivation of this model. Applications to the Möbius band and to an end-loaded open ribbon are presented. Overall, the new model delivers highly accurate approximations to the solutions of the Wunderlich model in the limit $w \ll \ell$ while avoiding the numerical difficulties associated with cone-like singularities.

1 Introduction

It is well known that twisting a thin elastic ribbon may induce stress localisations at points on the long edges of the structure. The elastic Möbius band shown in Figure 1a, for instance, contains a point of stress localisation on its edge (Starostin and van der Heijden, 2007). In the photograph, this singular point is the tip of a V-shaped pattern produced by the reflection of light. This pattern agrees with the elastic solution obtained by Starostin and van der Heijden (2007) for a Möbius band which, around the singularity, is close to a cone having its tip on the edge of the ribbon. By *cone*, we mean a general surface swept by a segment having one fixed end point (the singular point) while the other end point traces out a curve in space (this curve being the opposite edge of the ribbon). Considering a different geometry, Korte et al. (2011) have observed that a stretched and twisted ribbon produces the pattern shown in Figure 1b, consisting of nearly-flat triangular facets bounded by relatively sharp creases radiating out from these points (or vertices) of high bending stress. This pattern is obtained by arranging several cone-like singularities head-to-tail, as shown by the brown wedge symbols in the figure. A similar cone-like pattern has also been reported by Yu and Hanna (2019) in ribbons subjected to a combination of shearing and bending.

The goal of this paper is to explain these ubiquitous cone-like singularities and describe their inner structure, starting from the equations governing the equilibria of thin elastic ribbons.

The triangular creasing patterns in stretched and pulled ribbons shown in Figure 1b have been analysed using von Kármán plate theory. Chopin et al. (2015), for example, use scaling analysis

to identify various 'phases' of twisted ribbons, as well as instabilities causing transitions between them, depending on their length to thickness ratio as well as loading parameters (tension and twist rate). Further results from a rigorous energy analysis of the same extensible plate model, giving estimates on the amplitude and wavelength of small-scale tensile central wrinkles, are reported by Kohn and O'Brien (2018).

In the present work, we limit attention to the inextensional theory, valid for sufficiently thin ribbons: in the absence of stretching, an intrinsically flat ribbon is described by a developable surface. Using developability, one can reduce the strain energy of the ribbon to its centreline, giving the *one-dimensional* Wunderlich functional (Wunderlich, 1962). The equilibrium equations for this functional obtained by the Euler-Lagrange method are ordinary differential equations (Starostin and van der Heijden, 2007) and therefore much easier to analyse than the usual partial differential equations of plate theory. The stress localisation patterns appearing on the edge of the ribbon correspond to singularities in these ordinary differential equations, in the form of logarithmic divergences of the strain energy density at inflection points of the ribbon's centreline. These singularities, with associated rapid variation of bending and torsional strains, greatly complicate the study of deformed ribbon configurations, both analytically and numerically. Although numerical solutions have been constructed (Starostin and van der Heijden, 2007; Korte et al., 2011; Starostin and van der Heijden, 2015) and some regularity results have been obtained (Hornung, 2011; Bartels and Hornung, 2015), the singularities of twisted ribbons have so far resisted an analytical description.

Here, we present a matched asymptotic analysis valid for ribbons with small width to length ratio $w/\ell \ll 1$, in which the cone-like singularities are described as *inner layers*. In appropriately scaled form, these cone-like singularities are found to be universal, with no parameter dependence. The equilibrium equations within the layer reduce to a second-order differential equation for a single degree of freedom that is the angle between the local generator and the centreline. A matching procedure selects the layer solution to be the heteroclinic orbit of this system, corresponding to the generator sweeping through a 90° sector from $-45°$ to 45°, while the slaved normal curvature of the ribbon remains small, in good agreement with the experimentally observed pattern.

In the narrow limit $w/\ell \to 0$, the equilibrium of the ribbon is governed by the Sadowsky functional (Sadowsky, 1931), which predicts an even 'harder' singularity than the Wunderlich model. In the Sadowsky model the curvature has a finite jump (rather than rapid variation) through singularities. This behaviour is associated with non-convexity of Sadowsky's strain energy, which predicts a microstructure (Paroni and Tomassetti, 2019) that is reminiscent of the small-scale tensile central wrinkles observed by Chopin and Kudrolli (2013) and analysed by Kohn and O'Brien (2018). The Sadowsky model has recently attracted a great amount of interest

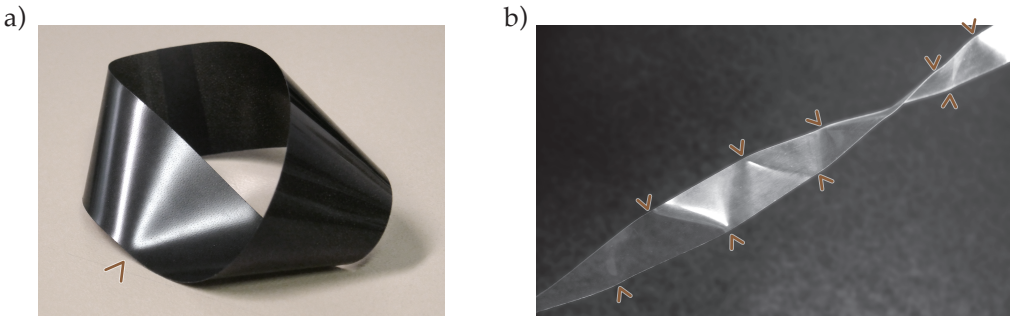

Figure 1: Spontaneous formation of cone-like singularities, revealed by light reflection in a thin, transparent ribbon: (a) isolated singularity in a Möbius band made of blackened transparency film with dimensions 20.1 cm × 2.7 cm (Starostin and van der Heijden, 2007) and (b) multiple singularities in a pulled and twisted transparency ribbon of dimensions 27.5 cm × 1.85 cm (Korte et al., 2011). The overlaid wedge symbols highlight the tips of the cone-like singularities.

(Freddi et al., 2015; Paroni and Tomassetti, 2019; Starostin and van der Heijden, 2018), while generalisations to intrinsically curved and residually-stressed narrow ribbons are considered by Dias and Audoly (2015); Efrati (2015); Freddi et al. (2016).

The main practical benefit of our analysis is to identify jump conditions applicable to the Sadowsky model, that capture in an effective way the rapidly varying bending and torsional strains predicted by the more accurate but also more complex Wunderlich model at cone-like singularities. Our analysis therefore deals with three different models for elastic ribbons:

- The inextensional Wunderlich model is geometrically exact and is valid for all values of w/ℓ. It is a one-dimensional model obtained by reducing the elastic energy of an inextensional, rectangular plate to its centreline. As a result of this reduction, the energy depends on the strain gradient $\eta' = (\omega_3/\omega_2)' = \frac{\omega_3' \, \omega_2 - \omega_3 \, \omega_2'}{\omega_3^2}$, where ω_2 and ω_3 are the curvature and torsion of the centreline. This strain-gradient model features inner-layer behaviour at cone-like singularities, and is challenging to solve numerically. In the present work, the Wunderlich model is used to produce reference solutions and is the starting point of our matched asymptotic analysis.

- The Sadowsky model describes narrow ribbons and is obtained from the Wunderlich model in the limit $w/\ell \to 0$. Its strain energy does not depend on the strain gradients ω_2' and ω_3'. Its solutions are therefore much easier to compute but agree with the exact Wunderlich model to first order in $w/\ell \ll 1$ only. Moreover, the Sadowsky model cannot account for the detailed structure of the rapidly varying, exact solution near cone-like singularities.

- The outcome of our matched asymptotic analysis is a third model that shares some of the best features of the previous two. It endows the Sadowsky model with new jump conditions capturing in an effective way the inner layers of the Wunderlich model. It is accurate to second order in $w/\ell \ll 1$, not just to first order. It does not depend on the strain gradient, thereby remaining easy to solve numerically.

We compare the predictions of these models in application to two cases featuring stress singularities: the elastic Möbius band (§7) and the pulled and twisted ribbon (§8).

2 Background: the Wunderlich and Sadowsky models

We start with a short summary of the classical Wunderlich and Sadowsky models for inextensible ribbons.

2.1 Kinematic equations for an inextensible ribbon

We consider an inextensible ribbon of length ℓ, width w and thickness h. It will always be assumed that $h \ll w \ll \ell$. A one-dimensional model of the ribbon is derived by focussing on the centreline, which we denote by $\boldsymbol{x}(S)$, where $S \in [0, \ell]$ is a Lagrangian arclength coordinate. We introduce an orthonormal material frame of directors $\boldsymbol{d}_i(S)$ $i = 1, 2, 3$, with $\boldsymbol{d}_3$ in the tangent direction and $\boldsymbol{d}_1$ normal to the surface of the ribbon (see Figure 2), and denote as $\omega_i(S)$ the local components of the rotation gradient, also known as the Darboux vector.

The centreline position $\boldsymbol{x}(S)$ and the directors $\boldsymbol{d}_i(S)$ are subject to the inextensibility, adaptation and developability conditions from the classical theory of inextensible ribbons:

$$\boldsymbol{d}_i(S) \cdot \boldsymbol{d}_j(S) = \delta_{ij} \tag{2.1}$$

$$\boldsymbol{x}'(S) = \boldsymbol{d}_3(S) \tag{2.2}$$

$$\boldsymbol{d}_i'(S) = \left(\sum_{j=2}^{3} \omega_j(S) \, \boldsymbol{d}_j(S) \right) \times \boldsymbol{d}_i(S). \tag{2.3}$$

Here δ_{ij} is the Kronecker symbol, equal to 1 if $i = j$ and to 0 otherwise.

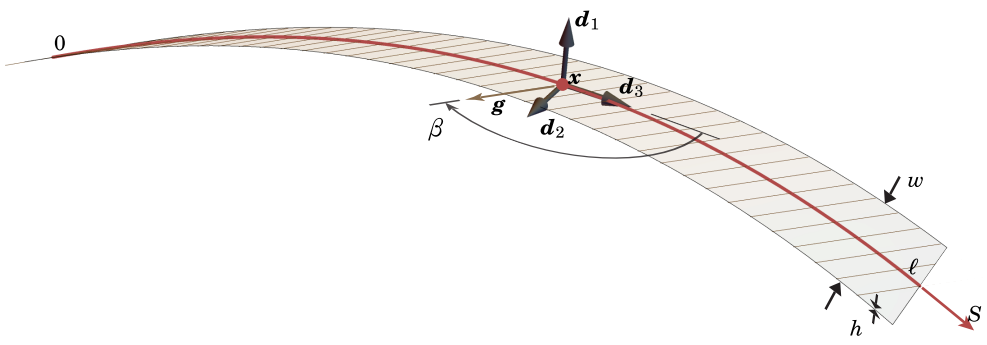

Figure 2: An inextensible ribbon is parametrised by its centreline $\boldsymbol{x}(S)$ and by a set of orthonormal directors $\boldsymbol{d}_i(S)$. The ribbon midsurface is developable, hence ruled.

Equation (2.3) serves two purposes. First, excluding the value $j = 1$ from the sum effectively suppresses the stiff bending mode of the ribbon, a condition classically written as $\omega_1 = 0$: this ensures that the geodesic curvature of the centreline on the midsurface remains zero, thereby enforcing the kinematic constraint of midsurface developability. Second, Equation (2.3) enforces the usual definition of the strain measures ω_2 and ω_3, which are the components in the director basis of the rotation gradient (the latter being the quantity in parentheses).

The ribbon midsurface can be reconstructed from the centreline $\boldsymbol{x}(S)$ as

$$\boldsymbol{U}(S,T) = \boldsymbol{x}(S) + T\,\boldsymbol{g}(S), \qquad S \in [0,\ell], T \in [-w/2, w/2]. \tag{2.4}$$

Here, $\boldsymbol{U}(S,T)$ is a point on the midsurface of the deformed ribbon, and $\boldsymbol{g}$ is the field of generators of the ribbon defined as $\boldsymbol{g}(S) = \boldsymbol{d}_2(S) + \eta(S)\,\boldsymbol{d}_3(S)$ in terms of the strain ratio

$$\eta(S) = \frac{\omega_3(S)}{\omega_2(S)}. \tag{2.5}$$

Geometrically, $\eta = \cot\beta$, where β is the angle the local generator makes with the centreline (see Figure 2). Equation (2.4) and (2.5) together give the parametrisation of a developable surface (Spivak, 1999). When extended into infinite lines, the generators meet along a caustic (also called edge of regression); see Figure 6c. For the midsurface to remain smooth, this caustic has to remain outside the physical domain of the ribbon. This leads to the condition (Starostin and van der Heijden, 2015)

$$w\,|\eta'(S)| < 2. \tag{2.6}$$

The above kinematic description of inextensible ribbons applies to both the Wunderlich and Sadowsky models.

2.2 Force and moment balance

For both the Wunderlich and Sadowsky models, the force and moment balance is expressed by the classical Kirchhoff equations,

$$\begin{aligned} \boldsymbol{n}'(S) &= \boldsymbol{0} \\ \boldsymbol{m}'(S) + \boldsymbol{x}'(S) \times \boldsymbol{n}(S) &= \boldsymbol{0}, \end{aligned} \tag{2.7}$$

where $\boldsymbol{n}(S)$ is the internal force and $\boldsymbol{m}(S)$ the internal moment. Mathematically, $\boldsymbol{n}(S)$ is the Lagrange multiplier associated with the adaptation constraint (2.2). The internal moment can be decomposed onto the directors as

$$\boldsymbol{m}(S) = m_1(S)\,\boldsymbol{d}_1(S) + m_2(S)\,\boldsymbol{d}_2(S) + m_3(S)\,\boldsymbol{d}_3(S). \tag{2.8}$$

The first bending moment $m_1(S) = \boldsymbol{m}(S) \cdot \boldsymbol{d}_1(S)$ is a Lagrange multiplier associated with the developability condition $\omega_1 = 0$.

2.3 Constitutive relations

The second bending moment $m_2(S) = \boldsymbol{m}(S)\cdot\boldsymbol{d}_2(S)$ and the twisting moment $m_3(S) = \boldsymbol{m}(S)\cdot\boldsymbol{d}_3(S)$ appearing in (2.8) are given by different constitutive relations in the Wunderlich and Sadowsky models.

2.3.1 Wunderlich model

The strain energy functional of the Wunderlich model (Wunderlich, 1962) is given by

$$\mathcal{E}_{\mathrm{Wd}}[\omega_2,\omega_3] = 4\,D\,w\int_0^\ell \frac{\omega_2^2}{2}\,L(\eta)F\left(w\,\eta'\right)\,\mathrm{d}S = \int_0^\ell e_{\mathrm{Wd}}(\omega_2,\eta,\eta')\,\mathrm{d}S, \tag{2.9}$$

where $D = \frac{Y\,h^3}{12\,(1-\nu^2)}$ is the plate's bending rigidity, with Y Young's modulus and ν Poisson's ratio. The energy functional $\mathcal{E}_{\mathrm{Wd}}$ depends on $\eta(S)$ through the function

$$L(\eta) = \left(\frac{1+\eta^2}{2}\right)^2 \tag{2.10}$$

and on the gradient $\eta'(S)$ through

$$F(q) = \frac{1}{q}\,\ln\frac{1+\frac{q}{2}}{1-\frac{q}{2}} \quad (\text{for } |q|<2). \tag{2.11}$$

The singularity of $F(q)$ at $q=0$ is removable and F can be extended into a smooth function by setting

$$F(0) = 1, \qquad F'(0) = 0, \quad \ldots \tag{2.12}$$

On the other hand, the function F has a true singularity at $q = w\,\eta' = \pm 2$ which is connected to the *cone-like* singularities investigated in this paper: for a cone η' is constant and the value $q = w\,\eta' = \pm 2$ corresponds to a cone whose tip lies on one of the edges of the ribbon by (2.6) (see also B).

Equation (2.9) is nothing but the bending energy of a rectangular thin plate whose midsurface configuration is given by (2.4), after partial integration with respect to the transverse coordinate T.

The variational derivation of the equilibrium equations yields the internal equilibrium equation for η as

$$-\frac{\mathrm{d}}{\mathrm{d}S}\left(\frac{\partial e_{\mathrm{Wd}}}{\partial \eta'}\right) + \frac{\partial e_{\mathrm{Wd}}}{\partial \eta} - m_3\,\omega_2 = 0, \tag{2.13}$$

and the constitutive law for the bending moment as

$$m_2 = \frac{\partial e_{\mathrm{Wd}}}{\partial \omega_2} - \eta\,m_3, \tag{2.14}$$

as first shown by Starostin and van der Heijden (2007).

Inserting the expression of e_{Wd} in (2.9) into (2.14), we have $m_2 = 4\,D\,w\,\left(\omega_2\,F\left(w\,\eta'\right)\,L(\eta) - \eta\,\frac{m_3}{4\,D\,w}\right)$, which can be solved for ω_2 as

$$\omega_2 = \frac{1}{F\left(w\,\eta'\right)\,L(\eta)}\,\frac{m_2+\eta\,m_3}{4\,D\,w}. \tag{2.15}$$

We also state here that the Hamiltonian of the Wunderlich model is given by

$$\mathcal{H}_{\mathrm{Wd}}(S) = \boldsymbol{d}_3\cdot\boldsymbol{n} + 4\,D\,w\,\frac{\omega_2^2}{2}\,L(\eta)\,\left(F(w\,\eta') + w\,\eta'\,F'(w\,\eta')\right). \tag{2.16}$$

$\mathcal{H}_{\mathrm{Wd}}$ is an invariant for any solution of the model, as shown in A. It will be used later to derive the inner layer equation.

2.3.2 Sadowsky model

The Sadowsky model is the limit of the Wunderlich model when $|w\,\eta'| \ll 1$, corresponding to narrow ribbons (small w) with slowly varying $\eta(S)$—this includes cylinders ($\eta' = 0$) but excludes cone-like singularities ($w\eta' = \pm 2$).

By Equation (2.12) the function F can be approximated as $F(w\,\eta') = 1$ when $|w\,\eta'| \ll 1$. Setting $F \equiv 1$ in (2.9), we obtain the energy functional originally derived by Sadowsky (1931),

$$\mathcal{E}_{\mathrm{Sd}}[\omega_2, \omega_3] = 4\,D\,w \int_0^\ell \frac{\omega_2^2}{2}\,L(\eta)\,\mathrm{d}S = \int_0^\ell e_{\mathrm{Sd}}(\omega_2, \eta)\,\mathrm{d}S. \tag{2.17}$$

The constitutive relations of the Sadowsky model are

$$\begin{aligned} m_2(S) &= \frac{\partial e_{\mathrm{Sd}}\left(\omega_2, \frac{\omega_3}{\omega_2}\right)}{\partial \omega_2} = 4\,D\,w\,\omega_2\,\left(L(\eta) - \tfrac{\eta}{2}\,L'(\eta)\right) = D\,w\,\omega_2(S)\,(1-\eta^4(S)) \\ m_3(S) &= \frac{\partial e_{\mathrm{Sd}}\left(\omega_2, \frac{\omega_3}{\omega_2}\right)}{\partial \omega_3} = 4\,D\,w\,\omega_2\,\tfrac{L'(\eta)}{2} = 4\,D\,w\,\omega_2(S)\,\eta(S)\,\tfrac{1+\eta^2(S)}{2}. \end{aligned} \tag{2.18}$$

3 Setting up the matched asymptotic expansions

We carry out a matched asymptotic analysis of the Wunderlich model. It accounts for the existence of inner layers where the solution varies on a short length scale, of order w with $w \ll \ell$. The asymptotic expansions are set up in this section. In the following sections, we obtain an inner solution valid in the layers (§4), an outer solution valid far away from the layers (§6), as well as matching conditions that ensure that the inner and outer solutions are consistent (§5). Altogether, the procedure delivers a solution of the Wunderlich model in the limit $w/\ell \to 0$ that is valid over the entire domain $0 \le S \le \ell$.

3.1 Scaling analysis

Following the method of matched asymptotic expansions, we construct a solution of the Wunderlich equation having qualitatively different behaviour in different parts of the domain $[0, \ell]$, as sketched in Figure 3:

- in the *inner region* (also called *inner layer*), the solution varies over a length scale comparable to the width w;
- in the *outer region*, the solution varies over a much larger length scale $\frac{w}{\varepsilon}$ ($\gg w$).

The separation of scales is captured by a dimensionless parameter ε,

$$\varepsilon \ll 1. \tag{3.1}$$

The parameter $\varepsilon = w/\ell$ will be defined as the ratio of the ribbon width w to a macroscopic length ℓ whose exact definition varies from problem to problem:

- for the Möbius band studied in Section 7, ℓ is the arclength of the ribbon, so that $\varepsilon = w/\ell$ is the geometrical aspect ratio;
- for the infinitely long, twisted band studied in Section 8, ℓ is given by the wavelength of the triangular pattern.

The inner regions featured by the Wunderlich solutions are regularised versions of the jump singularities predicted by the Sadowsky model at inflection points of the ribbon's centreline. In this section, we analyse the solution of the Wunderlich model in these inner regions. To keep the

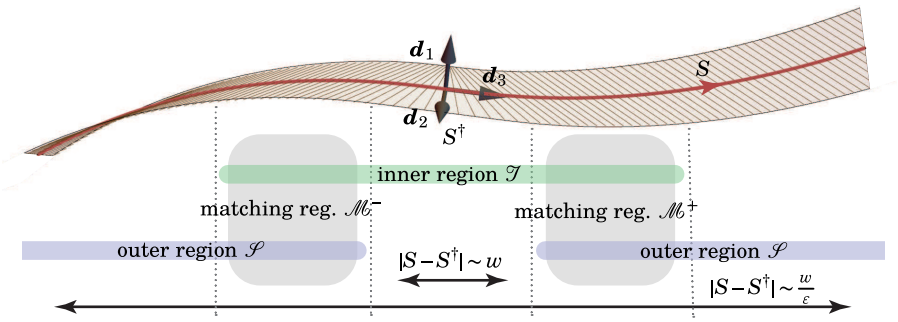

Figure 3: Solution of the Wunderlich model by a matched asymptotic expansion. The variable $\eta(S)$ that sets the direction of the generators varies quickly in an *inner region* $\mathcal{I}$ of length $\sim w$, centred at $S^\dagger$. In the *outer region* $\mathcal{S}$, $\eta(S)$ varies slowly and the Sadowsky model is valid. The *matching regions* $\mathcal{M}^\pm$ are defined as the overlap of the inner and outer regions.

notation simple, we address the case of a single inner layer and denote its centre by $S^\dagger$—for the moment, the centre $S^\dagger$ can be any particular point inside the inner layer but later on it will be defined accurately, see (4.14). The extension to multiple inner layers is straightforward as the layers are independent of each other.

The inner region $\mathcal{I}$ and the outer region $\mathcal{S}$ are defined, respectively, as the set of points S such that

$$\mathcal{I} : |S - S^\dagger| \ll \frac{w}{\varepsilon}, \qquad \mathcal{S} : |S - S^\dagger| \gg w. \tag{3.2}$$

They overlap in two matching regions $\mathcal{M}^\pm$ located on both sides of the inner region, see Figure 3,

$$\mathcal{M}^\pm : w \ll \pm(S - S^\dagger) \ll \frac{w}{\varepsilon}. \tag{3.3}$$

In the matching regions $\mathcal{M}^\pm$ we will require that the inner and outer solutions are equivalent, see Section 5.

The matched asymptotic expansion is based on the following scaling assumptions: the strain $\omega_j(S)$, the components of the internal moment m_j, and the internal force $\boldsymbol{n}$ are given in terms of ε as

$$\begin{array}{rcll} \omega_j(S) & = & \mathcal{O}\left(\frac{\varepsilon}{w}\right) & \text{for } 2 \leqslant j \leqslant 3 \\ \eta(S) & = & \mathcal{O}(1) & \\ m_j(S) & = & \mathcal{O}(D\,\varepsilon) & \text{for } 1 \leqslant j \leqslant 3 \\ \boldsymbol{n} & = & \mathcal{O}\left(\frac{D\,\varepsilon^2}{w}\right). & \end{array} \tag{3.4}$$

These scaling relations are motivated by the following qualitative arguments :

- our main assumption is that the characteristic length ℓ, defined as the order of magnitude of $1/\omega_i$ in the outer region, is much larger than the ribbon width w; with $\varepsilon = w/\ell$, this assumption is expressed by (3.1); in addition, note that $(3.4)_1$ holds in the outer region by construction;

- as the bending and twisting strains ω_j are both of order ε/ω, the ratio $\eta = \frac{\omega_3}{\omega_2}$ from (2.5) is of order 1, as stated in $(3.4)_2$;

- the constitutive law (2.15) suggests the scaling relation $\omega_j \sim \frac{m_j}{D\,w}$, which yields $(3.4)_3$ from $(3.4)_1$;

- in the outer region, the gradient $\left|\frac{\mathrm{d}\boldsymbol{m}}{\mathrm{d}S}\right|$ of the internal moment can be estimated in two equivalent ways, namely $\left|\frac{\mathrm{d}\boldsymbol{m}}{\mathrm{d}S}\right| \sim \frac{\mathrm{d}m_j}{\mathrm{d}S} \sim \frac{m_j}{w/\varepsilon} \sim D\,\varepsilon^2/w$ and $\left|\frac{\mathrm{d}\boldsymbol{m}}{\mathrm{d}S}\right| \sim m_j\,\frac{\mathrm{d}\boldsymbol{d}_j}{\mathrm{d}S} \sim m_j\,\omega_j \sim D\,\varepsilon^2/w$; inserting into the balance of moments $(2.7)_2$, we obtain $(3.4)_4$;

- having justified all the scaling assumptions in the *outer* region, we observe that the equations of equilibrium require that the internal force $\boldsymbol{n}$ and moments m_j each remain of the same order of magnitude in the *inner* region. This leads us to postulate that the scaling assumptions $(3.4)_{3,4}$ are also valid in the inner region. By using the inverse constitutive relation (2.15), we also conclude that $(3.4)_{1,2}$ extend to the inner region.

The consistency of the scaling assumptions (3.4), which suggest rapid variation (inner-layer behaviour) only in the strain variables ω_2, ω_3 and η, will be confirmed by the existence of solutions to the matched asymptotic procedure.

3.2 Inner and outer expansions

In view of the scaling assumptions $(3.4)_1$, we postulate the following expansion of the bending ($j = 2$) and twisting ($j = 3$) strains,

$$\omega_j(S) = \frac{\varepsilon}{w} \times \begin{cases} \overline{\mu}\,\left[\overline{\omega}_j\left(\frac{S-S^\dagger}{w}\right) + \varepsilon\,\overline{\overline{\omega}}_j\left(\frac{S-S^\dagger}{w}\right) + \cdots\right] & \text{in } \mathcal{I}, \\ \widetilde{\omega}_j\left(\varepsilon\,\frac{S-S^\dagger}{w}\right) + \varepsilon\,\widetilde{\widetilde{\omega}}_j\left(\varepsilon\,\frac{S-S^\dagger}{w}\right) + \cdots & \text{in } \mathcal{S}. \end{cases} \tag{3.5}$$

The implicit dependence on ε of the solution ω_j on the left-hand side has become explicit on the right-hand side.

As usual in matched asymptotic solutions, the successive terms $\overline{\omega}_j$, $\overline{\overline{\omega}}_j$, etc. in the inner solution are sought as functions of the fast variable $\overline{S}$, while those in the outer solution, $\widetilde{\omega}_j$, $\widetilde{\widetilde{\omega}}_j$, etc., are sought as functions of the slow variable $\widetilde{S}$,

$$\overline{S} = \frac{S - S^\dagger}{w}, \qquad \widetilde{S} = \varepsilon\,\frac{S - S^\dagger}{w}. \tag{3.6}$$

Anticipating the fact that the inner solution is unique up to a multiplicative constant, we have factored out on the right-hand side of (3.5) a coefficient $\overline{\mu}$ that will be defined later in (E.4). For the moment it suffices to know that $\overline{\mu}$ is a dimensionless quantity that is independent of ε.

Similarly, in view of the other assumptions in (3.4) we postulate the following expansions for $\eta(S)$,

$$\eta(S) = 1 \times \begin{cases} \overline{\eta}\left(\frac{S-S^\dagger}{w}\right) + \varepsilon\,\overline{\overline{\eta}}\left(\frac{S-S^\dagger}{w}\right) + \cdots & \text{in } \mathcal{I} \\ \widetilde{\eta}\left(\varepsilon\,\frac{S-S^\dagger}{w}\right) + \varepsilon\,\widetilde{\widetilde{\eta}}\left(\varepsilon\,\frac{S-S^\dagger}{w}\right) + \cdots & \text{in } \mathcal{S} \end{cases} \tag{3.7}$$

for the components $m_j(S)$ of the internal moment ($1 \leqslant j \leqslant 3$),

$$m_j(S) = D\,\varepsilon \times \begin{cases} \overline{\mu}\,\left[\overline{m}_j\left(\frac{S-S^\dagger}{w}\right) + \varepsilon\,\overline{\overline{m}}_j\left(\frac{S-S^\dagger}{w}\right) + \cdots\right] & \text{in } \mathcal{I} \\ \widetilde{m}_j\left(\varepsilon\,\frac{S-S^\dagger}{w}\right) + \varepsilon\,\widetilde{\widetilde{m}}_j\left(\varepsilon\,\frac{S-S^\dagger}{w}\right) + \cdots & \text{in } \mathcal{S} \end{cases} \tag{3.8}$$

and for the constant internal force, see $(2.7)_1$,

$$\boldsymbol{n} = \frac{D\,\varepsilon^2}{w}\,\left(\overline{\boldsymbol{n}} + \varepsilon\,\overline{\overline{\boldsymbol{n}}} + \cdots\right) \quad \text{in both } \mathcal{I} \text{ and } \mathcal{S}. \tag{3.9}$$

We proceed to insert these expansions into the equations of the Wunderlich model and obtain the equations for the dominant contribution $(\overline{\omega}_j, \overline{\eta}, \ldots)$ in the inner region first (§4) and for the dominant contribution $(\widetilde{\omega}_j, \widetilde{\eta}, \ldots)$ in the outer region next (§6). In principle, the expansion procedure could be continued to higher orders in ε but this is beyond the scope of the paper.

4 Analysis of the layer

4.1 Bending and twisting moments are constant in the layer

A consequence of our scaling assumptions is that the bending and twisting moments are effectively constant in the inner layer as we now show.

Let us consider the balance of moments $(2.7)_2$ in the inner layer. The first term can be expressed as $\frac{\mathrm{d}\boldsymbol{m}}{\mathrm{d}S} = \frac{\mathrm{d}(m_i\,\boldsymbol{d}_i)}{\mathrm{d}S} = \frac{\mathrm{d}m_i}{\mathrm{d}S}\,\boldsymbol{d}_i + m_i\,\sum_{j=1}^{2}\omega_j\,\boldsymbol{d}_j\times\boldsymbol{d}_i$; using the inner expansions (3.5) and (3.8), we have $m_i\,\sum_{j=1}^{2}\omega_j\,\boldsymbol{d}_j\times\boldsymbol{d}_i = \mathcal{O}\left(D\,\varepsilon^2/w\right)$, which leaves us with

$$\frac{\mathrm{d}\boldsymbol{m}}{\mathrm{d}S} = \frac{D\,\varepsilon}{w}\,\frac{\mathrm{d}\overline{m}_j}{\mathrm{d}\overline{S}}(\overline{S}) + \mathcal{O}\left(\frac{D\,\varepsilon^2}{w}\right) \quad \text{in } \mathcal{I}.$$

The second term in $(2.7)_2$ can be estimated using (2.2) as $\boldsymbol{x}'\times\boldsymbol{n} = \mathcal{O}\left(D\,\varepsilon^2/w\right)$. The balance of moments $(2.7)_2$ in the inner layer therefore shows that the components $\overline{m}_j(\overline{S})$ of the internal moment are all constant at leading order $\frac{D\,\varepsilon}{w}$,

$$\frac{\mathrm{d}\overline{m}_j}{\mathrm{d}\overline{S}}(\overline{S}) = 0 \quad \text{in } \mathcal{I}. \tag{4.1}$$

The constant twisting moment in the inner layer is given by (3.8) as $m_3(S) = D\,\varepsilon\,\overline{\mu}\,\overline{m}_3 + \cdots$. The coefficient $\overline{\mu}$ has not yet been defined and we use this degree of freedom to set the constant value of $\overline{m}_3(\overline{S})$ in the inner layer to the arbitrary value $\overline{m}_3(\overline{S}) = 4$, chosen so as to simplify the forthcoming calculations. The other constant moment $\overline{m}_2(\overline{S})$ is sought in the form $\overline{m}_2(\overline{S}) \equiv 4\,\zeta$, where the constant ζ will be determined by solving the inner problem, see (4.11). To sum up, we set

$$\overline{m}_2(\overline{S}) = 4\,\zeta \quad \text{and} \quad \overline{m}_3(\overline{S}) = 4 \qquad \text{in } \mathcal{I}.$$

Inserting into the inner layer expansion (3.8), we have

$$\begin{array}{rcl} m_2(S) & = & D\,\varepsilon\times\left(4\,\overline{\mu}\,\zeta + \varepsilon\,\overline{\overline{m}}_2(\overline{S}) + \ldots\right) \\ m_3(S) & = & D\,\varepsilon\times\left(\ 4\,\overline{\mu}\ + \varepsilon\,\overline{\overline{m}}_3(\overline{S}) + \ldots\right) \end{array} \quad \text{in } \mathcal{I}. \tag{4.2}$$

4.2 Derivation of the layer equation

We proceed to derive inner layer equations by inserting the inner expansions from Section 3.2 into the equations of the Wunderlich model. By reading off these equations at dominant order, we obtain a set of equations for the dominant contributions $(\overline{\omega}_j, \overline{m}_j, \overline{\eta}, \ldots)$ of the inner solution, which we refer to as the *layer equations*.

As a preliminary step, we note that the argument $q = w\,\eta'(S)$ can be expressed in the inner layer using (3.7) as

$$q = w\,\eta'(S) = \overline{\eta}'(\overline{S}) + \mathcal{O}(\varepsilon) \quad \text{in } \mathcal{I}. \tag{4.3}$$

In our notation, the prime is a derivative with respect to the natural argument of the function, which is S for $\eta'(S) = \frac{\mathrm{d}\eta}{\mathrm{d}S}$ but $\overline{S}$ for $\overline{\eta}'(S) = \frac{\mathrm{d}\overline{\eta}}{\mathrm{d}\overline{S}}$.

Inserting the expansions (3.5), (3.7) and (4.2) into (2.15) and retaining the dominant terms in ε, we obtain

$$\overline{\omega}_2(\overline{S}) = \frac{\zeta + \overline{\eta}(\overline{S})}{F(\overline{\eta}'(\overline{S}))\,L(\overline{\eta}(\overline{S}))} \tag{4.4}$$

Next, we derive the expression of the Hamiltonian invariant in the inner layer, by inserting (3.5), (3.7), (4.4) and (3.9) into (2.16),

$$\mathcal{H}_{\mathrm{Wd}} = \frac{D\,\varepsilon^2}{w}\,\left(\boldsymbol{d}_3\cdot\overline{\boldsymbol{n}} + 4\,\overline{\mu}^2\,\frac{(\zeta+\overline{\eta}(\overline{S}))^2}{2\,L(\overline{\eta}(\overline{S}))\,H(\overline{\eta}'(\overline{S}))}\right) + \mathcal{O}(\epsilon^3), \tag{4.5}$$

where H is the auxiliary function

$$H(q) = \frac{F^2(q)}{F(q) + q\,F'(q)}. \tag{4.6}$$

H can be calculated using (2.11) as

$$H(q) = \frac{1}{4}\,\left(\frac{1}{(q/2)^2} - 1\right)\,\ln^2\left(\frac{1+\frac{q}{2}}{1-\frac{q}{2}}\right) \qquad (\text{for } |q|<2)\,. \tag{4.7}$$

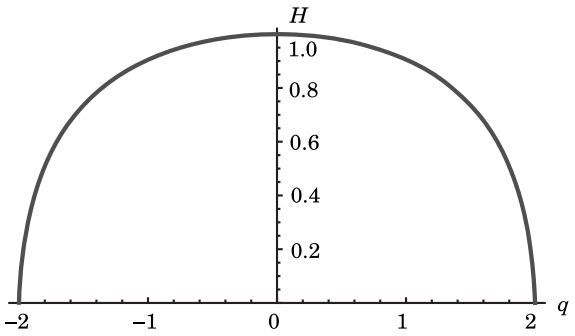

Figure 4: Auxiliary function $H(q)$ from Equation (4.7).

This function is plotted in Figure 4. It has a removable singularity at $q = 0$, where H can be continuously extended by setting

$$H(0) = 1. \tag{4.8}$$

In addition, we note that

$$H(q) > 0 \qquad \text{for } |q| < 2. \tag{4.9}$$

We return to Equation (4.5). The invariant $\mathcal{H}_{\mathrm{Wd}}$ on the left-hand side is constant, as shown in A.1. On the right-hand side, $\overline{\boldsymbol{n}}$ is constant by global equilibrium and $\boldsymbol{d}_3$ is constant to order $\mathcal{O}(\varepsilon^0)$ in the inner layer since its gradient is of order $|\omega_j| = \mathcal{O}(\varepsilon/w) \ll 1/w$. This shows that the fraction multiplying $4\,\overline{\mu}^2$ on the right-hand side of (4.5) is constant throughout the inner layer. Combining this observation with the definition of $L(\overline{\eta})$ in (2.10), we get

$$H(\overline{\eta}'(\overline{S})) = A \times \left(\frac{2\,(\overline{\eta}(\overline{S}) + \zeta)}{1 + \overline{\eta}^2(\overline{S})} \right)^2, \tag{4.10}$$

for some constant A. This result can also be obtained by directly integrating equations (2.13) and (2.14) to leading order in ε in the inner layer. Equation (4.10) is an implicit, first-order ordinary differential equation for $\overline{\eta}(\overline{S})$. The parameters A and ζ are undetermined on the right-hand side, ζ being the (scaled) constant value of $\overline{m}_2$ in the inner layer by $(4.2)_1$.

4.3 Selection of the constants A and ζ

The possible behaviours of the solutions $\overline{\eta}(\overline{S})$ to the differential equation (4.10) can be listed based on the phase portraits shown in Figure 5. By (4.10), the inner solution traces out a level curve of the function $H(\overline{\eta}')/\left(\frac{2\,(\overline{\eta}+\zeta)}{1+\overline{\eta}^2}\right)^2 = A$ when plotted in the phase plane $(\overline{\eta}, \overline{\eta}')$. The level curves of this function are plotted for the case $\zeta < 0$ in Figure 5a, and for the case $\zeta = 0$ in Figure 5b. The case $\zeta > 0$ can be obtained by reflecting Figure 5a about the vertical $\overline{\eta} = 0$ axis, see (4.10).

To allow matching with the outer solution, the inner solution $\overline{\eta}(\overline{S})$ must converge to two constants $\overline{\eta}^\star_\pm$ for $\overline{S} \to \pm\infty$, capturing the behaviour of the solution in the matching regions, see (3.3) and (3.6). Details on the matching procedure will be given in Section 5. In the phase portrait, these asymptotic limits appear as fixed points $(\overline{\eta}^\star_\pm, \overline{\eta}' = 0)$ located on the horizontal axis. In general, level curves of H can be approximated by a parabola when they cross the axis $\overline{\eta}' = 0$ (dashed curves and open circles in the figure), but X-shaped profiles are also encountered for special level curves, *i.e.*, for special values of A (solid, thick, coloured curves and solid disks in the figure). It can easily be shown that the traversal of the parabolic points involves a *finite* increment of $\overline{S}$, implying that these points cannot be attained asymptotically for $\overline{S} \to \pm\infty$.

We will therefore concentrate on X-shaped crossings (saddle points). It can be checked that the solution converges exponentially towards them as $\overline{S} \to \pm\infty$. For $\zeta \neq 0$, there are two such

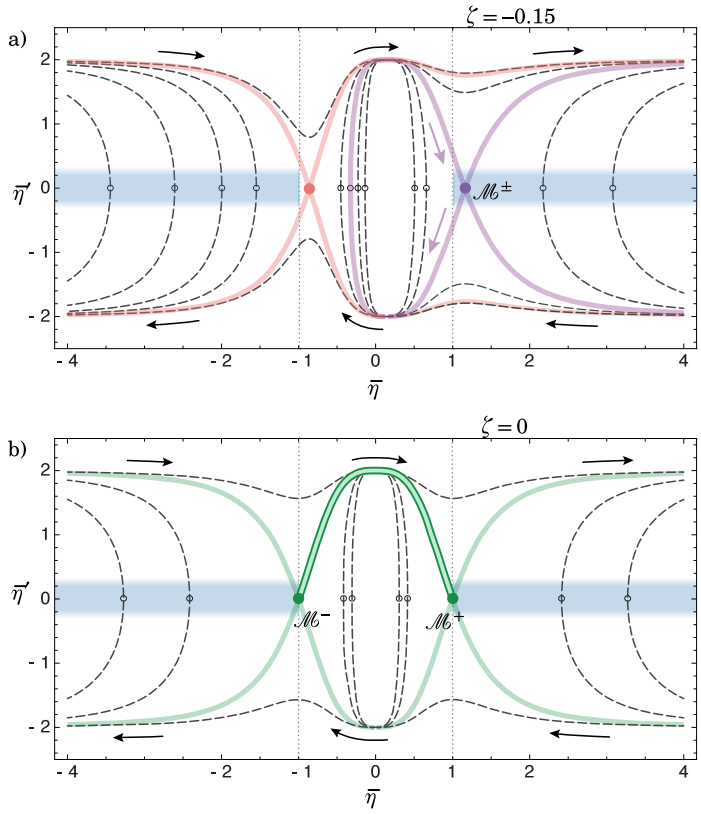

Figure 5: Phase portrait of the layer equation (4.10), obtained by plotting the level curves of $H(\overline{\eta}')/\left(2\,(\overline{\eta}+\zeta)/(1+\overline{\eta}^2)^2\right)$ in the $(\overline{\eta},\overline{\eta}')$ plane. (a) Case $\zeta \neq 0$, illustrated here by using the value $\zeta = -0.15$. The only solution connecting two X-shaped crossings is the purple homoclinic loop indicated by the two purple arrows. This homoclinic solution must however be discarded, as the point $\mathcal{M}^{\pm}$ that it attains asymptotically for $\overline{S} \to \pm\infty$ lies in the light blue region $|\overline{\eta}| > 1$ where the outer solution is expected to be unstable by the argument of Freddi et al. (2015), as detailed in C. (b) The case $\zeta = 0$ yields as valid inner layer solution the heteroclinic connection corresponding to the highlighted green contour, having $A = 1$ and analysed in Section 4.4. The inner solution obtained from this by a point symmetry about the origin of the coordinate axes is also valid and corresponds to a change in the orientation of the centreline.

crossing points, drawn in pink and purple in Figure 5a, and there is a single solution that attains a crossing point for both $\overline{S} \to -\infty$ and $\overline{S} \to +\infty$: this is the homoclinic solution following the closed loop in the purple level curve in Figure 5a, as shown by the pair of purple arrows. For this homoclinic solution, the asymptotic value $\overline{\eta}^\star_- = \overline{\eta}^\star_+$ of $\overline{\eta}(\overline{S})$ is identical in both matching regions ($S \to \pm\infty$), and a simple calculation shows that its absolute value is larger than 1, $|\overline{\eta}^\star_\pm| > 1$. As shown in C, the inequality $|\overline{\eta}^\star_\pm| > 1$ prevents this type of inner solution from matching with anything else but *unstable* outer solutions (this is shown graphically in Figure 5 by the fact that the purple dot at the centre of the X-shaped crossing lies inside the forbidden domain shown in a light shade of blue). Inner solutions with $\zeta < 0$ must therefore be discarded. Changing the sign of ζ corresponds to a mirror symmetry $\overline{\eta} \leftarrow -\overline{\eta}$ in the phase portrait in Figure 5a, so that inner solutions having $\zeta > 0$ can be discarded by a similar argument.

Having ruled out the case $\zeta \neq 0$, we proceed to analyse the case $\zeta = 0$. For $\zeta = 0$, there exists a heteroclinic orbit, shown by the highlighted green stroke in Figure 5b, which connects $\overline{\eta}^\star_- = -1$ for $\overline{S} \to -\infty$ (point labelled $\mathcal{M}^-$ in the figure) to $\overline{\eta}^\star_+ = +1$ for $\overline{S} \to +\infty$ (point labelled $\mathcal{M}^+$). The corresponding level curve is characterised by

$$\zeta = 0 \quad \text{and} \quad A = 1 \tag{4.11}$$

and the asymptotic limits are

$$\overline{\eta}(\overline{S}) \to \pm 1 \quad \text{for } \overline{S} \to \pm\infty. \tag{4.12}$$

Another solution is possible, corresponding to the heteroclinic orbit obtained by a point symmetry about the origin of the coordinate axes in the phase portrait. Its asymptotic limits (4.12) are swapped, *i.e.*, $\overline{\eta}(\overline{S}) \to \mp 1$ for $\overline{S} \to \pm\infty$. *In the following, we focus on the solution satisfying (4.12)*, keeping in mind that the other solution can be generated by reversing the orientation of the centreline, $\overline{S} \leftrightarrow -\overline{S}$.

Inserting (4.11) into (4.10), we obtain the final form of the first-order differential equation for the inner solution $\overline{\eta}(\overline{S})$ as

$$H(\overline{\eta}'(\overline{S})) = \left(\frac{2\,\overline{\eta}(\overline{S})}{1 + \overline{\eta}^2(\overline{S})} \right)^2 . \tag{4.13}$$

As the function H cannot be easily inverted, we will keep this differential equation in implicit form. Note that (4.13) is invariant under the symmetries $\eta \leftrightarrow -\eta$ and $\eta' \leftrightarrow -\eta'$.

In view of $(4.2)_1$, $\zeta = 0$ implies that the approximately constant bending moment $\overline{m}_2 = 4\,D\,\varepsilon\,\overline{\mu} \times 0 + \cdots$ in the inner layer is zero at leading order in ε.

4.4 Layer solution

The solution $\overline{\eta}(\overline{S})$ on the heteroclinic connection is unique up to a shift in the centreline coordinate $\overline{S}$. We lift this indeterminacy by defining the centre $\overline{S} = 0$ of the layer to be such that

$$\overline{\eta}(0) = 0. \tag{4.14}$$

In original variables, the centre of the layer $S^\dagger$ therefore satisfies $\eta(S^\dagger) = 0$.

The numerical solution $\overline{\eta}(\overline{S})$ of the differential equation (4.13) with initial condition (4.14) can be obtained by standard methods. We computed the solution in two different ways using Wolfram Mathematica (Inc.). In the first, we solved the implicit differential equation (4.13) directly with `NDSolve`. In the second, we tabulated the inverse function H^{-1} and rewrote the equation (4.13) in explicit form before calling `NDSolve`. Both methods give the same result up to numerical accuracy. They were used to generate the numerical results shown in this section. In yet another approach, the differential equation can be solved by inserting a central difference approximation for the derivative $\overline{\eta}'$: this approach was taken for the numerical results presented in Sections 7 and 8.

Having found $\overline{\eta}(\overline{S})$, one can then reconstruct the inner solution for the scaled bending and twisting strains $\overline{\omega}_j(\overline{S})$ using (4.4), (4.11) and (2.5) as

$$\begin{aligned} \overline{\omega}_2(\overline{S}) &= \frac{\overline{\eta}(\overline{S})}{F(\overline{\eta}'(\overline{S}))\left(\frac{1+\overline{\eta}^2(\overline{S})}{2}\right)^2} \\ \overline{\omega}_3(\overline{S}) &= \overline{\eta}(\overline{S})\,\overline{\omega}_2(\overline{S}). \end{aligned} \tag{4.15}$$

The original, non-scaled quantities are found by inserting these expressions into (3.5–3.7).

In terms of the inner solution (4.13–4.15), we also define the numerical constant

$$c = \left(\int_{-\infty}^{+\infty} (\overline{\omega}_3(\overline{S}) - 1) \, \mathrm{d}\overline{S} \right)^{-1}, \tag{4.16}$$

which will prove to be of particular interest for the matching problem. The convergence of the indefinite integral on the right-hand side is ensured by the estimate $|\overline{\omega}_3(\overline{S}) - 1| = \mathcal{O}\left(\exp(-2\sqrt{3}|\overline{S}|)\right)$ for $|\overline{S}| \gg 1$, which can be established by combining the differential equation (4.13) with the expansion $H(q) = 1 - \frac{q^2}{12} + \mathcal{O}(q^4)$. By evaluating the right-hand side of equation (4.16) numerically, we find

$$c = -1.642. \tag{4.17}$$

4.5 Graphical representation of the inner solution

The inner layer solutions $\overline{\eta}(\overline{S})$ and $\overline{\omega}_2(\overline{S})$ are universal, *i.e.*, they do not depend on any parameter. They are plotted in Figure 6a. In Figure 6b the inner layer solution is visualised as a path in the $(\overline{\omega}_2, \overline{\omega}_3)$ plane. In the limit $\overline{S} \to \pm\infty$, $\overline{\eta} \to \pm 1$ by (4.12) and $F(\overline{\eta}'(\overline{S})) \to F(0) = 1$ by (2.12), which yield the asymptotic behaviour of the inner solution as

$$\overline{\omega}_j(\overline{S}) \to \sigma_j^{\pm} \quad \text{for } \overline{S} \to \pm\infty, \quad \text{where } \sigma_j^{\pm} = \begin{cases} \pm 1 & \text{if } j = 2 \\ +1 & \text{if } j = 3. \end{cases} \tag{4.18}$$

This is in agreement with the asymptotes in Figure 6a, and with the end points $(\overline{\omega}_2, \overline{\omega}_3) = (\sigma_2^{\pm}, \sigma_3^{\pm}) = (\pm 1, +1)$ representing the matching regions $\mathcal{M}^{\pm}$, which are attained in the limit $\overline{S} \to \pm\infty$ in Figure 6b.

In Figure 6c, the inner layer predictions for the generators are shown in the planar development $(\overline{x}, \overline{y}) = (x/w, y/w)$ of the ribbon. The equation of the generator emanating from the point with coordinate $\overline{S}$ on the centreline is, by (2.4),

$$\overline{x} = \overline{S} + \overline{\eta}(\overline{S})\, \overline{y}. \tag{4.19}$$

The generators can be extended beyond the lateral edges $\overline{y} = \pm\frac{1}{2}$ and we define the caustic $\mathcal{C}$ as their envelope: differentiating (4.19) with respect to $\overline{S}$, one obtains the parametric equation of the caustic as

$$\overline{x}_{\mathcal{C}}(\overline{S}) = \overline{S} - \frac{\overline{\eta}(\overline{S})}{\overline{\eta}'(\overline{S})}, \qquad \overline{y}_{\mathcal{C}}(\overline{S}) = -\frac{1}{\overline{\eta}'(\overline{S})}. \tag{4.20}$$

The caustic is shown as the orange curve in Figure 6c. At the centre of the layer, $\overline{S} = 0$, $\overline{\eta}(0) = 0$ and $\overline{\eta}'(0) = 2$, so that $(\overline{x}_{\mathcal{C}}(0), \overline{y}_{\mathcal{C}}(0)) = (0, -1/2)$: at this point C, the tip of the caustic makes contact with the ribbon. The generators emanating from the region surrounding the centre $\overline{S} = 0$ *almost* converge to the point of contact C, implying that the centre of the layer resembles a cone. In B, the expansion of $\overline{\eta}(\overline{S})$ near $\overline{S} \approx 0$ is derived and it is found to be weakly singular. This weak singularity accounts for the pointed shape of the caustic at its tip, for the layout of the generators in the inner layer, as well as for the cone-like shape of the ribbon in this layer.

The mean curvature $\kappa(\overline{x}, \overline{y})$ of the mid-surface of the ribbon can be reconstructed in terms of the centreline using the inextensibility condition, and is given by $\kappa(\overline{x}, \overline{y}) = -\omega_2(\overline{x}, \overline{y}) \, \frac{1+\overline{\eta}^2(\overline{S}(\overline{x},\overline{y}))}{2\left(1+\overline{y}\,\overline{\eta}'(\overline{S}(\overline{x},\overline{y}))\right)}$; see for instance Equation (2) in Starostin and van der Heijden (2015). Here, $\overline{S}(\overline{x}, \overline{y})$ denotes the arclength parameter of the generator passing through the point $(\overline{x}, \overline{y})$, as obtained from (4.19). The mean curvature can be written as $\kappa(\overline{x}, \overline{y}) = \frac{\varepsilon\,\overline{\mu}}{w}\, \overline{\kappa}(\overline{x}, \overline{y})$ where

$$\overline{\kappa}(\overline{x}, \overline{y}) = -\overline{\omega}_2(\overline{x}, \overline{y}) \, \frac{1 + \overline{\eta}^2(\overline{S}(\overline{x}, \overline{y}))}{2\,\left(1 + \overline{y}\,\overline{\eta}'(\overline{S}(\overline{x}, \overline{y}))\right)}. \tag{4.21}$$

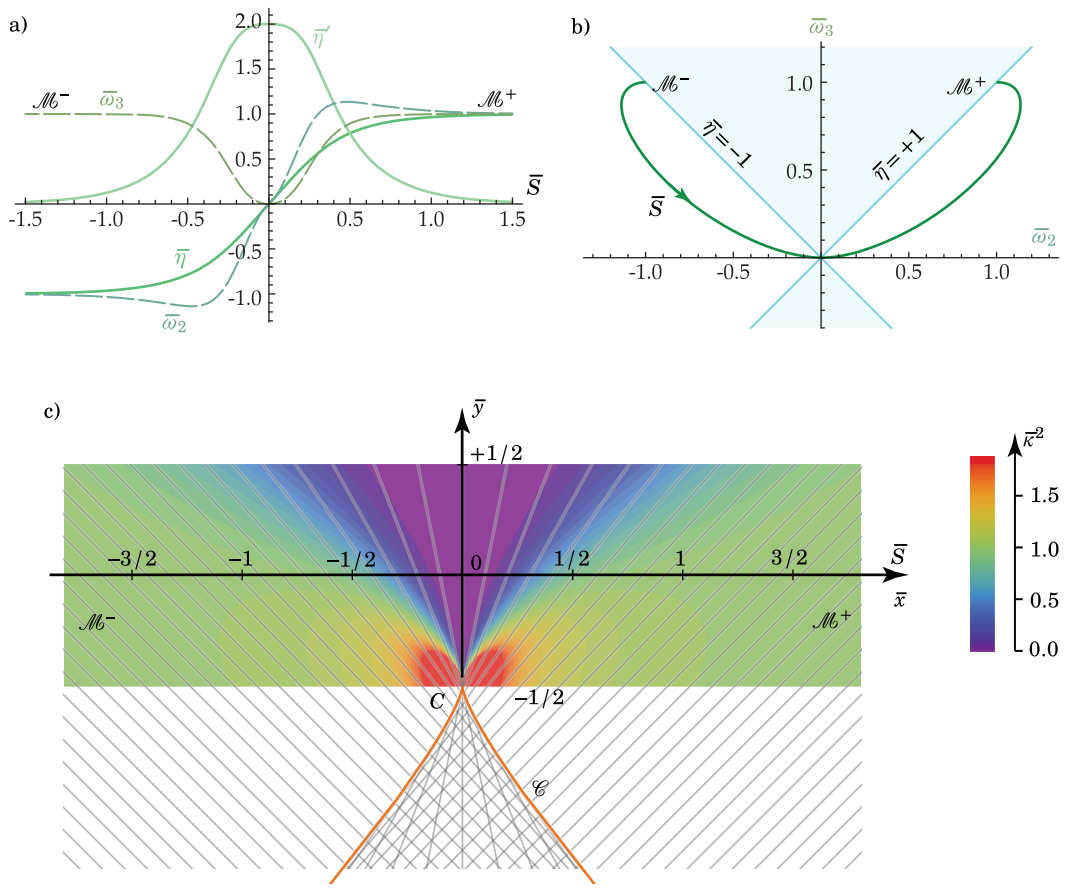

Figure 6: Inner solution obtained by integrating the differential equation (4.13–4.14) for $\overline{\eta}(\overline{S})$ numerically and by reconstructing the scaled bending and twisting strains $\overline{\omega}_j(\overline{S})$ using (4.15). The inner solution corresponds to the heteroclinic solution highlighted in green in the phase portrait in Figure 5b. (a) Plot of the inner solution. (b) Representation of the inner solution as a path in the $(\overline{\omega}_2, \overline{\omega}_3)$ plane: the path connects the points $\mathcal{M}^{\pm}$ representing the matching regions; the light blue region, defined by $|\overline{\eta}| = \left|\frac{\overline{\omega}_3}{\overline{\omega}_2}\right| > 1$, is where the Sadowsky functional is non-convex (Freddi et al., 2015). (c) Generators (grey lines) and distribution of bending energy (colours) shown in the planar development $(\overline{x}, \overline{y}) = (x/w, y/w)$ of the ribbon, from (4.19) and (4.21). The generators define a caustic $\mathcal{C}$ (orange curve), see (4.20), whose tip C makes contact with the lower edge of the ribbon. At C the mid-surface mean curvature $\overline{\kappa}$ is unbounded.

The *squared*, scaled mean curvature $\overline{\kappa}^2$ is shown as a colour map in Figure 6c; this quantity has been scaled in such a way that $\overline{\kappa}(\overline{x},\overline{y}) \to \pm 1$ in the matching regions, shown as the green areas away from the centre of the layer in the figure. The quantity $\overline{\kappa}^2$ is also proportional to the density of the bending energy per unit area in the two-dimensional plate energy underlying the one-dimensional Wunderlich functional $\mathcal{E}_{\mathrm{Wd}}$ (2.9). This bending energy *density* is unbounded in the vicinity of the point C with coordinates $(\overline{x},\overline{y}) = (0,-1/2)$ where the caustic makes contact with the ribbon; it is however integrable, as shown in B, so that the bending energy of the inner layer is *finite*.

5 Matching

We have just derived the inner solution, valid in the inner domain $\mathcal{I}$ (green region in Figure 7a). The outer solution, valid in the outer region $\mathcal{S}$ (blue regions), will be derived in the following section. They must be matched in the matching regions $\mathcal{M}^{\pm}$, attained by taking the limit $|\overline{S}| \gg 1$ from the inner solution or the limit $|\widetilde{S}| \ll 1$ from the outer solution, see Figure 7a and Equations (3.3) and (3.6). The matching procedure is carried out in the present section. Starting from the standard form of the matching conditions, see (5.2) below, we derive effective jump conditions for the outer solution, see (5.6). This approach is not standard. The jump conditions replace the inner layer by an equivalent point-like singularity, thereby hiding effectively the unimportant details of the inner solution.

5.1 Strategy: enforcing matching through jump conditions

Given a generic quantity f, we denote its inner and outer expansions as $f_{\mathrm{in}}(\overline{S})$ and $f_{\mathrm{out}}(\widetilde{S})$, respectively. The expansions in (3.5–3.8) are of the form

$$f(S) = \begin{cases} f_{\mathrm{in}}\left(\frac{S-S^\dagger}{w}\right) & \text{in } \mathcal{I} \\ f_{\mathrm{out}}\left(\varepsilon\,\frac{S-S^\dagger}{w}\right) & \text{in } \mathcal{S}. \end{cases} \tag{5.1}$$

When $f = \omega_2$ represents the bending strain, for instance, we can identify the inner and outer expansions from (3.5) as $\omega_2^{\mathrm{in}}(S) = \frac{\varepsilon}{w}\,\overline{\mu}\left(\overline{\omega}_2(\overline{S}) + \varepsilon\,\overline{\overline{\omega}}_2(\overline{S}) + \cdots\right)$ and $\omega_3^{\mathrm{out}}(\widetilde{S}) = \frac{\varepsilon}{w}\left(\widetilde{\omega}_2(\widetilde{S}) + \varepsilon\,\widetilde{\widetilde{\omega}}_2(\widetilde{S}) + \cdots\right)$, respectively. Both f_{in} and f_{out} are defined as *infinite* series in ε. The equal sign in (5.1) means that these infinite series converge to $f(S)$ in the domains $\mathcal{I}$ and $\mathcal{S}$, respectively, where they are assumed to converge. This formal notation is convenient but we will not attempt to compute these series beyond the leading orders.

In the matching regions $\mathcal{M}^{\pm}$ defined by (3.3), both expansions should be equivalent,

$$f_{\mathrm{out}}\left(\varepsilon\,\frac{S-S^\dagger}{w}\right) = f_{\mathrm{in}}\left(\frac{S-S^\dagger}{w}\right) \quad \text{for } 1 \ll \pm\left(\frac{S-S^\dagger}{w}\right) \ll \frac{1}{\varepsilon}. \tag{5.2}$$

This is the standard form of the matching conditions used in matched asymptotic analysis.

The function $f_{\mathrm{out}}(\widetilde{S})$ appearing in (5.2) is undefined in the core of the inner region, for $|\widetilde{S}| = \varepsilon\left|\frac{S-S^\dagger}{w}\right| \ll \varepsilon$, as sketched by the dotted part of the curve in Figure 7a. We can however *extend* this function smoothly on both sides of $\widetilde{S} = 0$. The result is a function f_{out} that is discontinuous at $\widetilde{S} = 0$, see Figure 7b. We denote as $[\![f_{\mathrm{out}}]\!] = f_{\mathrm{out}}(0^+) - f_{\mathrm{out}}(0^-)$ the apparent jump in f_{out}. The *'apparent'* qualifier emphasises that this jump is an artefact introduced by extending f_{out} inside the inner region.

Using the explicit inner solution from Section 4, one can obtain the asymptotic expansion of $f_{\mathrm{in}}(\overline{S})$ for $\overline{S} \to \pm\infty$ for various quantities f in the form

$$f_{\mathrm{in}}(\overline{S}) = \varepsilon\left(\alpha_\pm^{[2]}\,\overline{S}^2 + \alpha_\pm^{[1]}\,\overline{S} + \alpha_\pm^{[0]} + \frac{\alpha_\pm^{[-1]}}{\overline{S}} + \ldots\right) + \varepsilon^2\,(\ldots) \qquad \text{for } \overline{S} \to \pm\infty, \tag{5.3}$$

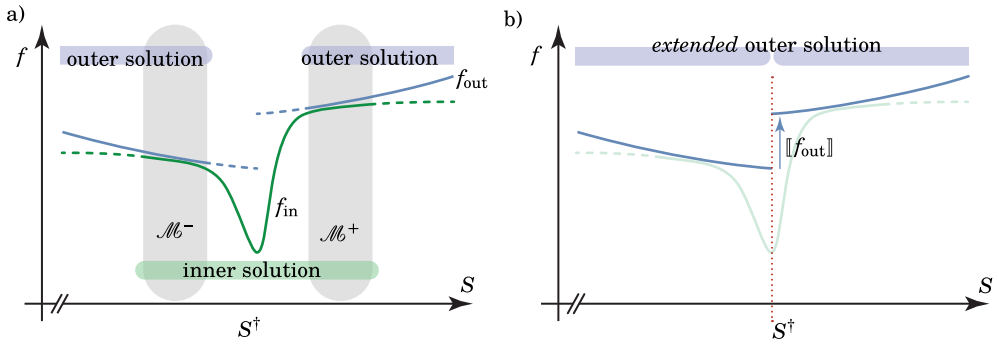

Figure 7: Derivation of a jump condition for the outer solution, expressing the matching condition with the inner solution. (a) Matched asymptotic solution of the Wunderlich model: inner expansion f_{in} (green) and outer expansion f_{out} (blue). Both solutions agree in the matching regions $\mathcal{M}^\pm$ (grey background). (b) By extending mathematically the outer solution f_{out} into the inner region, one obtains an apparent discontinuity $[\![f_{\text{out}}]\!]$, see Equations (5.3) and (5.6) in Section 5.1.

where the expansion coefficients $\alpha_\pm^{[i]}$ can be obtained from the layer solution $\overline{f}(\overline{S})$ and the final ellipsis stands for the inner layer solution to higher-order $\overline{\overline{f}}(\overline{S})$. The smallest powers in ε and in $\overline{S}$ have been arbitrarily chosen as ε^1 and $\overline{S}^2$ in (5.3), respectively, but these values may vary depending on the quantity f of interest.

In view of the matching condition (5.2), one can substitute $f_{\text{in}}(\overline{S})$ with $f_{\text{out}}(\widetilde{S})$ where $\widetilde{S} = \varepsilon\,\overline{S}$ on the left-hand side,

$$\begin{aligned} f_{\text{out}}(\widetilde{S}) &= \varepsilon\left(\alpha_\pm^{[2]}\left(\frac{\widetilde{S}}{\varepsilon}\right)^2 + \alpha_\pm^{[1]}\frac{\widetilde{S}}{\varepsilon} + \alpha_\pm^{[0]} + \dots\right) + \varepsilon^2(\dots) \\ &= \left(\frac{\alpha_\pm^{[2]}}{\varepsilon} + \cdots\right)\widetilde{S}^2 + (\alpha_\pm^{[1]} + \cdots)\,\widetilde{S} + \left(\varepsilon\,\alpha_\pm^{[0]} + \cdots\right) + \cdots \end{aligned} \tag{5.4}$$

This expansion holds for $\varepsilon \ll |\widetilde{S}| \ll 1$, see (5.2). Having extended the function f_{out} smoothly on both sides of the discontinuity at $\widetilde{S} = 0$, we can however relax the condition $\varepsilon \ll |\widetilde{S}|$, so that (5.4) ultimately applies to both intervals $|\widetilde{S}| \ll 1$ adjacent to the singularity $\widetilde{S} = 0$. Note that the sign $\pm$ in (5.4) denotes the sign of $\widetilde{S}$.

Taking the limit $\widetilde{S} \to 0^\pm$ in (5.4), we have in particular

$$f_{\text{out}}(\widetilde{S}) \to \varepsilon\,\alpha_\pm^{[0]} + \cdots \quad \text{for } \widetilde{S} \to 0^\pm. \tag{5.5}$$

Note that this limit would be meaningless if f_{out} had not been extended to $\widetilde{S} = 0^\pm$. The apparent jump in f_{out} can be obtained from (5.5) as

$$[\![f_{\text{out}}]\!] = \varepsilon\,(\alpha_+^{[0]} - \alpha_-^{[0]}) + \cdots, \tag{5.6}$$

where the ellipsis stands for higher-order terms. A graphical summary of the above argument, leading to the effective jump condition (5.6), is proposed in Figure 7.

For the various physical quantities f, the right-hand side $\varepsilon\,(\alpha_+^{[0]} - \alpha_-^{[0]})$ of (5.6) can be computed by expanding the inner solution obtained in Section 4 for large $|\overline{S}|$, see (5.3). In what follows, we will enforce the matching conditions in the form (5.6) rather than in the standard form (5.2). The benefit is that, by extending the outer solution right up to the singularity, we obtain a solution that is defined on the full domain and gives a coarse-grained description of the inner layer by means of simple jump conditions.

5.2 Explicit form of the jump conditions

The abstract matching procedure described above is applied in D to various concrete physical quantities f. The results can be summarised as follows.

- We start with $\boldsymbol{f} = (f_2, f_3)$, where f_2 is the bending angle and f_3 is the twisting angle, both being measured with respect to the director frame $\boldsymbol{d}_i(S^\dagger)$ at the centre of the layer. The argument in D.1 yields the apparent jump condition for the directors in the form

$$\begin{pmatrix} \boldsymbol{d}_1^{\mathrm{out}}(0^+) \\ \boldsymbol{d}_2^{\mathrm{out}}(0^+) \\ \boldsymbol{d}_3^{\mathrm{out}}(0^+) \end{pmatrix} = \begin{pmatrix} +\cos\varphi\, \boldsymbol{d}_1^{\mathrm{out}}(0^-) + \sin\varphi\, \boldsymbol{d}_2^{\mathrm{out}}(0^-) \\ -\sin\varphi\, \boldsymbol{d}_1^{\mathrm{out}}(0^-) + \cos\varphi\, \boldsymbol{d}_2^{\mathrm{out}}(0^-) \\ \boldsymbol{d}_3^{\mathrm{out}}(0^-) \end{pmatrix} + \mathcal{O}(\varepsilon^2), \tag{5.7}$$

  where $\varphi = \mathcal{O}(\varepsilon)$ in a small apparent discontinuity in the twist angle,

$$\varphi = \frac{\varepsilon\, \overline{\mu}}{c} + \mathcal{O}(\varepsilon^2). \tag{5.8}$$

  Note that the tangent director $\boldsymbol{d}_3^{\mathrm{out}}(S)$ in $(5.7)_3$ is continuous at this order. The constant $c = -1.642$ appearing in (5.8) was introduced in (4.16–4.17).

- Setting $\boldsymbol{f}(S) = \boldsymbol{x}(S) - \big(\boldsymbol{x}(S^\dagger) + S\, \boldsymbol{d}_3(S^\dagger)\big)$, we find that the apparent discontinuity in the centreline is small,

$$[\![\boldsymbol{x}_{\mathrm{out}}]\!] = \boldsymbol{0} \times w + \mathcal{O}\left(w\, \varepsilon\right), \tag{5.9}$$

  see Equation (D.11) in D.2. This small discontinuity is negligible in a sense that will be made precise later on.

- On setting $f = \frac{D\, w}{2} \int_{S^\dagger}^{S} 4\, F\left(w\, \eta'\right) \omega_2^2 \left(\frac{1+\eta^2}{2}\right)^2 \mathrm{d}S'$, we derive the apparent jump of the strain energy (2.9) of the Wunderlich model as

$$[\![\mathcal{E}_{\mathrm{Wd,out}}]\!] = \frac{4\, D\, c}{2}\, \varphi^2 + \mathcal{O}\left(D\, \varepsilon^3\right), \tag{5.10}$$

  see Equation (D.12) in D.3. The right-hand side $\frac{4\, D\, c}{2}\, \varphi^2 + \cdots$ is a point-like contribution to the strain energy representing the inner layer, see (6.9).

Additional continuity conditions can be derived as follows.

- By the balance of forces $(2.7)_1$, the internal force $\boldsymbol{n}$ is constant, hence the obvious condition

$$[\![\boldsymbol{n}_{\mathrm{out}}]\!] = \boldsymbol{0}. \tag{5.11}$$

- Integrating the balance of moments $(2.7)_2$, we find that $\boldsymbol{m}(S) + \boldsymbol{x}(S) \times \boldsymbol{n}$ is an invariant of the solutions of the Wunderlich model. Across the singularity, we therefore have $[\![\boldsymbol{m}_{\mathrm{out}}]\!] = -\,[\![\boldsymbol{x}_{\mathrm{out}}]\!] \times \boldsymbol{n}$. Using the estimates $(3.4)_4$ for $\boldsymbol{n}$ and (5.9) for $[\![\boldsymbol{x}_{\mathrm{out}}]\!]$, we get

$$[\![\boldsymbol{m}_{\mathrm{out}}]\!] = \boldsymbol{0} \times D\, \varepsilon^2 + \mathcal{O}\left(D\, \varepsilon^3\right). \tag{5.12}$$

- Since the tangent $\boldsymbol{d}_3^{\mathrm{out}}$ is continuous at dominant order by $(5.7)_3$, the continuity condition for $\boldsymbol{m}_{\mathrm{out}}$ at dominant order in (5.12) implies a similar condition for the twisting moment $m_3 = \boldsymbol{m} \cdot \boldsymbol{d}_3$, namely

$$[\![m_3^{\mathrm{out}}]\!] = 0 \times D\, \varepsilon^2 + \mathcal{O}\left(D\, \varepsilon^3\right). \tag{5.13}$$

- Finally, we consider the Hamiltonian invariant $\mathcal{H}_{\mathrm{Wd}}$ of the Wunderlich model from Equation (2.16). As shown in A.1, we have $\mathcal{H}_{\mathrm{Wd}}(S_1) = \mathcal{H}_{\mathrm{Wd}}(S_2)$ for any pair of points (S_1, S_2) and any equilibrium solution. Taking S_1 and S_2 to be in the matching regions $\mathcal{M}^-$ and $\mathcal{M}^+$, respectively, inserting the outer expansion f_{out} (5.1) into the expression (2.16) of $\mathcal{H}_{\mathrm{Wd}}$ and

denoting the result as $\mathcal{H}_{\rm Wd}^{\rm out}$, we have $\mathcal{H}_{\rm Wd}^{\rm out}(S_1) = \mathcal{H}_{\rm Wd}^{\rm out}(S_2)$ for $w \ll -(S_1 - S^\dagger) \ll w/\varepsilon$ and $w \ll +(S_2 - S^\dagger) \ll w/\varepsilon$. Using the smooth extrapolations of the outer solution to $(S^\dagger)_-$ and $(S^\dagger)_+$, we can relax the conditions $w \ll -(S_1 - S^\dagger)$ and $w \ll +(S_2 - S^\dagger)$ as earlier, and take the limits $S_1 \to (S^\dagger)_-$ and $S_2 \to (S^\dagger)_+$ on both sides of the apparent singularity: we conclude that the Hamiltonian invariant has no apparent discontinuity,

$$\big[\!\big[\mathcal{H}_{\rm Wd}^{\rm out}\big]\!\big] = 0. \tag{5.14}$$

In the above reasoning, the equation $\mathcal{H}_{\rm Wd}^{\rm out}(S_1) = \mathcal{H}_{\rm Wd}^{\rm out}(S_2)$ is valid for arbitrary values of ε and not just for $\varepsilon \to 0$. The left-hand side in (5.14) is therefore zero at all orders in ε, as implied by the absence of an error term in this equation. In E, we will use this equality at the leading orders 1 and ε only, *i.e.*, we will only make use of $[\![\mathcal{H}_{\rm Wd}^{\rm out}]\!] = \mathcal{O}(\varepsilon^2)$.

In this section we have used our knowledge of the inner solution to derive the jump conditions satisfied by the outer solution. They will be used in Section 6 to set up a complete set of equations for the outer solution. Before that, we make a small digression and derive a convenient, alternative form of the matched asymptotic solution called the composite representation.

5.3 Composite representation of the asymptotic expansion

In terms of the 4 signs $\sigma_j^\pm = \lim_{\overline{S}\to\pm\infty} \overline{\omega}_j(\overline{S})$ introduced in (4.18), one can rewrite the matching condition for the inner and outer expansions in (3.5) as $\omega_j^{\rm out}(0^\pm) = \lim_{\overline{S}\to\pm\infty} \omega_j^{\rm in}(\overline{S}) = \frac{\varepsilon\,\overline{\mu}}{w} \lim_{\overline{S}\to\pm\infty} \overline{\omega}_j(\overline{S}) = \frac{\varepsilon\,\overline{\mu}}{w}\,\sigma_j^\pm$. Given that $|\sigma_j^\pm| = 1$, this can be inverted as $\frac{\varepsilon\,\overline{\mu}}{w} = \sigma_j^\pm\,\omega_j^{\rm out}(0^\pm)$. The inner expansion can then be rewritten as $\omega_j^{\rm in}(\overline{S}) = \frac{\varepsilon\,\overline{\mu}}{w}\,\overline{\omega}_j(\overline{S}) = \sigma_j^\pm\,\omega_j^{\rm out}(0^\pm)\,\overline{\omega}_j(\overline{S})$, and the expansions (3.5) can be rewritten as

$$\omega_j(S) = \begin{cases} \sigma_j^\pm\,\omega_j^{\rm out}(0^\pm)\,\overline{\omega}_j(\overline{S}) + \cdots & \text{in } \mathcal{I} \\ \omega_j^{\rm out}(\widetilde{S}) + \cdots & \text{in } \mathcal{S}. \end{cases} \tag{5.15}$$

We claim that this expression is asymptotically equivalent to

$$\omega_j(S) = \sigma_j^{\mathrm{sign}(S-S^\dagger)}\,\omega_j^{\rm out}\left(\varepsilon\,\frac{S-S^\dagger}{w}\right)\,\overline{\omega}_j\left(\frac{S-S^\dagger}{w}\right) + \cdots \quad \text{in } \mathcal{I}\cup\mathcal{S}, \tag{5.16}$$

which we refer to as the *composite form* of the matched asymptotic solution. Note that the fast and slow variables $\overline{S}$ and $\widetilde{S}$ have been replaced by their expressions (3.6).

The equivalence of (5.15) and (5.16) is illustrated in Figure 8, and is established as follows:

- In the inner region, that is for fixed $\overline{S} = \frac{S-S^\dagger}{w}$ and for $\widetilde{S} = \varepsilon\,\frac{S-S^\dagger}{w} \to 0^{(\mathrm{sign}\,\overline{S})}$, the right-hand side in (5.16) can be expanded as $\omega_j(S) = \sigma_j^{\mathrm{sign}\,\overline{S}}\,\omega_j^{\rm out}(0^{(\mathrm{sign}\,\overline{S})})\,\overline{\omega}_j(\overline{S}) + \cdots$, which is nothing but the inner expansion in (5.15). Incidentally, this shows that the composite approximation (5.16) is smooth at $S = S^\dagger$, like the inner solution: for $j = 2$ both factors $\omega_j^{\rm out}$ and $\sigma_j^{\mathrm{sign}(S-S^\dagger)}$ flip sign at $S = S^\dagger$, as can be checked, while for $j = 3$ both functions are smooth.
- Similarly, in the outer region, that is for fixed $\widetilde{S} = \varepsilon\,\frac{S-S^\dagger}{w}$ and with $\overline{S} = \frac{S-S^\dagger}{w} \to (\mathrm{sign}\,\widetilde{S})\times\infty$, Equation (5.16) yields, with the help of (4.18), $\omega_j(S) = \sigma_j^{\mathrm{sign}\,\widetilde{S}}\,\omega_j^{\rm out}(\widetilde{S})\,\sigma_j^{\mathrm{sign}\,\widetilde{S}} + \cdots$, which can be further simplified as $\omega_j(S) = \omega_j^{\rm out}(\widetilde{S}) + \cdots$ since $|\sigma_j| = 1$: this is nothing but the outer expansion in (5.15).

By a similar argument, one can combine the discontinuous directors $\boldsymbol{d}_j^{\rm out}(S)$ in (5.7) with the inner solution to produce a uniform and smooth approximation of the directors,

$$\begin{array}{rcl} \boldsymbol{d}_1(S) &=& +\cos\psi(S)\,\boldsymbol{d}_1^{\rm out}(S) + \sin\psi(S)\,\boldsymbol{d}_2^{\rm out}(S) \\ \boldsymbol{d}_2(S) &=& -\sin\psi(S)\,\boldsymbol{d}_1^{\rm out}(S) + \cos\psi(S)\,\boldsymbol{d}_2^{\rm out}(S) \\ \boldsymbol{d}_3(S) &=& \boldsymbol{d}_3^{\rm out}(S), \end{array} \tag{5.17}$$

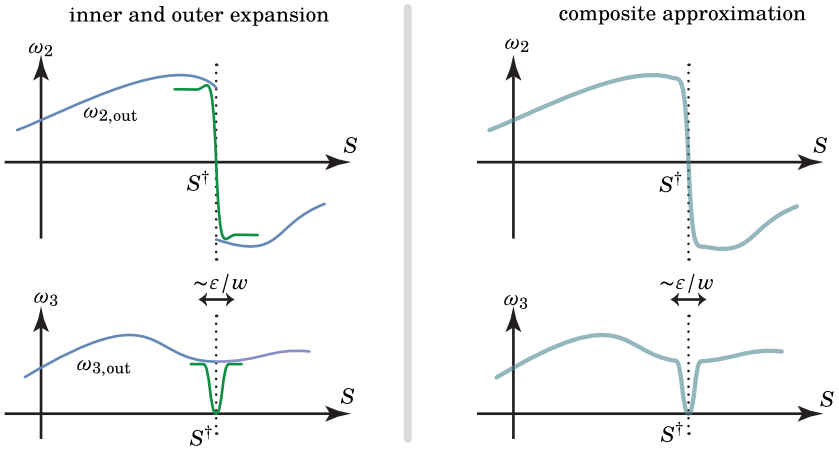

Figure 8: The inner and outer expansions (3.5) for ω_j (left) can be reformulated as a composite approximation (5.16) (right), both being asymptotically equivalent. While the matched inner and outer expansions are continuous in the limit $\varepsilon \to 0$ only, the composite approximation is smooth for arbitrary values of ε by construction.

where

$$\begin{aligned} \psi(S) &= \varepsilon\,\overline{\mu}\,\Psi\left(\tfrac{S-S^\dagger}{w}\right) - \tfrac{\varphi}{2}\,\operatorname{sign}(S-S^\dagger) \\ \Psi(\overline{S}) &= \textstyle\int_0^{\overline{S}} (\overline{\omega}_3(\overline{S}') - 1)\,\mathrm{d}\overline{S}'. \end{aligned} \tag{5.18}$$

A jump $[\![\psi]\!]'(S^\dagger) = -\varphi$ has been purposely introduced in $(5.18)_1$ to compensate the apparent discontinuity in the twisting angle of the frame $\boldsymbol{d}_i^{\text{out}}$, see (5.7); as a result, the director frame defined by (5.17) is smooth. In addition, its twisting strain $\boldsymbol{d}_1'(S)\cdot\boldsymbol{d}_2(S) = \omega_3^{\text{out}}(S) + \psi'(S)$ is designed to match both the inner and outer expansions of ω_3 in (3.5).

We will refer to (5.16) and to (5.17–5.18) as the composite approximations of the strains and of the directors, respectively. While being asymptotically equivalent to the original expansions from Section 3.2, the composite approximations offer the advantage of being smooth for arbitrary values of ε and not just in the limit $\varepsilon \to 0$, as sketched in Figure 8. When we compare the predictions of the matched asymptotic expansion to the original Wunderlich model later on, we will often use the composite representation of the former.

6 Outer problem

The last steps in our matched asymptotic expansion are (i) to set up a complete set of equations for the outer solution and (ii) to solve them. Task (i) is the topic of this section, while task (ii) will be illustrated in Sections 7 and 8 for specific ribbon geometries.

6.1 Second-order approximation of the outer solution

The task (i) involves two sub-steps:

- Inserting the outer expansions $f(S) = f_{\text{out}}(\overline{S})$ listed in (3.5–3.9) into the Wunderlich model: as the outer solution f_{out} depends on S through the slow variable $\overline{S} = \frac{S-S^\dagger}{w/\varepsilon}$, the outer solution is effectively governed by the *Sadowsky model* to the two leading orders in ε, as we will show.
- Applying the jump conditions from Section 5.2, which account for the inner layer in an effective way.

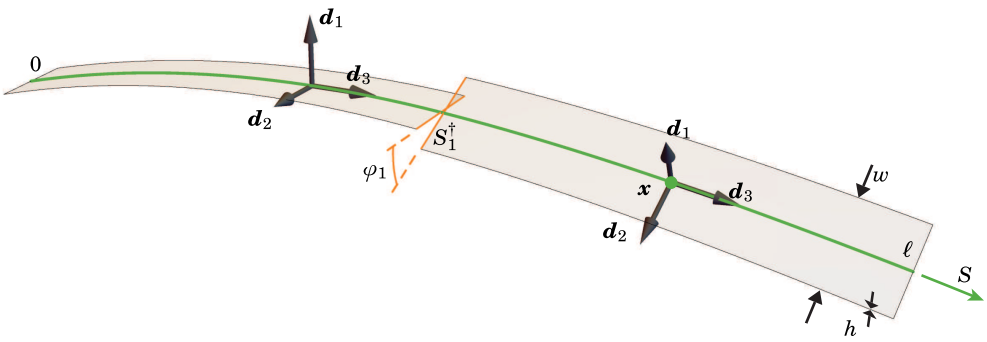

Figure 9: The outer solution features points of discontinuity representing the inner layer in an effective manner, where the twisting angle jumps by an amount φ_J. Here, a single discontinuity is shown ($N = 1$).

The outer solution f_{out} is an infinite series expansion in ε. Our goal is to determine the two leading terms, of order 1 and ε. Specifically, we propose in Section 6.2 a one-dimensional differential problem (or more accurately a boundary-value problem for an ordinary differential equation with finitely many discontinuities and associated jump conditions) whose solution $f^\star$ is a second-order approximation of the infinite series f_{out},

$$f^\star(S) = f_{\text{out}}(S) + \mathcal{O}\left(\varepsilon^2 f\right). \tag{6.1}$$

In (6.1), f denotes a generic unknown, such as $\boldsymbol{x}$, $\boldsymbol{d}_i$, ω_i, and $\mathcal{O}\left(\varepsilon^2 f\right)$ stands for an error term that is ε^2 smaller than the natural orders of magnitude listed in (3.4), namely

$$\boldsymbol{x} = \mathcal{O}\left(w/\varepsilon\right), \quad \boldsymbol{d}_i = \mathcal{O}(1), \quad \omega_j = \mathcal{O}\left(\varepsilon/w\right), \quad \eta = \mathcal{O}(1),$$
$$\boldsymbol{m} = \mathcal{O}\left(D\,\varepsilon\right), \quad \boldsymbol{n} = \mathcal{O}\left(D\,\varepsilon^2/w\right), \quad \mathcal{H} = \mathcal{O}\left(D\,\varepsilon^2/w\right), \quad \mathcal{E} = \mathcal{O}\left(D\,\varepsilon\right). \tag{6.2}$$

Our key contribution is to identify the simple differential problem satisfied by the unknowns $f^\star$. This differential problem is formulated in Section 6.2 below, and the order of accuracy announced in (6.1) is established in E.

So far, we have considered a single inner layer, with centre $S^\dagger$. In what follows, we revert to the general case with an arbitrary number, N, of inner layers whose centres are located at $S_J^\dagger$ for $1 \leqslant J \leqslant N$. While doing so, we also change the definition (3.6) of the slow variable $\widetilde{S} = \varepsilon\,(S - S^\dagger)/w$ to

$$\widetilde{S} = \frac{\varepsilon\, S}{w}. \tag{6.3}$$

In the absence of any ambiguity, we continue to use the same symbol $\widetilde{S}$. The outer solution is now a function of the new variable $\widetilde{S}$, having N points of discontinuity located at $\widetilde{S}_J^\dagger = \varepsilon\, S_J^\dagger/w$, rather than a single point of discontinuity at $\widetilde{S} = 0$ as earlier. One such point is shown in Figure 9. The apparent discontinuity of a physical quantity f at a singularity is denoted as

$$[\![f_{\text{out}}]\!]_J = f_{\text{out}}((\widetilde{S}_J^\dagger)^+) - f_{\text{out}}((\widetilde{S}_J^\dagger)^-). \tag{6.4}$$

6.2 Complete outer problem

The differential problem that yields the approximation $\boldsymbol{x}^\star(\widetilde{S})$, $\boldsymbol{d}_i^\star(\widetilde{S})$, $\omega_j^\star(\widetilde{S})$, $\boldsymbol{m}^\star(\widetilde{S})$, $\boldsymbol{n}^\star(\widetilde{S})$ is set up as follows. It is directly inspired by the matching results in Section 5.2.

- We consider N points of discontinuity, having scaled arclength coordinates $\widetilde{S}_J^\dagger$, for $1 \leqslant J \leqslant N$.
- *Away from discontinuities*: the equilibrium equations of the *Sadowsky model* listed in Equations (2.1–2.3), (2.7–2.8) and (2.18) are enforced on the intervals $(0, S_1^\dagger)$, $(S_1^\dagger, S_2^\dagger)$, ..., $(S_{N-1}^\dagger, S_N^\dagger)$ and $(S_N^\dagger, \ell)$.
- *At a discontinuity*:
  - *kinematic conditions*: the centreline $\boldsymbol{x}^\star$ and tangent $\boldsymbol{d}_3^\star$ are continuous, and the orthogonal director frame $\boldsymbol{d}_i^\star$ makes a jump through a discontinuity $\varphi_J^\star$ of the twisting angle, as sketched in Figure 9,

$$[\![\boldsymbol{x}^\star]\!]_J = \boldsymbol{0}, \qquad \begin{pmatrix} \boldsymbol{d}_1^\star(\widetilde{S}_J^+) \\ \boldsymbol{d}_2^\star(\widetilde{S}_J^+) \\ \boldsymbol{d}_3^\star(\widetilde{S}_J^+) \end{pmatrix} = \begin{pmatrix} +\cos\varphi_J^\star\, \boldsymbol{d}_1^\star(\widetilde{S}_J^-) + \sin\varphi_J^\star\, \boldsymbol{d}_2^\star(\widetilde{S}_J^-) \\ -\sin\varphi_J^\star\, \boldsymbol{d}_1^\star(\widetilde{S}_J^-) + \cos\varphi_J^\star\, \boldsymbol{d}_2^\star(\widetilde{S}_J^-) \\ \boldsymbol{d}_3^\star(\widetilde{S}_J^-) \end{pmatrix}. \tag{6.5}$$

  - *equilibrium conditions*: the balance of forces and moments takes the form

$$[\![\boldsymbol{n}^\star]\!]_J = \boldsymbol{0}, \qquad [\![\boldsymbol{m}^\star]\!]_J = \boldsymbol{0}, \tag{6.6}$$

    and the position $\widetilde{S}_J^\dagger$ of the singularity is fixed by the condition

$$[\![\mathcal{H}_{\mathrm{Sd}}^\star]\!]_J = 0, \tag{6.7}$$

    where $\mathcal{H}_{\mathrm{Sd}}^\star$ is the Hamiltonian invariant of the Sadowsky model from Equation (A.3).
  - *constitutive relation*: the twisting moment $m_3^\star = \boldsymbol{m}^\star \cdot \boldsymbol{d}_3^\star$ is continuous at a discontinuity by $(6.5)_2$ and $(6.6)_2$ and its value at the singularity is given by the constitutive relation

$$m_3^\star(\widetilde{S}_J^\dagger) = 4\, D\, c\, \varphi_J^\star, \tag{6.8}$$

    where $c = -1.642$ by (4.17). Equation (6.8) can be thought of as fixing the free parameters $\varphi_J^\star$ or, through (5.8), the corresponding parameter $\overline{\mu}_J$ capturing the amplitude of the inner layer solution.
- *At end points*: the relevant boundary conditions are applied, such as periodic boundary conditions for closed ribbons.

In E it is shown that the solution $f^\star$ of these equations gives a second-order accurate outer solution, as stated earlier in (6.1). Fundamentally, this comes from the fact that (i) the jump conditions comply with those derived in Section 5 and (ii) the Taylor expansion of the *even* function $F(q)$ about $q = 0$ has no linear term, $F(q) = 1 + \mathcal{O}(q^2)$; this, together with $q = w\,\eta' = \varepsilon\, \frac{\mathrm{d}\eta_{\mathrm{out}}}{\mathrm{d}\widetilde{S}} = \mathcal{O}(\varepsilon)$, yields $F(q) = 1 + \mathcal{O}(\varepsilon^2)$ in the outer region: there, the condition $F = 1$ under which the Wunderlich model reduces to the Sadowsky model is indeed satisfied up to terms of order ε^2.

The generic outer problem described above is solved in Sections 7 and 8 for two specific ribbon geometries.

6.3 Discussion

The only way the inner layer solution (§4) enters in the outer problem is through the constant $c = -1.642$ in Equation (6.8): this numerical value effectively captures all the details of the inner solution. Interestingly, the usual Sadowsky model is recovered by changing its value to $c = \infty$: in this limit, the jumps in the twisting angle are indeed suppressed, $\varphi_J^\star = 0$, see (5.8). The outer problem of Section 6.2 is therefore nothing but a Sadowsky model with *modified jump conditions*. These jump conditions introduce apparent discontinuities $\varphi_J^\star$ in the twisting angle, providing coarse-grained representations of the inner layers. The outer problem from Section 6.2 is about

as easy to solve as the standard Sadowsky model. Yet, its solutions agree with the Wunderlich model up to terms of order ε^2, see (6.1), while those of the standard Sadowsky model agree up to terms of order ε. This improvement in accuracy is demonstrated in Section 7. It is remarkable that refining the jump conditions, through $(6.5)_2$ and (6.8), suffices to improve the accuracy of the solution by one order.

The outer problem for $\boldsymbol{x}^\star(\widetilde{S})$, $\boldsymbol{d}_i^\star(\widetilde{S})$, $\omega_j^\star(\widetilde{S})$, $\boldsymbol{m}^\star(\widetilde{S})$, $\boldsymbol{n}^\star(\widetilde{S})$ has a simple variational structure. For ribbon configurations parametrised by $\boldsymbol{x}^\star$, $(\boldsymbol{d}_i^\star)_{1\leqslant i\leqslant 3}$ including discontinuities $(\widetilde{S}_J^\dagger, \varphi_J^\star)_{1\leqslant J\leqslant N}$, and satisfying the kinematic constraints (2.1–2.3) and (6.5), we introduce the energy functional

$$\mathcal{E}_{\mathrm{im}}[\omega_2, \omega_3, (S_J^\dagger, \varphi_J)_{1\leqslant J\leqslant N}] = \frac{D\,w}{2}\int_{\mathcal{D}} 4\,\omega_2^2\left(\frac{1+\eta^2}{2}\right)^2 \mathrm{d}S + \frac{4\,D\,c}{2}\sum_{J=1}^{N}\varphi_J^2, \tag{6.9}$$

which we will refer to as the *improved* Sadowsky functional. It is shown in F that the stationarity conditions for $\mathcal{E}_{\mathrm{im}}$ are nothing but the equilibrium equations (2.7–8), (6.6–6.7), together with the constitutive laws (2.18) and (6.8). In particular, (6.7) is a standard condition in problems in the calculus of variations with moving discontinuities, known as the Weierstrass-Erdmann corner condition.

The first term in the energy $\mathcal{E}_{\mathrm{im}}$ is the classical Sadowsky energy (2.17), integrated over a domain $\mathcal{D}$ from which the singularities have been removed,

$$\mathcal{D} = (0, S_1^\dagger) \cup (S_1^\dagger, S_2^\dagger) \cup \cdots \cup (S_N^\dagger, \ell). \tag{6.10}$$

The second term is a contribution coming from discontinuities, as intimated by (5.10). The energy $\frac{4\,Dc}{2}\,\varphi_J^2$ of a discontinuity is that of a torsional spring having a spring constant $4\,Dc$, an interpretation that is consistent with the constitutive relation of a singularity in (6.8).

As the constant c is negative, these spring constants are negative and none of the stationary points of $\mathcal{E}_{\mathrm{im}}$ are minima in the presence of singularities. This does not imply, however, that the corresponding matched asymptotic solutions are unstable equilibria of the Wunderlich model. Indeed, although we have shown that matched asymptotic solutions correspond to stationary points of $\mathcal{E}_{\mathrm{im}}$, their stability properties are not governed by this functional.

The Weierstrass–Erdmann corner condition (6.7) has the following consequences. Since both $\boldsymbol{n}^\star$ and $\boldsymbol{d}_3^\star$ are continuous at the singularity by (6.5–6.6), Equation (6.7) is equivalent to

$$\left[\!\!\left[\frac{D\,w}{2}\,(\omega_2^\star)^2\,(1+\eta^{\star 2})^2\right]\!\!\right]_J = 0. \tag{6.11}$$

Now, recalling that $m_3^\star = 4\,D\,w\,\omega_2^\star\,\eta^\star\,\frac{1+\eta^{\star 2}}{2}$ is continuous at a singularity, we can divide (6.11) by $(m_3^\star)^2$, which yields the equivalent continuity condition, $\left[\!\!\left[\frac{1}{8\,\eta^{\star 2}}\right]\!\!\right]_J = 0$ (this assumes that $m_3^\star(\widetilde{S}_J^\dagger) \neq 0$, which holds in general). The consequence is that $\eta^{\star 2}$ is continuous. Returning to (6.11), we then find that $(\omega_2^\star)^2$ is continuous. Using again the fact that $m_3^\star = 4\,D\,w\,\omega_2^\star\,\eta^\star\,\frac{1+\eta^{\star 2}}{2}$ is continuous, we find that $\omega_2^\star\,\eta^\star$ is also continuous across a singularity. Now, $\omega_2^\star$ and $\eta^\star$ cannot both be continuous across a singularity as there would then be no singularity at all. The only possibility is that both $\omega_2^\star$ and $\eta^\star$ flip sign, in agreement with the computed inner solution, see Figure 6a,

$$\omega_2^\star((\widetilde{S}_J^\dagger)^+) = -\omega_2^\star((\widetilde{S}_J^\dagger)^-), \qquad \eta^\star((\widetilde{S}_J^\dagger)^+) = -\eta^\star((\widetilde{S}_J^\dagger)^-). \tag{6.12}$$

The bending moment, given by $(2.18)_2$ as $m_2^\star = D\,w\,\omega_2^\star\,(1-\eta^{\star 4})$, then flips sign as well, a condition that we can rewrite as

$$\boldsymbol{m}^\star(\widetilde{S}_J)\cdot\frac{\boldsymbol{d}_2^\star((\widetilde{S}_J)^-) + \boldsymbol{d}_2^\star((\widetilde{S}_J)^+)}{2} = 0. \tag{6.13}$$

The quantity $\boldsymbol{m}^\star$ that appears on the left-hand side is continuous by $(6.6)_2$. Equation (6.13) has been derived from the Weierstrass–Erdmann corner condition (6.7) and appears to be the non-smooth analogue of the condition $m_2 = \boldsymbol{m}\cdot\boldsymbol{d}_2 = 0$ that holds at a singular point of the standard Sadowsky model—this condition $m_2 = 0$ is indeed implied by the equation $|\omega_2| = |\omega_3|$ defining the edge of the non-convex region identified by Freddi et al. (2015), and also appears explicitly in Equation [7.4] of (Audoly and Neukirch, 2021).

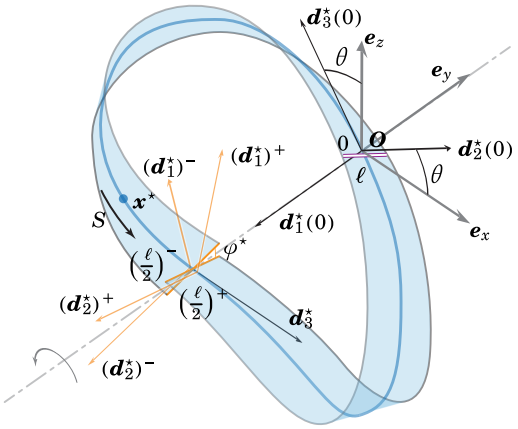

Figure 10: Sketch of the outer problem for the elastic Möbius band. The end points of the domain $S = 0$ and $S = \ell$ are shown by the double-struck purple line, whose midpoint coincides with the origin $\boldsymbol{O}$ of the coordinate system. There, the director frame is flipped: the directors at $S = \ell$ (not shown) are obtained by flipping those at $S = 0$ using (7.1). There is an apparent discontinuity at $S = \ell/2$ representing an inner layer. At the discontinuity, the directors are denoted using the shorthand notation $(\boldsymbol{d}_i^\star)^\pm = \boldsymbol{d}_i^\star((\ell/2)^\pm)$. Note that the picture is drawn with a *negative* jump in twisting angle, $\varphi^\star < 0$.

7 Application to a Möbius band

We apply the matched asymptotic construction to a Möbius strip. This requires adapting the general form of the outer problem stated in Section 6.2 (and in particular the boundary conditions) to this geometry, and solving it numerically.

7.1 Formulation of the outer problem

We limit attention to a solution that is invariant under a 180° rotation about a fixed axis cutting the centreline of the ribbon at two points. We take this axis to be the coordinate axis $(O\boldsymbol{e}_y)$, see Figure 10. There is a single singularity ($N = 1$) and it is located on this axis. With ℓ as the arclength of the ribbon, we use the domain $S \in [0, \ell]$ and designate $S = \ell/2$ as the position of the singularity, see Figure 10. The other point on the symmetry axis, corresponding to both end points $S = 0$ and $S = \ell$ of the domain, is taken as origin of the coordinate system. At this point we impose the frame flipping conditions required to comply with the topology of the Möbius band. Thus

$$\boldsymbol{x}^\star(0) = \boldsymbol{x}^\star(\ell) = \boldsymbol{0}, \qquad (\boldsymbol{d}_1^\star, \boldsymbol{d}_2^\star, \boldsymbol{d}_3^\star)(\ell) = (-\boldsymbol{d}_1^\star, -\boldsymbol{d}_2^\star, \boldsymbol{d}_3^\star)(0). \tag{7.1}$$

The Cartesian axes are oriented such that $\boldsymbol{d}_3^\star(\ell/2) = \boldsymbol{e}_x$. Denoting the coordinates of the centreline as $\boldsymbol{x}^\star = (x^\star, y^\star, z^\star)$, we can write

$$x^\star(0) = y^\star(0) = z^\star(0) = 0, \qquad (\boldsymbol{d}_1^\star, \boldsymbol{d}_2^\star, \boldsymbol{d}_3^\star)(0) = (-\boldsymbol{e}_y, \cos\theta\, \boldsymbol{e}_x + \sin\theta\, \boldsymbol{e}_z, -\sin\theta\, \boldsymbol{e}_x + \cos\theta\, \boldsymbol{e}_z) \tag{7.2}$$

and, allowing for the frame jump at the singularity,

$$x^\star\left(\frac{\ell}{2}\right) = z^\star\left(\frac{\ell}{2}\right) = 0, \qquad (\boldsymbol{d}_1^\star, \boldsymbol{d}_2^\star, \boldsymbol{d}_3^\star)\left(\frac{\ell^\pm}{2}\right) = \left(\mp\sin\frac{\varphi^\star}{2}\, \boldsymbol{e}_y + \cos\frac{\varphi^\star}{2}\, \boldsymbol{e}_z, \mp\sin\frac{\varphi^\star}{2}\, \boldsymbol{e}_z - \cos\frac{\varphi^\star}{2}\, \boldsymbol{e}_y, \boldsymbol{e}_x\right), \tag{7.3}$$

where the angles θ and $\varphi^\star$ are unknowns of the problem.

The assumed symmetry allows one half of the Möbius strip, $S \in [\ell/2, \ell]$, to be reconstructed in terms of the other half, $S \in [0, \ell/2]$, using $\boldsymbol{d}_1^\star(\ell - S) = -\boldsymbol{\mathcal{R}}_{(\pi, \boldsymbol{e}_y)} \boldsymbol{d}_1^\star(S)$, $\boldsymbol{d}_2^\star(\ell - S) = +\boldsymbol{\mathcal{R}}_{(\pi, \boldsymbol{e}_y)} \boldsymbol{d}_2^\star(S)$,

$\boldsymbol{d}_3^\star(\ell - S) = -\boldsymbol{\mathcal{R}}_{(\pi,\boldsymbol{e}_y)}\boldsymbol{d}_3^\star(S)$, $\omega_2(\ell - S) = -\omega_2(S)$, $\omega_3(\ell - S) = +\omega_3(S)$, $\eta(\ell - S) = -\eta(S)$, $\boldsymbol{n}^\star(\ell - S) = -\boldsymbol{\mathcal{R}}_{(\pi,\boldsymbol{e}_y)}\boldsymbol{n}^\star(S)$, $\boldsymbol{m}^\star(\ell - S) = -\boldsymbol{\mathcal{R}}_{(\pi,\boldsymbol{e}_y)}\boldsymbol{m}^\star(S)$. Here $\boldsymbol{\mathcal{R}}_{(\pi,\boldsymbol{e}_y)}$ is the 180° rotation about $\boldsymbol{e}_y$. We use this symmetry to set up a boundary-value problem on the interval $S \in [0, \ell/2]$.

The director frame $(\boldsymbol{d}_1^\star, \boldsymbol{d}_2^\star, \boldsymbol{d}_3^\star)$ is parametrised by means of Euler angles $(\bar\theta, \bar\psi, \bar\varphi)$ as

$$\boldsymbol{d}_1^\star = \begin{pmatrix} -\sin\bar\psi\sin\bar\varphi + \cos\bar\theta\cos\bar\psi\cos\bar\varphi \\ \cos\psi\sin\bar\varphi + \cos\bar\theta\sin\bar\psi\cos\bar\varphi \\ -\sin\bar\theta\cos\bar\varphi \end{pmatrix}, \quad \boldsymbol{d}_2^\star = \begin{pmatrix} -\sin\bar\psi\cos\bar\varphi - \cos\bar\theta\cos\bar\psi\sin\bar\varphi \\ \cos\bar\psi\cos\bar\varphi - \cos\bar\theta\sin\bar\psi\sin\bar\varphi \\ \sin\bar\theta\sin\bar\varphi \end{pmatrix},$$
$$\boldsymbol{d}_3^\star = \begin{pmatrix} \sin\bar\theta\cos\bar\psi \\ \sin\bar\theta\sin\bar\psi \\ \cos\bar\theta \end{pmatrix}. \tag{7.4}$$

This choice of angles avoids the Euler-angle singularity at $\bar\theta = 0$ in all computations in this and the next section.

We solve a system of 14 ordinary differential equations on the interval $[0, \ell/2]$ consisting of: 3 equations for $\boldsymbol{x}^\star$ obtained by projecting (2.2) on the Cartesian basis, 6 equations for $\boldsymbol{n}^\star$ and $\boldsymbol{m}^\star$ obtained from (2.7), 3 equations for $(\bar\theta, \bar\psi, \bar\phi)$, representing a reduced version of Equation (2.3), and 2 equations for (ω_2, η) obtained by differentiating the constitutive relations (2.18). The complete set of boundary conditions is:

$$\begin{aligned}
x^\star(0) &= 0, & x^\star(\ell/2) &= 0,\\
y^\star(0) &= 0, & z^\star(\ell/2) &= 0,\\
z^\star(0) &= 0, & \bar\theta(\ell/2) &= \frac{\pi}{2},\\
\bar\psi(0) &= \pi, & \bar\psi(\ell/2) &= 2\,\pi,\\
\bar\varphi(0) &= \frac{\pi}{2}, & \bar\varphi(\ell/2) &= \pi - \frac{\varphi^\star}{2},\\
n_1^\star(0) &= 0, & m_3^\star(\ell/2) &= 4\,D\,c\,\varphi^\star,\\
m_1^\star(0) &= 0,\\
m_2^\star(0) &= D\,w\,\omega_2(0)\,(1 - \eta^4(0)),\\
m_3^\star(0) &= 2\,D\,w\,\omega_2(0)\,\eta(0)\,(1 + \eta^2(0)).
\end{aligned} \tag{7.5}$$

The boundary-value problem is well-posed: the above 15 boundary conditions are used to solve the 14 differential equations and to fix the value of the free parameter $\varphi^\star$. The other free parameter θ does not appear in this boundary-value problem but can be reconstructed as $\theta = \bar\theta(0)$ using (7.2).

The boundary conditions in (7.5) on the kinematic variables $x^\star$, $y^\star$, $z^\star$, $\bar\theta$, $\bar\psi$ and $\bar\varphi$ come directly from (7.2–7.3); note that the second column of (7.5) uses the conditions applicable at $\ell^-/2$ as the boundary-value problem is formulated on the domain $[0, \ell/2]$. The boundary condition $\bar\varphi(\ell/2) = \pi - \varphi^\star/2$ creates a jump $\varphi^\star$ in the Euler angle $\bar\varphi$ across the singularity when the solution is reconstructed in the other half of the strip, in agreement with $(6.5)_2$. The other boundary conditions in (7.5) can be justified as follows: the $n_1^\star(0)$ and $m_1^\star(0)$ conditions ensure $\boldsymbol{n}^\star(0)\cdot\boldsymbol{e}_y = 0$ and $\boldsymbol{m}^\star(0)\cdot\boldsymbol{e}_y = 0$, as required by the rotation symmetry; the $m_2^\star(0)$ and $m_3^\star(0)$ conditions enforce the constitutive relations (2.18), which have been included in differentiated form only in the set of ordinary differential equations; the condition on $m_3^\star(\ell/2)$ is nothing but the equivalent constitutive law (6.8) of the singularity. Note that Equation (6.7), which sets the position of the singularity, is automatically satisfied as the singularity has been prescribed to lie on the symmetry axis.

It is easily verified that because $\boldsymbol{n}$ and $\boldsymbol{m} + \boldsymbol{x}\times\boldsymbol{n}$ are constant vectors in space, the above boundary conditions imply $\boldsymbol{n}^\star(\ell/2)\cdot\boldsymbol{e}_y = 0$ and $\boldsymbol{m}^\star(\ell/2)\cdot\boldsymbol{e}_y = 0$, as again required by rotation symmetry about $\boldsymbol{e}_y$. For later reference we also record here that with the help of $(7.3)_2$ these conditions can be written as

$$\begin{aligned}
n_1^\star(\ell/2)\sin\varphi^\star - n_2^\star(\ell/2)\cos\varphi^\star &= 0,\\
m_1^\star(\ell/2)\sin\varphi^\star - m_2^\star(\ell/2)\cos\varphi^\star &= 0.
\end{aligned} \tag{7.6}$$

7.2 Numerical results

We solve this boundary-value problem numerically for different widths, and compare solutions with those of the Wunderlich model. Our numerical calculations make use of particular length and energy units, such that $D\,w = 2$ and $\ell = 2\,\pi$. There is a one-parameter family of solutions depending on the aspect ratio w/ℓ. Having found a solution of the 14-dimensional system for a particular value of w/ℓ, we can plot the two-dimensional surface (or the field of straight generators) of the ribbon by using the parametrisation of the developable surface in Equation (2.4).

Figure 11 compares the curvature ω_2 and η of the inner, outer, Sadowsky and Wunderlich solutions for several aspect ratios w/ℓ and demonstrates convergence of the inner and outer solutions to the (exact) Wunderlich solution as $w \to 0$. The plots in Figure 11b", in particular, reveal that the agreement between the matched asymptotic solution and the Wunderlich solution is better than $\mathcal{O}(\varepsilon)$, in agreement with the $\mathcal{O}(\varepsilon^2)$ accuracy claim made in Section 6.1.

The plots confirm that the Sadowsky solution has $\eta(\ell/2) = 1$ at the singularity, corresponding to a 45° angle between generator and centreline—also known from Sadowsky's Möbius band application (Sadowsky, 1931)—, while the curvature there is found to be 0.785410, teasingly close to, but distinct from, $\pi/4$.

Figure 12 compares the composite form of the matched asymptotic solution for the selected values of w, also including the three-dimensional shape of the Möbius band. The agreement is excellent over the entire interval for $w/\ell = 0.2/(2\,\pi)$, and remains quite good for aspect ratios as large as $w/\ell = 1/(2\,\pi)$. The plots in the (ω_2, ω_3) plane in Figure 12c highlight the accuracy of the composite solution in the inner region.

Figure 13 shows how the jump $\varphi^\star$ in the twist angle predicted by the outer solution, as well as the strain energy $\mathcal{E}$ predicted by the various models, vary with the width w at fixed length $\ell = 2\,\pi$. The angle $\varphi^\star$ is negative, corresponding to overtwisting of the ribbon at the singularity. For small w, both the angle $\varphi^\star$ and the strain energy $\mathcal{E}$ vary linearly with w, and both these linear variations are captured by the perturbation analysis given in G (thin grey lines in the figure). The energy plot in Figure 13b, confirms that the Sadowsky, Wunderlich and matched asymptotic solutions all converge to the same limit as $w \to 0$, *i.e.*, the energies of all solutions agree up to terms of order ε. Since the last two share the same initial tangent, the matched asymptotic solution appears to predict the energy minimum with a better accuracy, up to terms of order ε^2, than the Sadowsky model, which introduces an error of order ε. This is in line with the statement made in Section 6.3 that the modified jump conditions used in our matched asymptotic solution improve the accuracy of the Sadowsky model by one order in ε.

The energy of the matched asymptotic solution plotted in Figure 13b is based on Equation (6.9). Our results show that the contribution of the singularity (last term on the right-hand side) is significant. This confirms that the energy functional proposed in (6.9) does not only deliver the equations of the outer problem variationally (§6.3) but also furnishes an accurate estimate of the energy of the Wunderlich solution.

8 Application to a pulled and twisted ribbon

Here we apply our asymptotic analysis to the pattern shown in Figure 1b obtained by twisting a thin ribbon held in tension. Specifically, we adapt the generic form of outer problem stated in Section 6.2 to this particular geometry. The figure shows that the pattern is, to a very high degree, symmetric; it consists essentially of an alternating sequence of vertices on the long edges of the ribbon with associated flat triangular facets very similar to those described by the inner layer in the Möbius solutions shown in Figure 12.

Following (Korte et al., 2011), we will therefore formulate a boundary-value problem for an elementary segment of the deformation pattern, namely half the segment between two successive vertices on opposite sides of the ribbon (see Figure 14). Suitable reflections of this elementary segment will allow us to construct twisted-ribbon solutions with any number of triangular facets. The vertices of the deformation pattern will therefore correspond to our cone-like singularities. We

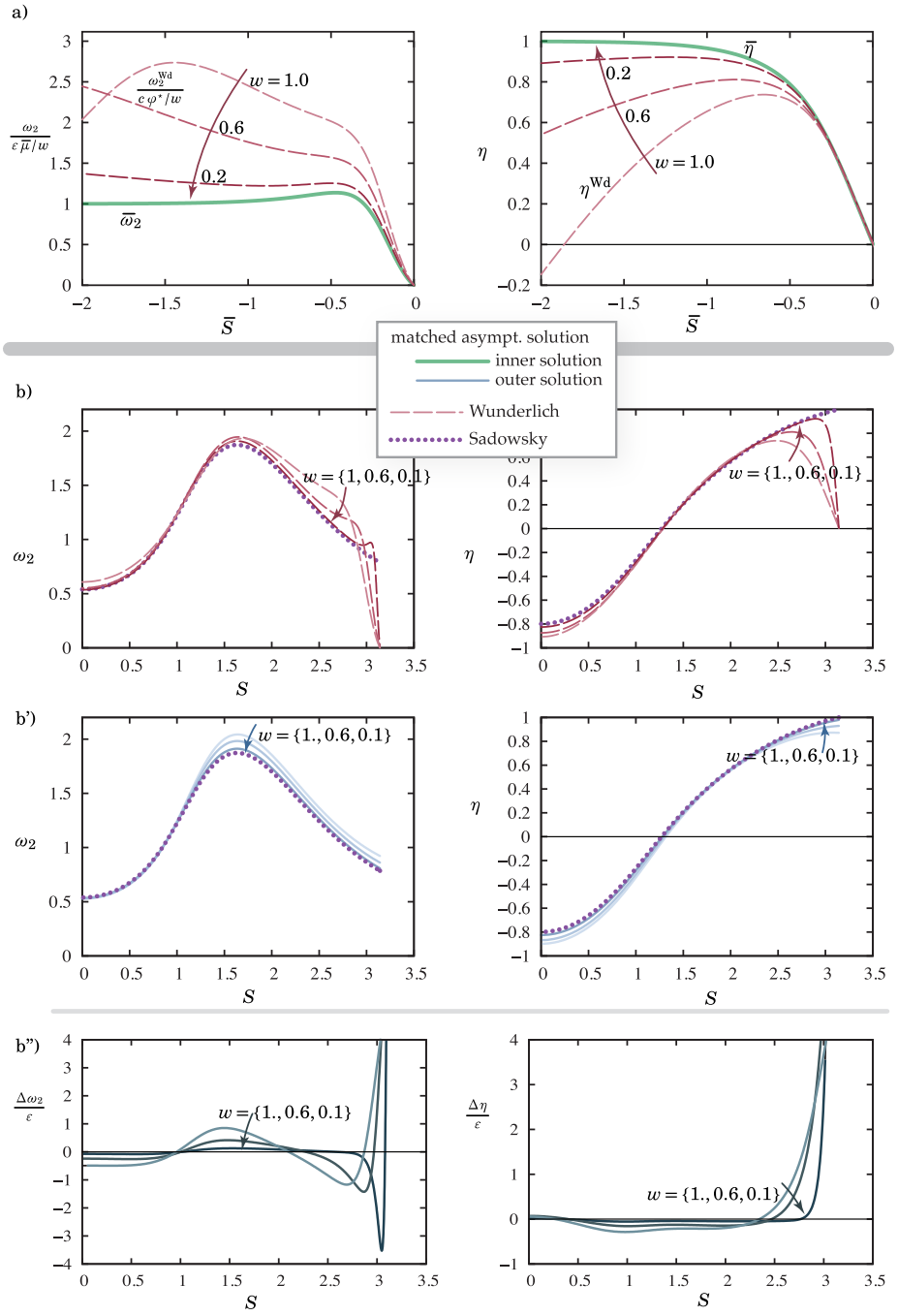

Figure 11: Convergence of the matched asymptotic solution to the Wunderlich solutions as $w \to 0$, for a Möbius strip with length $\ell = 2\,\pi$. (a) Convergence in the *inner region*, tested as a function of the stretched variable $\overline{S} = (S - \ell/2)/w$. In the plot on the left, the bending strain ω_2 is rescaled by the factor $\varepsilon\,\overline{\mu}/w$ appearing in the inner solution, see (3.5); to produce the prediction of the Wunderlich model, this scaling factor is evaluated as $\varepsilon\,\overline{\mu}/w = c\,\varphi^\star/w$ using (5.8), where $\varphi^\star$ is the jump in twisting angle in the matched asymptotic solution. In the plot on the right, the predictions for the dimensionless quantity η are compared directly. (b–b") Convergence in the *outer region* using the unstretched coordinate S. (b–b'): both the Wunderlich solution and the outer solution converge to the Sadowsky solution. (b"): the outer solution and the Wunderlich solution agree to a higher order than $\varepsilon = w/\ell$ in the outer region, as shown by the fact that $\Delta\omega_2/\varepsilon = \left(\omega_2^{\mathrm{out}} - \omega_2^{\mathrm{Wd}}\right)/\varepsilon$ and $\Delta\eta/\varepsilon = \left(\eta^{\mathrm{out}} - \eta^{\mathrm{Wd}}\right)/\varepsilon$ converge to zero, except near the singularity located at $S = \pi$.

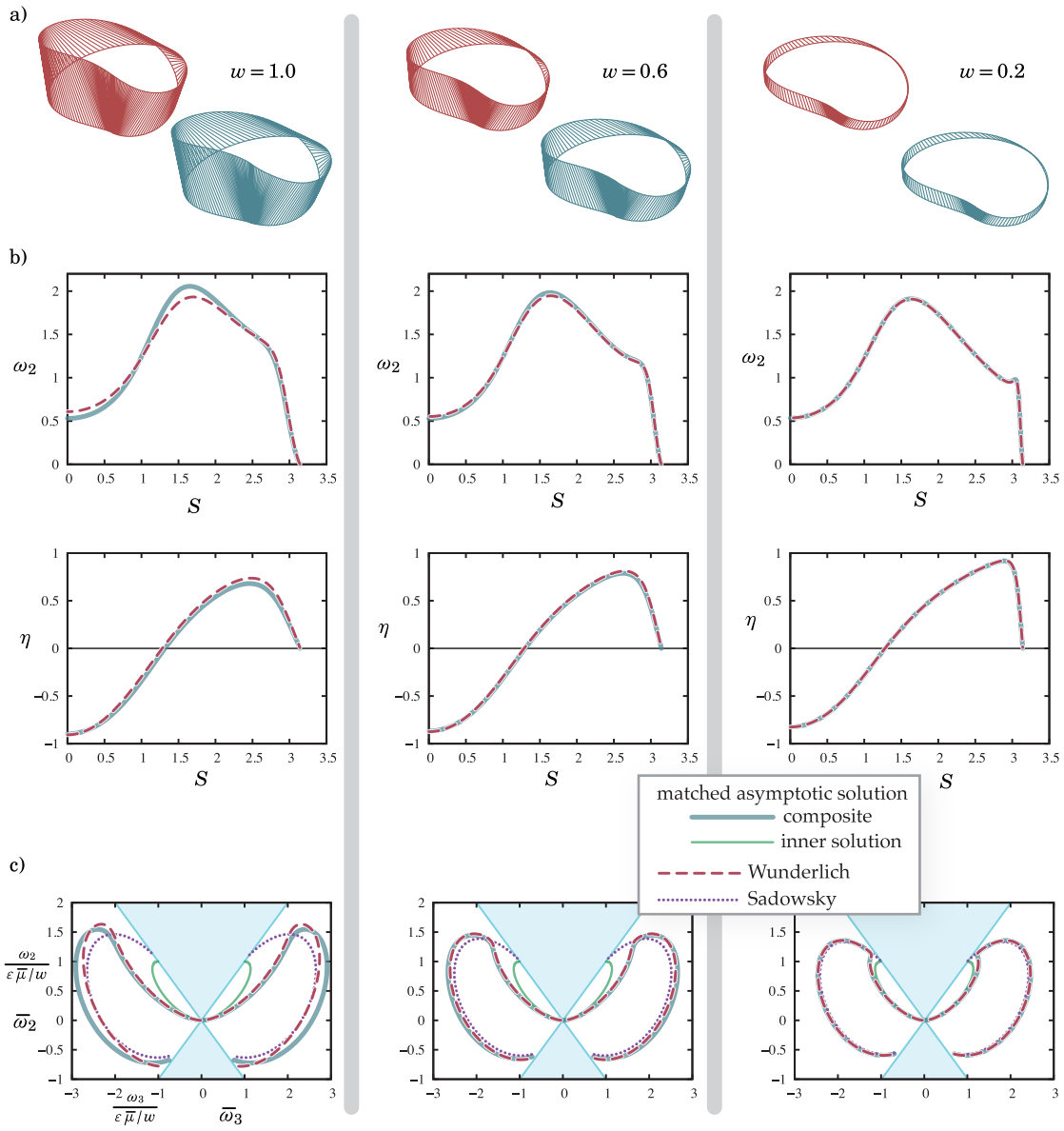

Figure 12: Composite form of the matched asymptotic solution for the Möbius strip with length $\ell = 2\,\pi$, and comparison to the Wunderlich solution for three different widths (columns). (a) True-view three-dimensional reconstruction of the ribbon. (b) Convergence of the bending strain ω_2 and strain ratio η versus the arclength coordinate S. (c) Paths traced out in the $(\overline{\omega}_2, \overline{\omega}_3)$ plane, including predictions from the inner solution and from the Sadowsky model (the quantities ω_2 and ω_3 are rescaled as earlier in Figure 11a). The domain $|\omega_2| < |\omega_3|$ shown in light blue is where the Sadowsky model is non-convex (Freddi et al., 2015).

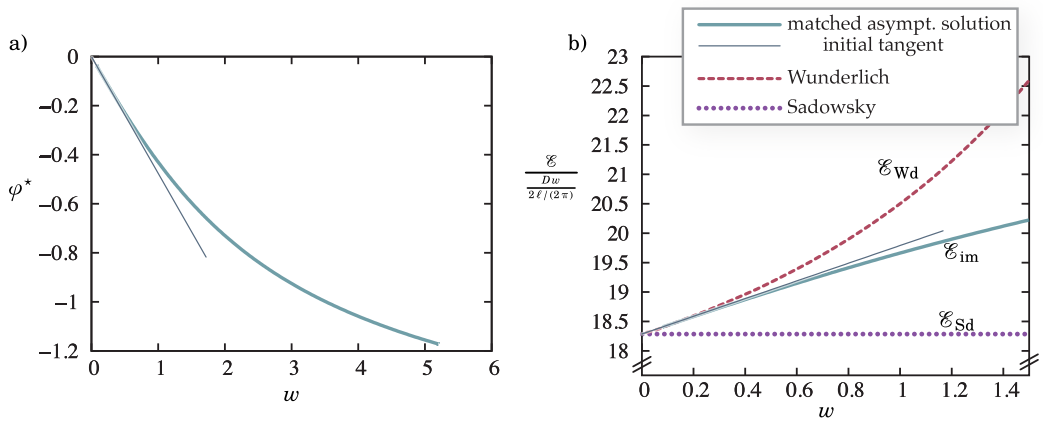

Figure 13: Dependence of the solution for a Möbius band on the width w, for a fixed length $\ell = 2\,\pi$. (a) Jump $\varphi^\star$ in twist angle predicted by the matched asymptotic solution; the initial tangent is the prediction (G.2) obtained by the perturbation analysis in G. (b) Comparison of strain energies of the equilibrium solutions of the various models: the initial tangent for the matched asymptotic solution is the prediction (G.3) from G. Using the (exact) Wunderlich model ($\mathcal{E}_{\mathrm{Wd}}$) as a reference, one can see that the Sadowsky model ($\mathcal{E}_{\mathrm{Sd}}$) and the matched asymptotic solution ($\mathcal{E}_{\mathrm{im}}$) predict the correct limiting value of the energy as $w \to 0$; however, the latter further captures its Taylor expansion to linear order correctly.

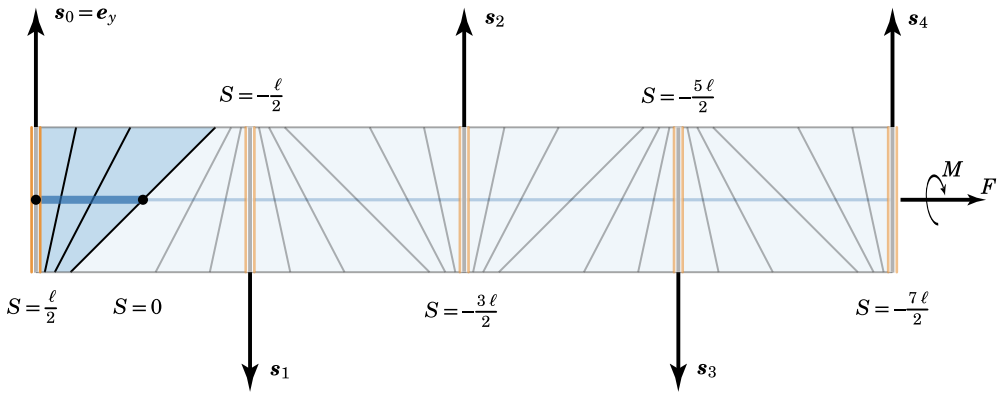

Figure 14: Schematic construction of a symmetric twisted-strip pattern of period two ($n = 4$) from the elementary segment on the arclength interval $[0, \ell/2]$ (darker blue shading). The symmetry operations consist of 180° rotation about the normal to the strip at $S = 0$, $-\ell$, -2ℓ, etc. and 180° rotation about the successive images $\boldsymbol{s}_1$, $\boldsymbol{s}_2$, $\boldsymbol{s}_3$, etc. of the symmetry axis $\boldsymbol{s}_0 = \boldsymbol{e}_y$ at $S = \ell/2$. The double-struck orange lines denote cone-line singularities.

thus take the wavelength of the deformation pattern, and hence the length scale ℓ of the problem, to be a parameter that can be set arbitrarily, and do not try to identify an optimal value. This assumption has possible implications for the stability of the computed solution, which we comment on at the end of this section.

To compute the elementary segment we need only slightly modify the boundary-value problem for half the Möbius band formulated in Section 7.1. We again solve our system of 14 equations on the interval $[0, \ell/2]$ with $S = \ell/2$ the position of the singularity. We keep the $\mathbf{e}_y$ axis as symmetry axis at $S = \ell/2$ and the kinematic alignment expressed by (7.3) with jump $\varphi^\star$ in the twist angle across the singularity. At $S = 0$ we still demand 180° rotation symmetry about the normal $\boldsymbol{d}_1^\star(0)$,

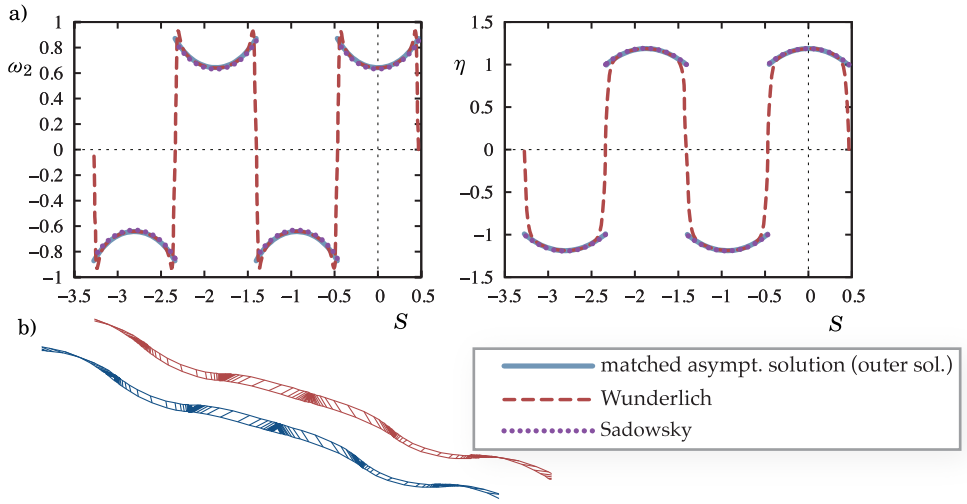

Figure 15: Twisted ribbon with end loads $F = 8.9528$ and $M = 6.4257$, $w = 0.08$, $\ell/2 = 0.46791$. (a) Plot of two periods ($n = 4$) of $\omega_2(S)$ and $\eta(S)$. (b) True-view three-dimensional reconstruction of the ribbon showing the generators: outer solution versus Wunderlich solution. The Sadowsky and outer solutions feature jumps in ω_2 and η, as seen in (a). Jumps in the twisting angle are also present, albeit hardly visible, in the blue outer solution plot in (b).

but no longer force $\boldsymbol{x}^\star(0)$ to lie on the $\mathbf{e}_y$ axis, thereby allowing for non-closed solutions. Thus we drop the conditions $x^\star(0) = 0$, $z^\star(0) = 0$ in (7.5) and impose the conditions (7.6) instead. We also need to replace two more kinematics conditions by two load conditions. We choose to drop the $\bar{\psi}(0)$ and $\bar{\varphi}(0)$ conditions and impose $\boldsymbol{n}\,(\ell/2)\cdot\hat{\boldsymbol{e}} = F$, $\boldsymbol{m}\,(\ell/2)\cdot\hat{\boldsymbol{e}} = M$ to fix the end force and end moment about the end-to-end axis (the unit vector $\hat{\boldsymbol{e}}$ that gives the direction of this axis is defined below). All other conditions of the Möbius problem can be retained.

A symmetric ribbon configuration with an arbitrary number of (equally spaced) singularities can be constructed from this elementary ribbon segment on $[0, \ell/2]$ as follows (see Figure 14). We define a section of the ribbon between two successive singularities as the half period of the ribbon's deformation pattern. A symmetric half period, of length ℓ, is obtained by reflection about the normal at $S = 0$ using rotations such as those introduced after Equation (7.3) but with $\boldsymbol{\mathcal{R}}_{(\pi,\mathbf{e}_y)}$ replaced by $\boldsymbol{\mathcal{R}}_{(\pi,\boldsymbol{d}_1^\star(0))}$. A full period is then computed by similar reflections about the resultant image $\boldsymbol{s}_1 := \boldsymbol{\mathcal{R}}_{(\pi,\boldsymbol{d}_1^\star(0))}(0,1,0)^T$ of the symmetry axis $\boldsymbol{s}_0 := \boldsymbol{e}_y$. This procedure can be iterated by successive reflections about $\boldsymbol{s}_1$, $\boldsymbol{s}_2$, etc. to construct a buckling pattern with any number, n, of half periods with $n-1$ interior singularities and two 'half' singularities at the ends of the ribbon at $S = S_n = -(2n-1)\ell/2$ and $S = S_0 = \ell/2$.

For a solution with n half periods we compute $\boldsymbol{e} = \boldsymbol{x}(S_0) - \boldsymbol{x}(S_n)$. The unit vector $\hat{\boldsymbol{e}} = \boldsymbol{e}/|\boldsymbol{e}|$ enters in the definition of the loading parameters F and M given above. As displacement measures we use the relative extension $e = |\boldsymbol{e}|/(n\,\ell)$ and the relative end rotation α of the components of the end edge directions $\boldsymbol{s}_n$ and $\boldsymbol{s}_0$ perpendicular to $\boldsymbol{e}$, *i.e.*, $\cos\alpha = \boldsymbol{a}_0 \cdot \boldsymbol{a}_n/|\boldsymbol{a}_0||\boldsymbol{a}_n|$, where $\boldsymbol{a}_0 = \boldsymbol{s}_0 - [\boldsymbol{s}_0 \cdot \hat{\boldsymbol{e}}]\hat{\boldsymbol{e}}$ and $\boldsymbol{a}_n = \boldsymbol{s}_n - [\boldsymbol{s}_n \cdot \hat{\boldsymbol{e}}]\hat{\boldsymbol{e}}$.

Numerical results are shown in Figures 15–18. All solutions are for $\ell/2 = 0.46791$. Figure 15 shows a period-2 solution ($n = 4$) for $w = 0.08$ and certain arbitrary end loads F and M given in the caption. Note that in both the ω_2 and η plots the reflection rules imply even *reflection* symmetry about the vertical at $S = 0, -\ell, -2\ell$, etc. (alternating maxima and minima) and odd *point* symmetry about the singularities at $S = \ell/2, -\ell/2, -3\ell/2$, etc. So we are letting the curvature change sign through an inflection point, while keeping the normal director $\boldsymbol{d}_1^\star$ continuous *i.e.*, we are not imposing a frame flip in this twisted-strip problem. The three-dimensional view in Figure 15 shows that, as a result of these reflection rules, the singularities (stress localisations) alternate between the two long edges of the ribbon, in agreement with the pattern seen in Figure 1b.

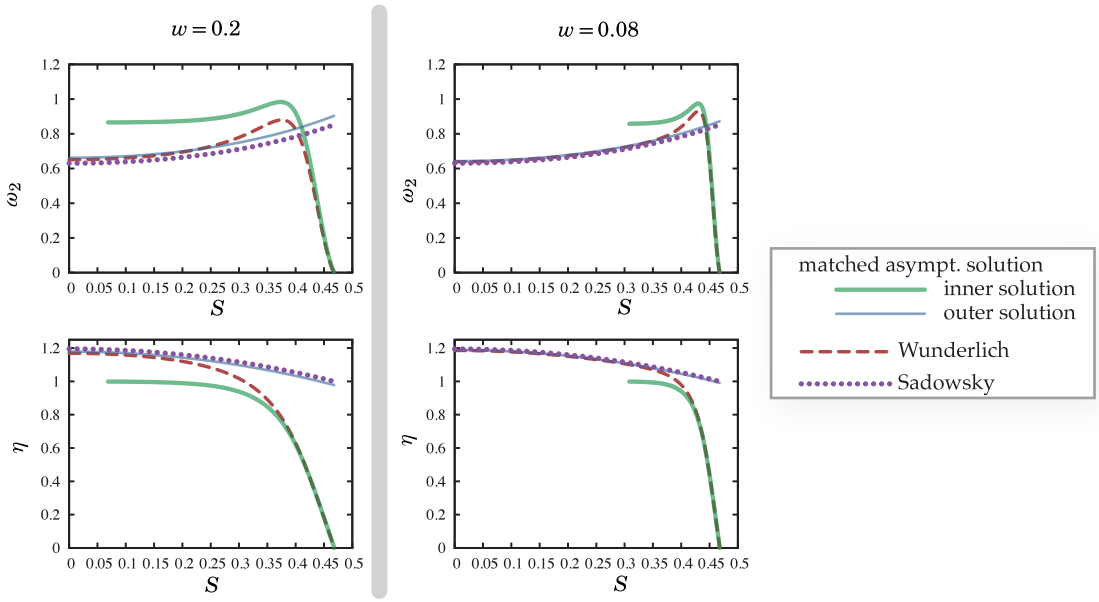

Figure 16: Twisted ribbon. Comparison of Sadowsky, matched asymptotic and Wunderlich solutions for a ribbon with end loads $F = 8.9528$ and $M = 6.4257$. $\ell/2 = 0.46791$. The solutions in the right column are for the same parameters as in Figure 15.

Figure 16 compares Sadowsky, Wunderlich and matched asymptotic solutions for $w = 0.08$ and $w = 0.2$, while Figure 17 displays the corresponding composite matched asymptotic solutions. In Figure 16 we see that the outer solutions have nearly constant ω_2 and η. They are essentially extensions of the inner solution away from the singularity. Moreover, η is close to 1, which corresponds to the local generator making an angle of 45° with the centreline. These twisted-ribbon solutions are therefore essentially concatenations of inner layers. They create a pattern of flat triangular facets, with the generator sweeping through a 90° sector at approximately uniform speed η', connected by nearly cylindrical segments with parallel generators running at a 45° angle, as confirmed in Figure 15c and as seen in an actual twisted strip in Figure 1b. Figure 17 clearly shows the benefit of the composite representation, which closely approximates the Wunderlich solution.

Figure 18 compares loading curves for the matched asymptotic solution and the exact (Wunderlich) model, under both varying force and varying twisting moment. The agreement of the force-extension curve is particularly good, for all displayed values of F. Force curves are seen to have a fold, predicting a buckling instability under pretwisted compressive loading (for comparison at $w = 0.08$, the fold occurs at $F = -8.3291$ in the matched asymptotic solution and at $F = -8.8379$ in the Wunderlich model). We generally observe that the matched asymptotic solution shows 'softer' behaviour than the Wunderlich model, under both force and moment loading, and this effect increases with w/ℓ (more so for the moment than for the force).

Overall we therefore have very good agreement with the Wunderlich solutions for the chosen parameter values. Although this study has not been about stability we like to end the discussion of this twisted-strip application with some more speculative comments on the stability of the computed solutions. Physically one expects the wavelength of the periodic pattern to be selected by energy minimisation through a length-scale dependence of the strain energy. The choice of value for ℓ is therefore tied up with issues of stability of solutions. In fact, all solutions shown in Figures 15–17 have $|\eta| > 1$ for almost all S, and we know that the Sadowsky strain energy is non-convex when $|\eta| > 1$, implying instability of the solution and the creation of a microstructure with its own intrinsic length scale. Now, looking at the three-dimensional shapes in Figure 15b, and comparing them with the shape shown in Figure 1b, one may easily be led to believe that the

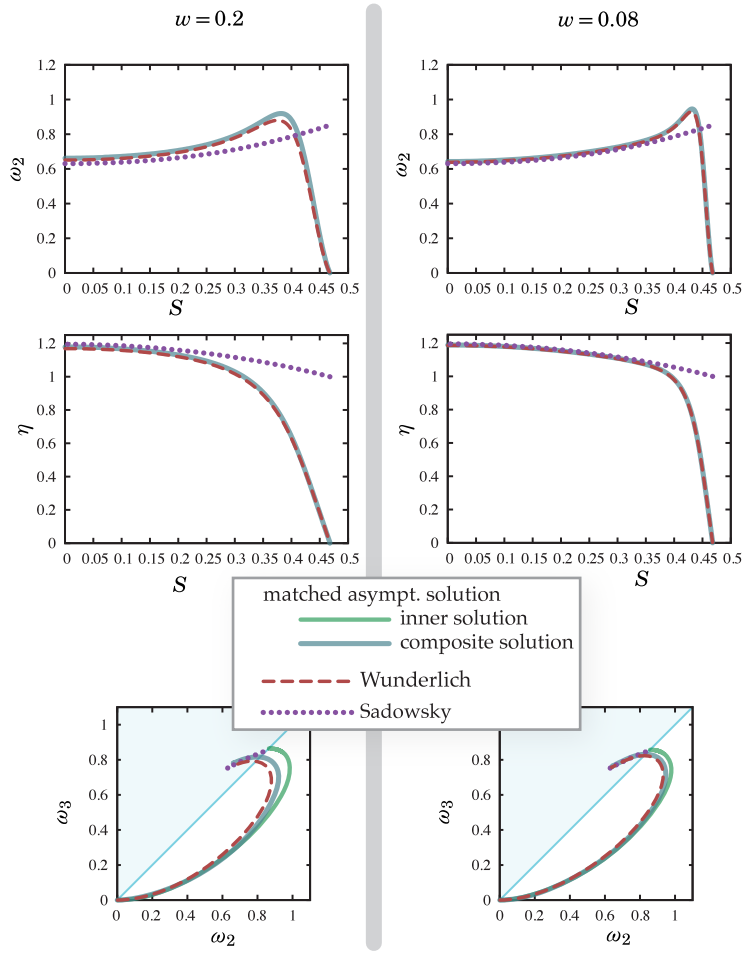

Figure 17: Twisted ribbon. Comparison of solutions including the composite matched asymptotic solution for the same parameters as in Figure 16.

chosen wavelength is too long, that the cylindrical part with nearly parallel generators given by the outer solution takes up too much of a wave. The solution is therefore likely to be unstable; there will instead be a tendency of the structure to fill in the cylindrical parts with additional conical stress singularities.

Under parameter variation η will generally vary; it does so along the loading curves shown in Figure 18. The marker on the force curves for the Sadowsky model in the figure indicates the point, at $F = -5.1194$, where $\eta(0) = 1$. Solutions to the right of this point have $|\eta| \geq 1$ for all S; those to the left have $|\eta| \leq 1$ for all S (and $|\eta| < 1$ for $0 \leq S < \ell/2$). By contrast, along the moment curves for the Sadowsky model all solutions have $\eta \geq 1$. The solutions of the other models (with $w > 0$) closely follow this η pattern. The parameter study reveals that there is a second solution at the same values of F and M used in Figures 15–17 having $|\eta| < 1$. However, the relative extension $e = 0.2336$ of this solution is unrealistically small for this (crumpled) solution to be stable. We therefore appear to have no stable solution in tension.

The right selection of ℓ is a problematic issue. Since the generator angle in the intermediate cylindrical regions is approximately 45°, ℓ may be close to w in case of a tightly packed triangular pattern as that observed in Figure 1b. This would cause a lack of separation of scales that would render our asymptotic analysis, which assumes $w/\ell \ll 1$, ineffective for such deformations. We hope to address this issue in future work.

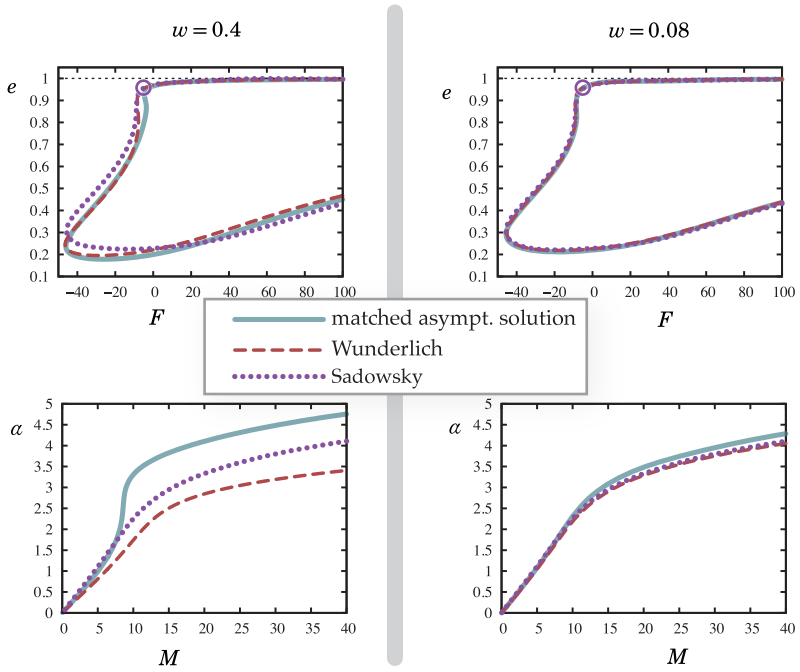

Figure 18: Load-displacement diagrams for a single-period twisted ribbon ($n = 2$). Top: extension e versus traction force F for $M = 6.4257$. Note that the curves have folds: the solutions on the lower branch have a very small extension e and are expected to be unstable. Bottom: rotation α versus twisting moment M for $F = 8.9528$. The curves for $w = 0.08$ contain the solutions shown in Figures 15–17 for this value at displacements $e = 0.9809$, $\alpha = 1.4241$. The circular marker indicates where the Sadowsky solution has $\eta(0) = 1$.

9 Discussion

The Sadowsky model for narrow ribbons ($w \ll \ell$) is known to have jump discontinuities at inflection points (i.e., at points where the curvature ω_2 is zero). From past numerical work we also know that wide strips, described by the Wunderlich model, feature cone-like stress concentrations on the edge of the ribbon at inflection points of its centreline. Thus the 'soft' (logarithmic) singularity of the finite-w Wunderlich model can be interpreted as a regularisation of the 'hard' (step) singularity of the zero-w Sadowsky model, with approximately flat right-angled triangles regularising the step in generator angle from $-45°$ to $45°$. This suggests that a singular perturbation analysis of the Wunderlich model valid for small w/ℓ might give further insight into the local cone-like behaviour with rapidly varying bending and torsional strains observed in twisted elastic ribbons.

Motivated by this, we have performed in this paper a matched asymptotic analysis valid for small w/ℓ in which the cone-like stress concentrations are described by inner layers, while the outer solution is given by a Sadowsky-like solution valid away from inflection points. Rather than enforcing matching conditions in the usual way, *i.e.*, in dedicated matching regions where both inner and outer solutions are asymptotically valid, we extend the outer solution into the inner region right up to the singularity. Matching then takes the form of jump conditions for the outer solution at this singularity. In addition to the discontinuity of the bending and torsional strains already present in the Sadowsky model, our outer solution therefore features a discontinuity in the twist angle, to first order in w/ℓ. This additional discontinuity lifts the Sadowsky-like outer solution to $\mathcal{O}(w/\ell)$ accuracy.

In the inner layer the forces and moments are constant to first order in w/ℓ. The layer is therefore governed by a reduced semi-decoupled planar system of equations for the strain ratio η and its derivative. The system does not depend on any remote boundary or closure conditions

or (in the case of an open ribbon) end loads. The two free parameters (integration constants) in the equations, A and ζ, can be determined uniquely from the equilibrium equations and from a stability argument. The inner layer solution constructed in this way is found to be symmetric to leading order. This is independent of any symmetry properties of the wider global solution. In the two examples we consider, the Möbius band and the twisted ribbon, we quite naturally impose global symmetry as expected under symmetric loading conditions. This imposed symmetry is consistent with the intrinsic symmetry of the inner layer. Under asymmetric loading conditions, however, the outer solution will lose symmetry but the symmetry of the inner layer, and hence the stress localisation, persists (to leading order). A further consequence of global asymmetry will be that the Weierstrass-Erdmann corner condition will have to be used to determine the location of singularities, while in our symmetric examples this condition is trivially satisfied.

The shape of the inner solution is universal, up to a single multiplicative constant, $\overline{\mu}$, representing the magnitude of the internal twisting moment in the layer, as set by the external forces and moments. It applies to all ribbon configurations with singularities, both open and closed, and including closed configurations with different linking number, as for instance studied in (Starostin and van der Heijden, 2015). The singularities in all these cases are characterised by flat triangular facets with the generator sweeping through a 90° sector from $-45°$ to 45° (see Figure 1), corresponding to η spanning the interval $[-1, 1]$ whose end points are exactly at the convexity boundary of the Sadowsky strain energy (Freddi et al., 2015).

The universal nature of the symmetric stress concentration at a cone-like singularity extends to circular *annular* ribbons (Starostin and van der Heijden, 2022). The strain energy in this case is given by an integral similar to Wunderlich's functional (2.9) but with a more complicated F of the form $F(\eta, w\,\eta')$ and with the torsion replaced by the geodesic torsion, the curvature by the normal curvature and with η the ratio of these two (Dias and Audoly, 2015; Starostin and van der Heijden, 2022). One easily verifies that in this case the (constant) geodesic curvature enters F only at order w. To first order in ε the layer equations (4.4) and (4.10) therefore remain valid, with F given by (2.11) and H by (4.7). Note, however, that the cone-like singularities are now associated with inflections of the surface rather than inflection points of the ribbon's centreline, which do not occur.

The advantage of our modified matching approach is that it gives us a new standalone model, called the improved Sadowsky model, defined over the full domain of the ribbon (§6.2). The model is independent of the strain gradient η' and offers a coarse-grained description of the singularities (stress localisations) in which the associated rapid strain variations are taken into account in an effective way by means of simple jump conditions, with dependence on the inner layer only through a single numerical constant, $c = -1.642$. This description is suited to situations where one is predominantly interested in the global, large-scale features of solutions and not in the detail of the singularities as, for instance, in questions of folding of ribbons into compact shapes or of overall shapes of ribbons with different linking numbers (Starostin and van der Heijden, 2015). We have also constructed a continuous composite solution, by inserting the universal inner layer at inflection points, for use when more detail of the singularity is required. In any case, the $\mathcal{O}(w/\ell)$ accuracy of solutions means that, at relatively little numerical cost, the improved Sadowsky model takes w-dependence into account, which may be important for instance in situations where self-contact may be expected.

For ribbon configurations without singularities (*e.g.*, cylindrical configurations), the improved Sadowsky model is equivalent to the Sadowsky model, as these models differ only in their jump conditions at singularities. In such regular situations the equations of either the Wunderlich or Sadowsky model are easy to solve. In the presence of singularities, the improved Sadowsky model reduces to the classical Sadowsky model in the formal limit $c \to \infty$, in which the twist angle discontinuities are suppressed.

Although all our inner and composite solutions are of course approximations, they are geometrically faithful in the sense that the corresponding ribbon shapes are given by developable surfaces. This is by construction: the developability condition $\omega_1 = 0$ is always satisfied and we are using the general parametrisation (2.4) of a developable surface to plot our ribbon shapes (*i.e.*, we are drawing straight generators that make an angle $\operatorname{arccot}(\eta)$ with the centreline). The surface

generated by the outer solution of our matched asymptotic construction, however, is usually not developable, as the generators intersect each other near the singularity in a ribbon of finite width (η does not tend to zero). This effect can be seen in Figure 15b. It could have been avoided by using the composite solution. However, as the figure demonstrates, the effect is only local and, in the spirit of the coarse-grained improved Sadowsky model, the unpolished solution will be sufficient as long as we do not care about these local details.

In closing, we comment on the inextensibility assumption which is at the heart of the Wunderlich model, on which the present work is founded. As shown by Shield (1992) in the planar case and by Audoly and Neukirch (2021) in general, the inextensibility assumption is consistent as long as the bending and twisting strains ω_i are much larger than the typical strain $\omega^\star \sim h/w^2$. Combining the expression of the typical strain $\omega \sim \varepsilon\,\overline{\mu}/w$ underlying our asymptotic analysis with $\varepsilon \sim w/\ell$, we find $\omega_i/\omega^\star \sim w^2/(h\,\ell)\,\overline{\mu}$, which is the product of the large number w/h by the small number w/ℓ and by the number $\overline{\mu} = \mathcal{O}(1)$. When this number $\omega_i/\omega^\star$ is large, the inextensibility assumption is correct and our analysis of the cone-like singularity is valid. When it is not, extensibility must be taken into account but this requires an extension of the Wunderlich model that is not currently available: the only extensible ribbon model available to date (Audoly and Neukirch, 2021) ignores the effect of the strain gradient which is clearly important near cone-like singularities.

We would like to thank Sébastien Neukirch for his suggestion to use the Hamiltonian invariant in the derivation of the inner layer equations, which helped making it more concise.

A Hamiltonian invariants

A.1 Hamiltonian of the Wunderlich model

Given a solution of the Wunderlich model and an interval $(S_1, S_2) \ni S$, consider the variation of the strain energy density e_{Wd} defined in (2.9) from S_1 to S_2,

$$[e_{\mathrm{Wd}}(\omega_2(S), \eta(S), \eta'(S))]_{S_1}^{S_2} = \int_{S_1}^{S_2} \left(\frac{\partial e_{\mathrm{Wd}}}{\partial \omega_2}\,\omega_2' + \frac{\partial e_{\mathrm{Wd}}}{\partial \eta}\,\eta' + \frac{\partial e_{\mathrm{Wd}}}{\partial \eta'}\,\eta'' \right) \mathrm{d}S.$$

Using the equilibrium equations (2.13–2.14), we have

$$\begin{aligned}
[e_{\mathrm{Wd}}(\omega_2(S), \eta(S), \eta'(S))]_{S_1}^{S_2} &= \int_{S_1}^{S_2} \left((m_2 + \eta\, m_3)\;\omega_2' + \left(\tfrac{\mathrm{d}}{\mathrm{d}S} \left(\tfrac{\partial e_{\mathrm{Wd}}}{\partial \eta'} \right) + m_3\,\omega_2 \right) \eta' + \tfrac{\partial e_{\mathrm{Wd}}}{\partial \eta'}\,\eta'' \right) \mathrm{d}S \\
&= \int_{S_1}^{S_2} \left(m_2\,\omega_2' + m_3\,\omega_3' + \tfrac{\mathrm{d}}{\mathrm{d}S} \left(\tfrac{\partial e_{\mathrm{Wd}}}{\partial \eta'}\,\eta' \right) \right) \mathrm{d}S \\
&= \left[m_2\,\omega_2 + m_3\,\omega_3 + \tfrac{\partial e_{\mathrm{Wd}}}{\partial \eta'}\,\eta' \right]_{S_1}^{S_2} - \int_0^\ell (m_2'\,\omega_2 + m_3'\,\omega_3)\;\mathrm{d}S \\
&= \left[m_2\,\omega_2 + m_3\,\omega_3 + \tfrac{\partial e_{\mathrm{Wd}}}{\partial \eta'}\,\eta' \right]_{S_1}^{S_2} - \int_0^\ell (m_1'\,\boldsymbol{d}_1 + m_2'\,\boldsymbol{d}_2 + m_3'\,\boldsymbol{d}_3) \cdot \boldsymbol{\omega}\,\mathrm{d}S,
\end{aligned}$$

where $\boldsymbol{\omega} = \omega_2\,\boldsymbol{d}_2 + \omega_3\,\boldsymbol{d}_3$ is the rotation gradient. Grouping the boundary terms and observing that $(m_1'\,\boldsymbol{d}_1 + m_2'\,\boldsymbol{d}_2 + m_3'\,\boldsymbol{d}_3) = \boldsymbol{m}' - \left(m_1\,\boldsymbol{d}_1' + m_2\,\boldsymbol{d}_2' + m_3\,\boldsymbol{d}_3'\right) = \boldsymbol{m}' - \boldsymbol{\omega} \times \boldsymbol{m} = -(\boldsymbol{d}_3 \times \boldsymbol{n} + \boldsymbol{\omega} \times \boldsymbol{m})$ by (2.7), we have

$$\begin{aligned}
\left[m_2\,\omega_2 + m_3\,\omega_3 + \tfrac{\partial e_{\mathrm{Wd}}}{\partial \eta'}\,\eta' - e_{\mathrm{Wd}}(\omega_2, \eta, \eta') \right]_{S_1}^{S_2} &= -\int_0^\ell (\boldsymbol{d}_3 \times \boldsymbol{n} + \boldsymbol{\omega} \times \boldsymbol{m}) \cdot \boldsymbol{\omega}\,\mathrm{d}S \\
&= -\int_0^\ell (\boldsymbol{\omega} \times \boldsymbol{d}_3) \cdot \boldsymbol{n}\,\mathrm{d}S \\
&= -\int_0^\ell \boldsymbol{d}_3' \cdot \boldsymbol{n}\,\mathrm{d}S \\
&= -[\boldsymbol{d}_3 \cdot \boldsymbol{n}]_{S_1}^{S_2}.
\end{aligned}$$

This shows that the Hamiltonian

$$\mathcal{H}_{\mathrm{Wd}}(S) = m_2\,\omega_2 + m_3\,\omega_3 + \frac{\partial e_{\mathrm{Wd}}}{\partial \eta'}\,\eta' + \boldsymbol{d}_3 \cdot \boldsymbol{n} - e_{\mathrm{Wd}}(\omega_2, \eta, \eta') \tag{A.1}$$

is an invariant for any solution of the Wunderlich model, *i.e.*, $\mathcal{H}_{\mathrm{Wd}}(S_1) = \mathcal{H}_{\mathrm{Wd}}(S_2)$ for any pair of points (S_1, S_2).

Inserting the constitutive relationship (2.14) and the expression of e_{Wd} from (2.9), we obtain the Hamiltonian in explicit form as

$$\begin{aligned}\mathcal{H}_{\mathrm{Wd}}(S) &= \boldsymbol{d}_3 \cdot \boldsymbol{n} + \left(\frac{\partial e_{\mathrm{Wd}}}{\partial \omega_2} - \eta\, m_3\right) \omega_2 + m_3\, \eta\, \omega_2 + \frac{\partial e_{\mathrm{Wd}}}{\partial \eta'}\, \eta' - e_{\mathrm{Wd}} \\ &= \boldsymbol{d}_3 \cdot \boldsymbol{n} + \left(\frac{\partial e_{\mathrm{Wd}}}{\partial \omega_2}\, \omega_2 - e_{\mathrm{Wd}}\right) + \frac{\partial e_{\mathrm{Wd}}}{\partial \eta'}\, \eta' \\ &= \boldsymbol{d}_3 \cdot \boldsymbol{n} + 4\, D\, w\, \frac{\omega_2^2}{2}\, L(\eta)\, \left(F(w\,\eta') + w\,\eta'\, F'(w\,\eta')\right) \end{aligned} \tag{A.2}$$

A.2 Hamiltonian of the Sadowsky model

A similar reasoning shows that the Hamiltonian of the Sadowsky model

$$\begin{aligned}\mathcal{H}_{\mathrm{Sd}}(S) &= m_2\, \omega_2 + m_3\, \omega_3 + \boldsymbol{d}_3 \cdot \boldsymbol{n} - e_{\mathrm{Sd}}(\omega_2, \eta) \\ &= \boldsymbol{d}_3 \cdot \boldsymbol{n} + 4\, D\, w \frac{\omega_2^2}{2}\, L(\eta) \end{aligned} \tag{A.3}$$

is an invariant for any solution of the Sadowsky model. This Hamiltonian can be obtained by taking formally $F \equiv 1$ in (A.2).

B Weak, cone-like singularity at the centre of the inner layer

In this appendix we analyse the weakly singular behaviour of the inner solution at the centre $\overline{S} = 0$ of the inner layer. This corresponds to the point C in Figure 6c where the caustic makes contact with the physical domain of the ribbon.

For $\overline{S} = 0$, $\overline{\eta}(0) = 0$, $\overline{\eta}'(0) = 2$, implying that the left-hand side $H(\overline{\eta}')$ of the differential equation (4.13) diverges logarithmically. By seeking a solution of (4.13) in the form of a series in $\overline{S}$ near $\overline{S} = 0$, one obtains

$$\overline{\eta}(\overline{S}) \approx 2\,\overline{S} - \frac{16}{3}\, \frac{\overline{S}^3}{\ln^2 |\overline{S}|} + \cdots \tag{B.1}$$

The first term in the expansion $\overline{\eta}(\overline{S}) \approx 2\,\overline{S}$ corresponds to a *conical approximation*: the generators predicted by (4.19) would then all pass through the tip of the cone C with coordinates $(\overline{x}, \overline{y}) = (0, -1/2)$. With this approximation, the argument q of F is $q = w\,\eta' = \overline{\eta}'(\overline{S}) = 2$, implying that the term $F(q)$ in the integrand of the strain energy $\mathcal{E}_{\mathrm{Wd}}$ in (2.9) is infinite: the conical approximation predicts an infinite energy, as is well-known in the theory of elastic plates. Even though the inner layer solution looks similar to a cone in the centre, the cone is not a suitable approximation as far as the elastic energy is concerned.

Inserting (B.1) into (4.20), one can derive the following approximation for the caustic near its tip C,

$$|\overline{x}_{\mathcal{C}}| \approx \frac{1}{3}\, \left(-\frac{1}{2} - \overline{y}_{\mathcal{C}}\right)^{3/2}\, \left[-\ln\left(-\frac{1}{2} - \overline{y}_{\mathcal{C}}\right)\right]. \tag{B.2}$$

The power $3/2$ being larger than 1, this corresponds to a sharp tip at C, in accordance with Figure 6c. By contrast, in the conical approximation $\overline{\eta}(\overline{S}) \approx 2\,\overline{S}$, the caustic would shrink to the point C.

Next, we proceed to check that the singularity (B.1) is weak enough for the elastic energy $\mathcal{E}_{\mathrm{Wd}}$ to remain finite. Using successively the expression of $\overline{\omega}_2$ in $(4.15)_1$, and the expansion (B.1) of the

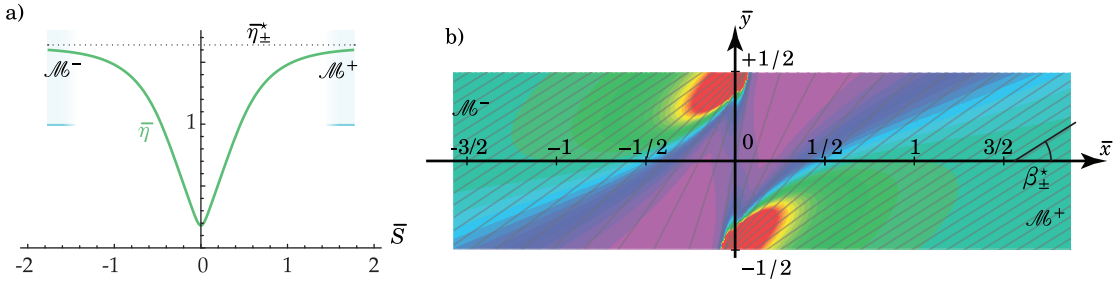

Figure 19: Inner layer solution for $\zeta = -0.5$ corresponding to a homoclinic loop similar to that in Figure 5a. (a) Layer solution $\overline{\eta}(\overline{S})$. (b) Distribution of the scaled bending energy $\overline{\kappa}^2$ shown in the unfolded ribbon domain, using the same colour code and conventions as in Figure 5c. There are two points on opposite sides of the ribbon where $\overline{\kappa}$ becomes unbounded, corresponding to tips of caustics where generators intersect.

solution, one can derive an approximation for the integrand of $\mathcal{E}_{\mathrm{Wd}}$ in (2.9) in dimensionless form as

$$4\,F(\overline{\eta}')\,\overline{\omega}_2^2\left(\frac{1+\overline{\eta}^2}{2}\right)^2 = 16\,\frac{\overline{\eta}^2(\overline{S})}{F(\overline{\eta}'(\overline{S}))\,(1+\overline{\eta}^2(\overline{S}))^2} \approx \frac{128\,\overline{S}^2}{-\ln\frac{4\,\overline{S}^2}{\ln^2|\overline{S}|}}. \tag{B.3}$$

This quantity is indeed integrable around $\overline{S}=0$: the logarithmic divergence of the factor $F(\overline{\eta}')$ on the left-hand side predicted by the conical approximation is cancelled by the small correction in (B.1).

C A stability argument for ruling out layer solutions having $\zeta \neq 0$

In this Appendix we briefly analyse the family of inner layer solutions with $\zeta \neq 0$ corresponding to the homoclinic loop shown using a purple curve in Figure 5a, and elaborate on the argument proposed in Section 4.3 for discarding them.

By processing an inner solution of this kind in the same way as we did with the other kind of inner solutions in Sections 4.4–4.5, we obtain the plots shown in Figure 19. These plots are for $\zeta = -0.5$; plots generated with different values of ζ are similar. In the rest of this appendix, we will limit attention to the case $\zeta < 0$: the inner layer solutions for $\zeta > 0$ can be obtained by applying the transformation $\overline{\eta}(\overline{S}) \leftarrow -\overline{\eta}(\overline{S})$, see Equation (4.10).

Using Taylor expansions, one can show that the values $\overline{\eta}_X$ of $\overline{\eta}$ where X-crossings occur in the level curves of Figure 5a are the roots of $-1+2\,\zeta\,\overline{\eta}+\overline{\eta}^2=0$. For the case $\zeta<0$ studied here, the X-crossing corresponding to the homoclinic loop (purple curve in the figure) is the positive root

$$\overline{\eta}_X = |\zeta| + \sqrt{1+\zeta^2}, \tag{C.1}$$

which satisfies the inequality $\overline{\eta}_X > 1$.

Now, this X-crossing is attained asymptotically for $\overline{S} \to \pm\infty$ by the homoclinic inner solution. The limits of $\overline{\eta}(\overline{S})$ for $\overline{S} \to \pm\infty$, denoted as $\overline{\eta}^\star_\pm$ in Section 4.3 and shown in Figure 19a, are therefore nothing but $\overline{\eta}^\star_+ = \overline{\eta}^\star_- = \overline{\eta}_X$. This shows that the asymptotic limits $|\overline{\eta}^\star_\pm|$ of $\overline{\eta}$ satisfy

$$|\overline{\eta}^\star_\pm| > 1. \tag{C.2}$$

The inequality $|\overline{\eta}| > 1$ is represented by the light blue domains in Figures 5a and 19a: Equation (C.2) is consistent with the fact that the points labelled $\mathcal{M}^\pm$ in these two figures fall inside the light blue domains.

The inequality also implies that the angle $\beta = \operatorname{arccot}(\overline{\eta})$ between the centreline and the generators is less that $\pi/4$ in the matching regions,

$$0 < |\beta^\star_\pm| < \frac{\pi}{4}, \tag{C.3}$$

as can indeed be seen in Figure 19b sufficiently far away from the centre of the layer.

In the matching regions $\mathcal{M}^\pm$ present on both sides of the singularity, this inner layer solution must be matched with an outer solution such that $\eta_{\text{out}}(S) \to \overline{\eta}^\star_\pm$, implying that the outer solution must satisfy $\eta_{\text{out}}(S) > 1$ in a finite-length domain near the matching region. However, we know from Section 6 that the outer solution is governed locally and away from singularities by the Sadowsky model, and from the work of Freddi et al. (2015); Paroni and Tomassetti (2019) we know that solutions of the Sadowsky model with $|\eta| > 1$ are unstable to the formation of a microstructure—see also Section 7 in (Audoly and Neukirch, 2021). This instability is due to the non-convex nature of the Sadowsky energy when $|\eta| > 1$. The matched asymptotic solutions obtained from the inner solutions having $\zeta < 0$ are therefore unstable and should be discarded. A similar reasoning applies to the case $\zeta > 0$. This justifies the selection of the parameter $\zeta = 0$ in (4.3).

By discarding layer solutions with $|\overline{\eta}^\star_\pm| > 1$ in the matching region, we also ensure consistency with the jump singularities predicted by the Sadowsky model, which involve a sign flip for the quantity ω_2 *at a point where* $|\eta| = 1$.

Note that both the 'heteroclinic' inner layer solution ($\zeta = 0$) in Figure 6 and the 'homoclinic' ones of the kind shown in Figure 19 ($\zeta \neq 0$) are symmetric, but with different kinds of symmetries: $\overline{\eta}$ is an even function of $\overline{S}$ in the former case, and an odd function in the latter. The 'heteroclinic' layer features a single point of stress focussing, located on the edge of the ribbon, while the 'homoclinic' ones feature two such points, in a bicone-like arrangement with conical tips on opposite sides of the ribbon. This bicone-like stress pattern does not look like the patterns seen in Figure 1. It is tempting, however, to interpret the triangular pattern in Figure 1b as a nascent microstructure similar to that considered in Paroni and Tomassetti (2019) formed in a stabilisation process in which the conical tips of the initially unstable 'homoclinic' pattern in Figure 19b separate and the two cones eventually become independent symmetric stress focussings.

D Derivation of apparent jump conditions

D.1 Apparent discontinuity in the twist angle

The general strategy from Section 5.1 is applied here to derive the apparent jump condition for the twist angle across an inner layer. To this end, we let $\boldsymbol{f}$ be the cumulative rotation, *i.e.*, we define

$$\boldsymbol{f}(S) = (f_2(S), f_3(S)) = \left(\int_{S^\dagger}^{S} \omega_2(S')\ \mathrm{d}S', \int_{S^\dagger}^{S} \omega_3(S')\ \mathrm{d}S' \right). \tag{D.1}$$

The quantity $\boldsymbol{f}(S)$ measures the rotation of the director frame $\boldsymbol{d}_i(S)$ with respect to the director frame $\boldsymbol{d}_i(S^\dagger)$ at the centre of the layer. This relative rotation is a small quantity in both the inner layer and the matching regions. Indeed, by combining the estimates for $S - S^\dagger$ from (3.3) and for ω_i in (3.5), we have

$$|\boldsymbol{f}(S)| \ll 1 \qquad \text{in } \mathcal{I} \cup \mathcal{M}^\pm.$$

Linearising and integrating equation (2.3), we obtain the directors in the vicinity of the inner layer as

$$\begin{pmatrix} \boldsymbol{d}_1(S) \\ \boldsymbol{d}_2(S) \\ \boldsymbol{d}_3(S) \end{pmatrix} = \begin{pmatrix} \boldsymbol{d}_1(S^\dagger) \\ \boldsymbol{d}_2(S^\dagger) \\ \boldsymbol{d}_3(S^\dagger) \end{pmatrix} + f_2(S) \begin{pmatrix} -\boldsymbol{d}_3(S^\dagger) \\ \boldsymbol{0} \\ \boldsymbol{d}_1(S^\dagger) \end{pmatrix} + f_3(S) \begin{pmatrix} \boldsymbol{d}_2(S^\dagger) \\ -\boldsymbol{d}_1(S^\dagger) \\ \boldsymbol{0} \end{pmatrix} + \mathcal{O}(|\boldsymbol{f}|^2). \tag{D.2}$$

If $\boldsymbol{f}(S)$ were not small, we would have to use a geometrically nonlinear extension of this equation.

Inserting the inner expansion (3.5) of ω_j into (D.1), we have

$$\boldsymbol{f}_{\rm in}(\overline{S}) = \varepsilon\,\overline{\mu}\,\left(\int_0^{\overline{S}} \overline{\omega}_2(\overline{S}')\;\mathrm{d}\overline{S}', \int_0^{\overline{S}} \overline{\omega}_3(S')\;\mathrm{d}\overline{S}'\right) + \mathcal{O}\left(\varepsilon^2\,\left|\int_0^{\overline{S}} \overline{\overline{\omega}}_j\,\mathrm{d}\overline{S}'\right|\right).$$

By (4.18), $\overline{\omega}_2(\overline{S}) \to \pm 1$ and $\overline{\omega}_3(\overline{S}) \to 1$ for $\overline{S} \to \pm\infty$. In addition, it can be shown that both $\int_0^{\pm\infty}(\overline{\omega}_2(\overline{S}') \mp 1)\;\mathrm{d}\overline{S}'$ and $\int_0^{\pm\infty}(\overline{\omega}_3(\overline{S}') - 1)\;\mathrm{d}\overline{S}'$ are convergent integrals, by a similar argument to that used earlier to justify (4.16). This yields the following expansion in the matching regions, for $w \ll |S - S^\dagger| \ll \frac{w}{\varepsilon}$:

$$\boldsymbol{f}_{\rm in}(\overline{S}) = \varepsilon\,\overline{\mu}\,\left(\pm\overline{S} + \int_0^{\pm\infty}(\overline{\omega}_2(\overline{S}') \mp 1)\;\mathrm{d}\overline{S}', \overline{S} + \int_0^{\pm\infty}(\overline{\omega}_3(\overline{S}') - 1)\;\mathrm{d}\overline{S}'\right) + \varepsilon^2 \times \cdots, \qquad \text{(D.3)}$$

where the symbols $\pm$ and $\mp$ stand for the signs of $(S - S^\dagger)$ and $-(S - S^\dagger)$, respectively. The expansion (D.3) is of the type anticipated in (5.3) and the coefficients in the expansion can be identified as

$$\boldsymbol{\alpha}_\pm^{[1]} = (\pm\overline{\mu}, \overline{\mu}), \qquad \boldsymbol{\alpha}_\pm^{[0]} = \overline{\mu}\,\left(\int_0^{\pm\infty}(\overline{\omega}_2(\overline{S}') \mp 1)\;\mathrm{d}\overline{S}', \int_0^{\pm\infty}(\overline{\omega}_3(\overline{S}') - 1)\;\mathrm{d}\overline{S}'\right), \qquad \ldots$$

Using (5.6), we obtain the apparent jump $[\![\boldsymbol{f}_{\rm out}]\!] = ([\![f_{2,\rm out}]\!], [\![f_{3,\rm out}]\!])$ as

$$[\![\boldsymbol{f}_{\rm out}]\!] = \varepsilon\,\left(\boldsymbol{\alpha}_+^{[0]} - \boldsymbol{\alpha}_-^{[0]}\right) + \mathcal{O}(\varepsilon^2).$$

Using the fact that $\overline{\omega}_2$ and $\overline{\omega}_3$ are odd and even functions, respectively, we get

$$\begin{array}{rcl} [\![\boldsymbol{f}_{\rm out}]\!] & = & \varepsilon\,\overline{\mu}\,\left(0, \int_{-\infty}^{+\infty}(\overline{\omega}_3(\overline{S}') - 1)\;\mathrm{d}\overline{S}'\right) + \mathcal{O}(\varepsilon^2) \\ & = & \left(0, \varepsilon\,\frac{\overline{\mu}}{c}\right) + \mathcal{O}(\varepsilon^2), \end{array} \qquad \text{(D.4)}$$

where c is the constant introduced in (4.16).

Combining with (D.2), we find the apparent discontinuity in the directors as

$$\begin{pmatrix} [\![\boldsymbol{d}_1^{\rm out}]\!] \\ [\![\boldsymbol{d}_2^{\rm out}]\!] \\ [\![\boldsymbol{d}_3^{\rm out}]\!] \end{pmatrix} = \frac{\varepsilon\,\overline{\mu}}{c}\begin{pmatrix} \boldsymbol{d}_2(S^\dagger) \\ -\boldsymbol{d}_1(S^\dagger) \\ \mathbf{0} \end{pmatrix} + \mathcal{O}(\varepsilon^2). \qquad \text{(D.5)}$$

Since $\boldsymbol{d}_i(S^\dagger) = \boldsymbol{d}_i^{\rm out}(0^-) + \mathcal{O}(\varepsilon)$, it is also possible to rewrite this in the following equivalent forms:

$$\begin{pmatrix} [\![\boldsymbol{d}_1^{\rm out}]\!] \\ [\![\boldsymbol{d}_2^{\rm out}]\!] \\ [\![\boldsymbol{d}_3^{\rm out}]\!] \end{pmatrix} = \frac{\varepsilon\,\overline{\mu}}{c}\begin{pmatrix} \boldsymbol{d}_2^{\rm out}(0^-) \\ -\boldsymbol{d}_1^{\rm out}(0^-) \\ \mathbf{0} \end{pmatrix} + \mathcal{O}(\varepsilon^2), \qquad \text{(D.6)}$$

or

$$\begin{pmatrix} \boldsymbol{d}_1^{\rm out}(0^+) \\ \boldsymbol{d}_2^{\rm out}(0^+) \\ \boldsymbol{d}_3^{\rm out}(0^+) \end{pmatrix} = \begin{pmatrix} +\cos\varphi\,\boldsymbol{d}_1^{\rm out}(0^-) + \sin\varphi\,\boldsymbol{d}_2^{\rm out}(0^-) \\ -\sin\varphi\,\boldsymbol{d}_1^{\rm out}(0^-) + \cos\varphi\,\boldsymbol{d}_2^{\rm out}(0^-) \\ \boldsymbol{d}_3^{\rm out}(0^-) \end{pmatrix} + \mathcal{O}(\varepsilon^2), \qquad \text{(D.7)}$$

where

$$\varphi = \frac{\varepsilon\,\overline{\mu}}{c} + \mathcal{O}(\varepsilon^2). \qquad \text{(D.8)}$$

Indeed, the right-hand sides of Equations (D.5–D.7) differ only by terms of order ε^2. The form (D.8) will be preferred as it preserves the orthonormal character of the director frame even when φ is finite, which will be useful for our numerical illustrations.

D.2 Apparent discontinuity of the centreline

A similar reasoning applied to the quantity $\boldsymbol{f}(S) = \boldsymbol{x}(S)$ yields the apparent discontinuity in the centreline position. The quantity $\boldsymbol{f}(S) = \boldsymbol{x}(S^\dagger) + \int_{S^\dagger}^{S} \boldsymbol{d}_3(S')\,\mathrm{d}S'$ can be estimated using (D.2) as

$$\boldsymbol{f}(S) = \boldsymbol{x}(S^\dagger) + (S - S^\dagger)\,\boldsymbol{d}_3(S^\dagger) + \left(\int_{S^\dagger}^{S} f_2(S')\,\mathrm{d}S'\right)\boldsymbol{d}_1(S^\dagger) + \cdots,$$

where f_2 is the cumulative bending angle from (D.1). This can be approximated in the inner layer as

$$\boldsymbol{f}_{\mathrm{in}}(\overline{S}) = \boldsymbol{x}(S^\dagger) + w\,\overline{S}\,\boldsymbol{d}_3(S^\dagger) + w\,\left(\int_{0}^{\overline{S}} f_2(\overline{S}')\,\mathrm{d}\overline{S}'\right)\boldsymbol{d}_1(S^\dagger) + \cdots \tag{D.9}$$

Using (D.3), one can obtain an expansion of the integral for $\overline{S} \to \pm\infty$ as

$$\int_{0}^{\overline{S}} f_2(\overline{S}')\,\mathrm{d}\overline{S}' = \varepsilon\,\overline{\mu}\,\left(\pm\frac{\overline{S}^2}{2} + \overline{S}\int_{0}^{\pm\infty}(\overline{\omega}_2(\overline{S}') \mp 1)\,\mathrm{d}\overline{S}' + C_\pm + \cdots\right), \tag{D.10}$$

where $C_\pm$ are two numerical constants of order 1 that can be expressed as integrals involving $\overline{\omega}_2$; we will not need their actual value.

Identifying (D.9–D.10) with the generic expansion (5.3), we can read off the constants

$$\alpha_\pm^{[2]} = \pm\frac{\overline{\mu}\,w}{2}, \qquad \alpha_\pm^{[1]} = w\,\left(\boldsymbol{d}_3(S^\dagger) + \overline{\mu}\,\left(\int_{0}^{\pm\infty}(\overline{\omega}_2(\overline{S}') \mp 1)\,\mathrm{d}\overline{S}'\right)\boldsymbol{d}_1(S^\dagger)\right), \qquad \alpha_\pm^{[0]} = \boldsymbol{x}(S^\dagger) + w\,\overline{\mu}\,C_\pm, \qquad \ldots$$

Equation (5.6) then yields the apparent discontinuity in the centreline position as

$$[\![\boldsymbol{x}_{\mathrm{out}}]\!] = [\![\boldsymbol{f}_{\mathrm{out}}]\!] = \varepsilon\,w\,\overline{\mu}\,(C_+ - C_-) + \mathcal{O}\left(w\,\varepsilon^2\right). \tag{D.11}$$

The factor w in the error term $\mathcal{O}\left(w\,\varepsilon^2\right)$ has been anticipated on dimensional grounds.

D.3 Equivalent point-like energy of a discontinuity

Consider now the energy (2.9) of the ribbon model integrated over a portion of the ribbon starting at the centre of the inner layer, *i.e.*, let

$$f(S) = \frac{D\,w}{2}\int_{S^\dagger}^{S} 4\,F\,(w\,\eta')\;\omega_2^2\,\left(\frac{1+\eta^2}{2}\right)^2\,\mathrm{d}S'.$$

In the inner layer, this can be approximated using $(3.6)_1$, (3.5), (3.7), (4.3) as

$$f_{\mathrm{in}} = \frac{D\,\varepsilon^2\,\overline{\mu}^2}{2}\int_{0}^{\overline{S}} 4\,F(\overline{\eta}')\,\overline{\omega}_2^2\,\left(\frac{1+\overline{\eta}^2}{2}\right)^2\,\mathrm{d}\overline{S} + \cdots,$$

and by using the expression of $\overline{\omega}_2$ in $(4.15)_1$, we obtain

$$f_{\mathrm{in}} = \frac{D\,(\varepsilon\,\overline{\mu})^2}{2}\int_{0}^{\overline{S}} \frac{4\,\overline{\eta}^2(\overline{S})}{F(\overline{\eta}'(\overline{S}))\,\left(\frac{1+\overline{\eta}^2(\overline{S})}{2}\right)^2}\,\mathrm{d}\overline{S} + \cdots$$

Observing that the asymptotic value of the integrand for $\overline{S} \to \pm\infty$ is 4 (since $\overline{\eta} \to \pm 1$, $\overline{\eta}' \to 0$ and $F \to 1$), we can take this constant out of the integral and rewrite this as

$$f_{\mathrm{in}} = \frac{D\,(\varepsilon\,\overline{\mu})^2}{2}\,\left(4\,\overline{S} + \int_{0}^{\overline{S}}\left(\frac{4\,\overline{\eta}^2(\overline{S})}{F(\overline{\eta}'(\overline{S}))\,\left(\frac{1+\overline{\eta}^2(\overline{S})}{2}\right)^2} - 4\right)\,\mathrm{d}\overline{S}\right) + \cdots$$

For $\overline{S} \to \pm\infty$, it can be shown that the integral converges, and that the limit is $\pm 2/c$. We can therefore identify the constants appearing in (5.3) as

$$\alpha_{\pm}^{[1]} = 4\,\frac{D\,\overline{\mu}^2}{2}, \qquad \alpha_{\pm}^{[0]} = \frac{D\,\overline{\mu}^2}{2}\,\int_0^{\pm\infty}\left(\frac{4\,\overline{\eta}^2(\overline{S})}{F(\overline{\eta}'(\overline{S}))\,\left(\frac{1+\overline{\eta}^2(\overline{S})}{2}\right)^2} - 4\right)\,\mathrm{d}\overline{S}, \qquad \dots$$

Note that since the leading order of f_{in} is ε^2, we need a version of (5.3) in which the powers of ε are increased by one to obtain these identifications. The integral appearing in $\alpha_{\pm}^{[0]}$ can be calculated to be $\pm 2/c$, which yields

$$\alpha_{\pm}^{[0]} = \pm\frac{D\,\overline{\mu}^2}{2} \times \frac{2}{c}.$$

Applying (5.6) to account for the leading power ε^2, we get the apparent jump as

$$\begin{aligned}\llbracket f_{\mathrm{out}} \rrbracket &= \varepsilon^2\,(\alpha_+^{[0]} - \alpha_-^{[0]}) + \mathcal{O}(\varepsilon^3)\\ &= \tfrac{D\,(\varepsilon\,\overline{\mu})^2}{2} \times \tfrac{4}{c} + \mathcal{O}\left(D\,\varepsilon^3\right).\end{aligned}$$

The factor D in the error term $\mathcal{O}\left(D\,\varepsilon^3\right)$ has been anticipated on dimensional grounds.

This can be rewritten in terms of the discontinuity φ in the twisting angle appearing in (5.8) as

$$\llbracket f_{\mathrm{out}} \rrbracket = \frac{4\,D\,c}{2}\,\varphi^2 + \mathcal{O}\left(D\,\varepsilon^3\right). \tag{D.12}$$

E The $f^\star$-problem is accurate to second order

In this appendix the equations proposed in Section 6.2 ($f^\star$-problem) are compared to those of the outer solution f_{out} in the matched asymptotic expansion. We check that both sets of equations are consistent up to terms of relative order ε^2, thereby justifying the error claim in (6.1).

Away from discontinuities, the equations for the outer solution are obtained by inserting the expansion $f(S) = f_{\mathrm{out}}\,(\varepsilon\,S/w)$ into the Wunderlich model and reading off the result order by order in ε. As noted in Section 2.3, the Wunderlich and Sadowsky models differ only through their constitutive relations, and we proceed to show that the constitutive relations of the Wunderlich model become equivalent to those of the Sadowsky model up to terms of relative order ε^2 when the scaling assumptions applicable to the outer solution are used: this will establish that the Sadowsky model is applicable in the outer region. In the constitutive relation (2.13), we insert the identity $e_{\mathrm{Wd}} = e_{\mathrm{Sd}}\,F(w\,\eta')$ and the scaling relation $\mathrm{d}/\mathrm{d}S \sim \varepsilon/w$, to estimate the first term as $-\frac{\mathrm{d}}{\mathrm{d}S}(\partial e_{\mathrm{Wd}}/\partial\eta') = \mathcal{O}(\frac{\varepsilon}{w})\,e_{\mathrm{Sd}}\,w\,F'(w\,\eta')$. The argument $q = w\,\eta'$ of F' being small in the outer region, $q = \mathcal{O}(\varepsilon)$, we have $F'(q) = \mathcal{O}(q) = \mathcal{O}(\varepsilon)$ by (2.12), which yields $-\frac{\mathrm{d}}{\mathrm{d}S}(\partial e_{\mathrm{Wd}}/\partial\eta') = \mathcal{O}(\varepsilon^2\,e_{\mathrm{Sd}})$. For the second term in (2.13), we have $\partial e_{\mathrm{Wd}}/\partial\eta = \partial e_{\mathrm{Sd}}/\partial\eta\,F(w\,\eta')$. In view of (2.12), the F term can be expanded in the outer region as

$$F(w\,\eta') = 1 + \mathcal{O}((w\,\eta')^2) = 1 + \mathcal{O}(\varepsilon^2). \tag{E.1}$$

and we have $\partial e_{\mathrm{Wd}}/\partial\eta = \partial e_{\mathrm{Sd}}/\partial\eta\,(1 + \mathcal{O}(\varepsilon^2))$. Up to terms of relative order ε^2, it is therefore possible to discard the first term $-\frac{\mathrm{d}}{\mathrm{d}S}(\partial e_{\mathrm{Wd}}/\partial\eta')$ in the constitutive relation (2.13) entirely, and to approximate the second term by $\partial e_{\mathrm{Sd}}/\partial\eta$, which yields

$$\frac{\partial e_{\mathrm{Sd}}}{\partial\eta}\,(1 + \mathcal{O}(\varepsilon^2)) - m_3\,\omega_2 = 0. \tag{E.2}$$

By a similar reasoning, the second constitutive relation (2.14) can be rewritten as

$$m_2 = \frac{\partial e_{\mathrm{Sd}}}{\partial\omega_2}\,(1 + \mathcal{O}(\varepsilon^2)) - \eta\,m_3 \tag{E.3}$$

in the outer region. Up to the ε^2 correction terms, Equations (E.2–E.3) are nothing but the constitutive relations (2.18) of the Sadowsky model, as can be checked. This shows that the Sadowsky model is accurate up to terms of order ε^2 in the outer region.

Next, we proceed to review the jump conditions. The jump condition (5.9) for $\boldsymbol{x}_{\mathrm{out}}$ has been derived in the framework of the matched asymptotic expansion: it shows that $[\![\boldsymbol{x}_{\mathrm{out}}]\!] = \boldsymbol{0}$, up to terms of order $w\,\varepsilon$, which are precisely ε^2 times smaller than the typical magnitude w/ε of $\boldsymbol{x}$ given in $(6.2)_1$. This confirms that the jump condition $[\![\boldsymbol{x}^\star]\!] = \boldsymbol{0}$ proposed in $(6.5)_1$ is accurate up to a relative order ε^2. The same reasoning shows that the jump condition $(6.5)_2$ for the directors is consistent to this order with that derived asymptotically in (5.7). By a similar argument, the continuity conditions (6.6) for $\boldsymbol{n}$ and $\boldsymbol{m}$ are clearly consistent with those derived asymptotically in (5.11–5.12), since the error term in (5.11–5.12) is ε^2 times smaller than the relevant order of magnitude in $(6.2)_{5,6}$.

Using $(4.2)_2$ and the matching condition (5.2) on $f = m_3$, we can obtain the parameter $\overline{\mu} = \overline{\mu}_J$ characterising the magnitude of the inner solution centred at $S_J^\dagger$ as

$$\overline{\mu}_J = \frac{m_3^{\mathrm{out}}(\widetilde{S}_J^\dagger)}{4\,D\varepsilon} + \mathcal{O}(\varepsilon), \tag{E.4}$$

where we recall that the quantity $m_3^{\mathrm{out}} = \boldsymbol{m}_3^{\mathrm{out}} \cdot \boldsymbol{d}_3$ appearing in the numerator is continuous to the required order by (5.13). Combining with (5.8), we have $\varphi_J = \frac{m_3^{\mathrm{out}}(\widetilde{S}_J^\dagger)}{4\,Dc} + \mathcal{O}(\varepsilon^2)$, which matches the constitutive law announced in (6.8). This error of order ε^2 in φ_J propagates to the directors $\boldsymbol{d}_i^{\mathrm{out}}$ via the jump conditions $(5.7)_{1,2}$, in accordance with the accuracy claim (6.1).

It can also be checked that the invariant $\mathcal{H}_{\mathrm{Sd}}^\star$ proposed in (6.7) is consistent, up to terms of relative order ε^2, with the invariant $\mathcal{H}_{\mathrm{Wd}}^{\mathrm{out}}$ derived in (5.14). This is shown by inserting the outer expansion into (A.1) and checking that the result is consistent with (A.3) up to terms of relative order ε^2. This verification is similar to that done earlier for the constitutive laws at the start of this Appendix, and is left to the reader. It proceeds again from Equation (E.1), which implies that the Wunderlich and Sadowsky models are effectively indistinguishable.

F Variational derivation of the outer problem

In this appendix we start from the strain energy functional which we proposed in (6.9) and derive the equilibrium equations announced in Section 6.2 using a variational approach.

We consider perturbations (variations) $\hat{\boldsymbol{x}}(S)$, $\hat{\boldsymbol{\psi}}(S)$, $\hat{S}_J^\dagger$, $\hat{\varphi}_J$ to the quantities $\boldsymbol{x}^\star(S)$, $\boldsymbol{d}_i^\star(S)$, $S_J^\dagger$ and $\varphi_J^\star$, with $1 \leqslant J \leqslant N$. Note that the arclength coordinates $S_J^\dagger$ of the discontinuities are perturbed as well.

Specifically, the quantity $\hat{\boldsymbol{\psi}}$ is an infinitesimal rotation angle, such that the orthogonal directors are perturbed as

$$\hat{\boldsymbol{d}}_i(S) = \hat{\boldsymbol{\psi}}(S) \times \boldsymbol{d}_i^\star(S). \tag{F.1}$$

This particular form of $\hat{\boldsymbol{d}}_i(S)$ ensures that the orthonormality condition (2.1) is satisfied in the perturbed configuration, to first order in the perturbation.

The perturbation $\widehat{[\![f]\!]}_J = [\![f + \hat{f}]\!]_{S_J^\dagger + \hat{S}_J^\dagger} - [\![f]\!]_{S_J^\dagger}$ of the jump $[\![f]\!]_J = f((S_J^\dagger)^+) - f((S_J^\dagger)^-)$ of an arbitrary quantity $f(S)$ at a moving point can be expanded as

$$\widehat{[\![f]\!]}_J = [\![\hat{f}]\!]_J + \hat{S}_J^\dagger [\![f']\!]_J. \tag{F.2}$$

Here, the first term on the right-hand side comes from the perturbations to the function f itself on either side of the discontinuity, while the second term arises from the motion of the discontinuity.

The continuity of the centreline position $\boldsymbol{x}^\star(S)$ in $(6.5)_1$ must hold both for the original configuration $\boldsymbol{x}^\star$ and for the perturbed configuration $\boldsymbol{x}^\star + \hat{\boldsymbol{x}}$. Using (F.2), we get $[\![\hat{\boldsymbol{x}}]\!]_J + \hat{S}_J^\dagger [\![\boldsymbol{d}_3^\star]\!]_J = \boldsymbol{0}$. Now, $\boldsymbol{d}_3^\star$ is continuous by $(6.5)_2$, and we obtain

$$[\![\hat{\boldsymbol{x}}]\!]_J = \boldsymbol{0}. \tag{F.3}$$

In incremental form, the jump condition $(6.5)_2$ can be written as

$$[\![\hat{\boldsymbol{\psi}}]\!]_J + \hat{S}_J^\dagger \left[\!\!\left[\sum_{i=1}^{2} \omega_i^\star \, \boldsymbol{d}_i^\star \right]\!\!\right]_J = \hat{\varphi}_J \, \boldsymbol{d}_3^\star(S_J^\dagger) \tag{F.4}$$

and the adaptation condition (2.2) as

$$\hat{\boldsymbol{x}}'(S) - \hat{\boldsymbol{\psi}}(S) \times \boldsymbol{d}_3^\star(S) = \boldsymbol{0}. \tag{F.5}$$

By a classical argument, the increments $\widehat{\omega_i}$ of the bending and twisting strains ω_i can be obtained from (2.3) as

$$\widehat{\omega_i} = \hat{\boldsymbol{\psi}}' \cdot \boldsymbol{d}_i^\star. \tag{F.6}$$

This follows for instance from Equation [65] in the work of Dias and Audoly (2014), with $1/r_0 = 0$. Having identified the incremental kinematic conditions, we proceed to write the stationarity condition of the total potential energy

$$\mathcal{E}_{\rm im}[\omega_2, \omega_3, (S_J^\dagger, \varphi_J)_{1 \leqslant J \leqslant N}] + \int_{\mathcal{D}} (-\boldsymbol{f}(S) \cdot \boldsymbol{x}(S) + g(\boldsymbol{d}_i(S))) \, \mathrm{d}S, \tag{F.7}$$

where $\boldsymbol{f}(S)$ represents a density of any applied forces, and $g(\boldsymbol{d}_i(S))$ is the potential associated with the density of applied moments.

The first variation of the energy must be zero,

$$\begin{aligned} \forall (\hat{\boldsymbol{x}}, \hat{\boldsymbol{\psi}}, \hat{S}_J^\dagger, \hat{\varphi}_J) \text{ k.a.} \quad & - \int_{\mathcal{D}} (m_1^\star \, \widehat{\omega_1} + m_2^\star \, \widehat{\omega_2} + m_3^\star \, \widehat{\omega_3}) \, \mathrm{d}S - 4 \, D \, c \sum_{J=1}^{N} \varphi_J^\star \, \hat{\varphi}_J + \sum_{J=1}^{N} [\![e_{\rm Sd}^\star]\!]_J \, \hat{S}_J^\dagger \cdots \\ & + \int_{\mathcal{D}} (\boldsymbol{f} \cdot \hat{\boldsymbol{x}} + \boldsymbol{q} \cdot \hat{\boldsymbol{\psi}}) \, \mathrm{d}S - \int_{\boldsymbol{\mathcal{D}}} \boldsymbol{n}^\star \cdot (\hat{\boldsymbol{x}}' - \hat{\boldsymbol{\psi}} \times \boldsymbol{d}_3^\star) \, \mathrm{d}S = 0. \end{aligned} \tag{F.8}$$

Here, 'k.a.' means that we limit attention to kinematically admissible perturbations, *i.e.*, to perturbations satisfying (F.3–F.4).

Equation (F.8) can be justified as follows:

- m_1 is a Lagrange multiplier enforcing the condition $\omega_1 = 0$;
- m_2 and m_3 are the bending and twisting moments introduced in (2.18), which allow the variation of the integral term in (6.9) to be written as $\int_{\mathcal{D}} (m_2^\star \, \widehat{\omega_1} + m_3^\star \, \widehat{\omega_3}) \, \mathrm{d}S$;
- $e_{\rm Sd}^\star$ is the strain energy density in the Sadowsky model, see (2.17);
- $\boldsymbol{q}$ is the density of external moments, such that $\hat{g} = -\boldsymbol{q} \cdot \hat{\boldsymbol{\psi}}$;
- $\boldsymbol{n}^\star$ is the Lagrange multiplier associated with the adaptation constraint, see (F.5).

Using (F.6) and identifying the internal moment $\boldsymbol{m}^\star = m_i^\star \, \boldsymbol{d}_i^\star$, one can rewrite (F.8) as

$$\begin{aligned} \forall (\hat{\boldsymbol{x}}, \hat{\boldsymbol{\psi}}, \hat{S}_J^\dagger, \hat{\varphi}_J) \text{ k.a.} \quad & - \textstyle\int_{\mathcal{D}} \boldsymbol{m}^\star \cdot \hat{\boldsymbol{\psi}}' \, \mathrm{d}S + \sum_{J=1}^{N} \left(-4 \, D \, c \varphi_J^\star \, \hat{\varphi}_J + [\![e_{\rm Sd}^\star]\!]_J \, \hat{S}_J^\dagger \right) \cdots \\ & + \textstyle\int_{\mathcal{D}} (\boldsymbol{f} \cdot \hat{\boldsymbol{x}} + \boldsymbol{q} \cdot \hat{\boldsymbol{\psi}}) \, \mathrm{d}S - \int_{\boldsymbol{\mathcal{D}}} \boldsymbol{n}^\star \cdot (\hat{\boldsymbol{x}}' - \hat{\boldsymbol{\psi}} \times \boldsymbol{d}_3) \, \mathrm{d}S = 0. \end{aligned} \tag{F.9}$$

In the presence of discontinuities, integrations by parts are carried out using

$$\int_{\mathcal{D}} u \, v' \, \mathrm{d}S = [u \, v]_0^\ell - \sum_{J=1}^{N} [\![u \, v]\!]_J, \tag{F.10}$$

where $[u\,v]_0^\ell = (u\,v)(\ell) - (u\,v)(0)$ denotes the variation across the entire domain and $\mathcal{D}$ is the integration domain without singularities from (6.10). Applying this to (F.9), we obtain

$$\forall(\hat{\boldsymbol{x}},\hat{\boldsymbol{\psi}},\hat{S}_J^\dagger,\hat{\varphi}_J)\text{ k.a.}\quad -[\boldsymbol{n}^\star\cdot\hat{\boldsymbol{x}}+\boldsymbol{m}^\star\cdot\hat{\boldsymbol{\psi}}]_0^\ell+\sum_{J=1}^{N}\Big(\llbracket\boldsymbol{n}^\star\cdot\hat{\boldsymbol{x}}+\boldsymbol{m}^\star\cdot\hat{\boldsymbol{\psi}}\rrbracket_J-4\,D\,c\varphi_J^\star\,\hat{\varphi}_J+\llbracket e_{\mathrm{Sd}}^\star\rrbracket_J\,\hat{S}_J^\dagger\Big)\cdots$$
$$+\int_{\mathcal{D}}((\boldsymbol{n}^{\star\prime}+\boldsymbol{f})\cdot\hat{\boldsymbol{x}}+(\boldsymbol{m}^{\star\prime}+\boldsymbol{d}_3^\star\times\boldsymbol{n}^\star+\boldsymbol{q})\cdot\hat{\boldsymbol{\psi}})\,\mathrm{d}S=0.\quad\text{(F.11)}$$

The stationarity conditions associated with the integral on the second line are the Kirchhoff equations stated in (2.7) but with external loads $\boldsymbol{f}$ and $\boldsymbol{q}$ included. The variation $[\ldots]_0^\ell$ on the first line yields the usual boundary conditions on $\boldsymbol{n}^\star$ and $\boldsymbol{m}^\star$ from rod theory—in the absence of kinematic constraints at end points, for instance, the stress-free boundary conditions $\boldsymbol{n}^\star(0)=\boldsymbol{0}$, $\boldsymbol{m}^\star(0)=\boldsymbol{0}$, $\boldsymbol{n}^\star(\ell)=\boldsymbol{0}$ and $\boldsymbol{m}^\star(\ell)=\boldsymbol{0}$ are recovered.

The remaining terms associated with the discontinuities can be rewritten as

$$\forall(\hat{\boldsymbol{x}},\hat{\boldsymbol{\psi}},\hat{S}_J^\dagger,\hat{\varphi}_J)\ \text{k.a.}\quad\sum_{J=1}^{N}\Big(\llbracket\boldsymbol{n}^\star\rrbracket_J\cdot\hat{\boldsymbol{x}}+\langle\boldsymbol{m}^\star\rangle_J\cdot\llbracket\hat{\boldsymbol{\psi}}\rrbracket_J+\llbracket\boldsymbol{m}^\star\rrbracket_J\cdot\langle\hat{\boldsymbol{\psi}}\rangle_J-4\,D\,c\varphi_J^\star\,\hat{\varphi}_J+\llbracket e_{\mathrm{Sd}}^\star\rrbracket_J\,\hat{S}_J^\dagger\Big)=0,\quad\text{(F.12)}$$

after using (F.3) and after decomposing both $\boldsymbol{m}^\star$ and $\hat{\boldsymbol{\psi}}$ according to

$$h((S_J^\dagger)^\pm)=\langle h\rangle_J\pm\frac{\llbracket h\rrbracket_J}{2},$$

where $\langle h\rangle_J=\frac{1}{2}\,(h((S_J^\dagger)^-)+h((S_J^\dagger)^+))$ denotes the average value of a discontinuous quantity h at the singularity.

In (F.12), the stationarity condition associated with the quantity $\hat{\boldsymbol{x}}$ is the balance of forces $\llbracket\boldsymbol{n}^\star\rrbracket_J=\boldsymbol{0}$ announced in $(6.6)_1$.

Using (F.4) to eliminate $\llbracket\hat{\boldsymbol{\psi}}\rrbracket_J$, we can then rewrite the remaining terms in (F.12) as

$$\forall(\langle\hat{\boldsymbol{\psi}}\rangle_J,\hat{S}_J^\dagger,\hat{\varphi}_J)\,\text{k.a.}\qquad\sum_{J=1}^{N}\Bigg(\llbracket\boldsymbol{m}^\star\rrbracket_J\cdot\langle\hat{\boldsymbol{\psi}}\rangle_J+\Big(\langle\boldsymbol{m}^\star\rangle_J\cdot\boldsymbol{d}_3^\star(S_J^\dagger)-4\,D\,c\varphi_J^\star\Big)\,\hat{\varphi}_J$$
$$-\left(\langle\boldsymbol{m}^\star\rangle_J\cdot\left\llbracket\sum_{i=1}^{2}\omega_i^\star\,\boldsymbol{d}_i^\star\right\rrbracket_J-\llbracket e_{\mathrm{Sd}}^\star\rrbracket_J\right)\,\hat{S}_J^\dagger\Bigg)=0.$$

Setting to zero the coefficients of $\langle\hat{\boldsymbol{\psi}}\rangle_J$ and $\hat{\varphi}_J$ first, we obtain the balance of moments $\llbracket\boldsymbol{m}^\star\rrbracket_J=\boldsymbol{0}$ announced in $(6.6)_2$, as well as the conditions $\langle\boldsymbol{m}^\star\rangle_J\cdot\boldsymbol{d}_3^\star(S_J^\dagger)=4\,D\,c\varphi_J^\star$. Since we know that $\boldsymbol{m}^\star$ is continuous, the latter yields the effective constitutive law (6.8) of the discontinuity.

Next, setting to zero the coefficient of $\hat{S}_J^\dagger$ and using $\llbracket\boldsymbol{m}^\star\rrbracket_J=\boldsymbol{0}$, we get the condition

$$\left\llbracket\boldsymbol{m}^\star\cdot\sum_{i=1}^{2}\omega_i^\star\,\boldsymbol{d}_i^\star-e_{\mathrm{Sd}}^\star\right\rrbracket_J=0.\quad\text{(F.13)}$$

This is equivalent to the Weierstrass–Erdmann corner condition (6.7): the quantity inside the double brackets can be identified with the Hamiltonian $\mathcal{H}_{\mathrm{Sd}}$ in (A.3) up to the continuous (hence unimportant) term $\boldsymbol{n}^\star\cdot\boldsymbol{d}_3^\star$.

G First-order energy estimate for the Möbius band

With the aim to predict the initial slope of the strain energy plotted in Figure 13b as a function of w, we present a perturbation analysis of the outer problem of the Möbius band (§7.1) in powers of ε, capturing the contributions of orders 1 and ε.

The dominant order corresponds to setting $\varepsilon = w/\ell = 0$. In this limit, the matched asymptotic solution is equivalent to the (discontinuous) Sadowsky solution for the Möbius band. Solving it numerically in scaled form first, and reverting to unscaled variables next, we obtain its strain energy in the form

$$\mathcal{E}_{\rm Sd}^0 = \frac{D\,w}{\ell}\,57.449.$$

The twisting moment at the singular point is found to be

$$(m_3^{\rm Sd})^0\left(\frac{\ell}{2}\right) = \frac{D\,w}{\ell}\,19.7395,$$

where the numerical factor on the right-hand side corresponds to the numerical value 0.785410 of the curvature observed in Section 7.2.

One can transition from this Sadowsky solution to the solution of the outer problem stated in Section 6.2 by progressively increasing the twist angle discontinuity at the singular point $S = \ell/2$, from 0 (Sadowsky solution) to $\varphi^\star$ (outer solution). The difference in strain energy $\mathcal{E}_{\rm Sd}$ between these two solutions equals the work done to create this twist angle discontinuity. Since the angle $\varphi^\star = \mathcal{O}(\varepsilon)$ is small, the twisting couple $m_3(\ell/2)$ opposing the creation of the discontinuity remains approximately equal to $m_3^{\rm Sd}(\ell/2) = \varepsilon$, implying that the work done is equal to $-(m_3^{\rm Sd})^0(\ell/2)\,\varphi^\star + \mathcal{O}(\varepsilon^3)$. We conclude that the Sadowsky energy $\mathcal{E}_{\rm Sd}(\varphi^\star)$ of the matched asymptotic solution, as given by (2.17), can be written as

$$\mathcal{E}_{\rm Sd}(\varphi^\star) = \mathcal{E}_{\rm Sd}^0 - (m_3^{\rm Sd})^0\left(\frac{\ell}{2}\right)\,\varphi^\star + \mathcal{O}(\varepsilon^3).$$

The strain energy functional $\mathcal{E}_{\rm im}$ introduced in (6.9) equally has an additional contribution from the singularity,

$$\mathcal{E}_{\rm im}(\varphi^\star) = \mathcal{E}_{\rm Sd}^0 - (m_3^{\rm Sd})^0\left(\frac{\ell}{2}\right)\,\varphi^\star + \frac{4\,D\,c}{2}\,\varphi^{\star 2} + \mathcal{O}(\varepsilon^3). \tag{G.1}$$

As shown in F, this energy functional is stationary with respect to $\varphi^\star$ at equilibrium. The stationarity condition yields the equilibrium value of the twist angle discontinuity as

$$\varphi^\star = \frac{1}{4\,D\,c}\,(m_3^{\rm Sd})^0 + \mathcal{O}(\varepsilon^2) = 4.93488\,\frac{\varepsilon}{c} + \mathcal{O}(\varepsilon^2). \tag{G.2}$$

This prediction is verified in Figure 13a. Note that (G.2), by comparison with (5.8), fixes the dimensionless coefficient $\overline{\mu}$ that sets the scale of internal moments in the inner layer: $\overline{\mu} = 4.93488$ (this being π times the jump in curvature across the singularity in the Sadowsky model, where π refers to half the length of the strip in our units).

Inserting (G.2) into (G.1), we have

$$\begin{aligned}\mathcal{E}_{\rm im}(\varphi^\star) &= \mathcal{E}_{\rm Sd}^0 - 48.7060\,\frac{D\varepsilon^2}{c} + \mathcal{O}(\varepsilon^3)\\ &= D\,\left(57.449\,\varepsilon - 48.7060\,\frac{\varepsilon^2}{c}\right) + \mathcal{O}(\varepsilon^3)\\ &= \frac{D\,w}{2\,\ell/(2\,\pi)}\,\left(18.287 + 3.00536\,\frac{w}{2\,\ell/(2\,\pi)}\right) + \mathcal{O}(\varepsilon^3).\end{aligned} \tag{G.3}$$

This prediction is shown as the thin straight line in Figure 13b. We see that it predicts the initial slope of the energy $\mathcal{E}_{\rm im}$ as a function of w very accurately.

References

Audoly, B., Neukirch, S., 2021. A one-dimensional model for elastic ribbons: a little stretching makes a big difference. Journal of the Mechanics and Physics of Solids 153, 104457.

Bartels, S., Hornung, P., 2015. Bending paper and the Möbius strip. Journal of Elasticity 119, 113–136.

Chopin, J., Démery, V., Davidovitch, B., 2015. Roadmap to the morphological instabilities of a stretched twisted ribbon. Journal of Elasticity 119, 137–189.

Chopin, J., Kudrolli, A., 2013. Helicoids, wrinkles, and loops in twisted ribbons. Physical Review Letters 111, 174302.

Dias, M.A., Audoly, B., 2014. A non-linear rod model for folded elastic strips. Journal of the Mechanics and Physics of Solids 62, 57—80.

Dias, M.A., Audoly, B., 2015. "Wunderlich, meet Kirchhoff": A general and unified description of elastic ribbons and thin rods. Journal of Elasticity 119, 49–66.

Efrati, E., 2015. Non-Euclidean ribbons: generalized Sadowsky functionals for incompatible ribbons. Journal of Elasticity 119, 251–261.

Freddi, L., Hornung, P., Mora, M.G., Paroni, R., 2015. A corrected Sadowsky functional for inextensible elastic ribbons. Journal of Elasticity 123, 125–136.

Freddi, L., Hornung, P., Mora, M.G., Paroni, R., 2016. A variational model for anisotropic and naturally twisted ribbons. SIAM Journal on Mathematical Analysis 48, 3883–3906.

Hornung, P., 2011. Euler-Lagrange equation and regularity for flat minimizers of the Willmore functional. Communications on Pure and Applied Mathematics 63, 367–441.

Inc., W.R., . Mathematica, Version 12.3.1. URL: `https://www.wolfram.com/mathematica`. champaign, IL, 2021.

Kohn, R.V., O'Brien, E., 2018. The wrinkling of a twisted ribbon. Journal of Nonlinear Science 28, 1221–1249.

Korte, A.P., Starostin, E.L., van der Heijden, G.H.M., 2011. Triangular buckling patterns of twisted inextensible strips. Proceedings of the Royal Society of London, A 467, 285–303.

Paroni, R., Tomassetti, G., 2019. Macroscopic and microscopic behavior of narrow elastic ribbons. Journal of Elasticity 135, 409–433.

Sadowsky, M., 1931. Theorie der elastisch biegsamen undehnbaren Bänder mit Anwendungen auf das Möbius'sche Band, in: Oseen, A.C.W., Weibull, W. (Eds.), Verhandl. des 3. Intern. Kongr. f. Techn. Mechanik, AB Sveriges Litografiska Tryckerier, Stockholm. pp. 444–451.

Shield, R.T., 1992. Bending of a beam or wide strip. Quarterly Journal of Mechanics and Applied Mathematics 45, 567–573.

Spivak, M., 1999. A comprehensive introduction to differential geometry. volume 3. 3^{rd} ed., Publish or perish, Inc., Houston, TX.

Starostin, E.L., van der Heijden, G.H.M., 2007. The shape of a Möbius strip. Nature Materials 6, 563–567.

Starostin, E.L., van der Heijden, G.H.M., 2015. Equilibrium shapes with stress localisation for inextensible elastic möbius and other strips. Journal of Elasticity 119, 67–112.

Starostin, E.L., van der Heijden, G.H.M., 2018. Forceless Sadowsky strips are spherical. Physical Review E 97, 023001.

Starostin, E.L., van der Heijden, G.H.M., 2022. Forceless folding of thin annular strips. submitted .

Wunderlich, W., 1962. Über ein abwickelbares Möbiusband. Monatshefte für Mathematik 66, 276–289.

Yu, T., Hanna, J.A., 2019. Bifurcations of buckled, clamped anisotropic rods and thin bands under lateral end translations. Journal of the Mechanics and Physics of Solids 122, 657–685.